Aalto University
School of Chemical
Engineering

School of Chemical Technology
Degree Programme of Materials Science and Engineering

Keiran Holland

DISTRIBUTION OF TRACE ELEMENTS IN THE BLISTER COPPER - WHITE METAL SYSTEM: COPPER BLOW CONDITIONS

Master's thesis for the degree of Master of Science in Technology submitted for inspection, Espoo, 08 July, 2018.

Supervisor **Ari Jokilaakso**

Instructors **Pekka Taskinen, Prof. Emer.**

Dmitry Sukhomlinov, PhD

Author Keiran Holland

Title of thesis: Distribution of Trace Elements in the Blister Copper - White Metal System: Copper Blow Conditions

Department Materials Science and Engineering

Professorship Metallurgy **Code of professorship** MTG

Thesis supervisor Ari Jokilaakso

Thesis advisor(s) / Thesis examiner(s) Pekka Taskinen, Dmitry Sukhomlinov

Date Kirjoita tekstiä napsauttamalla tätä. **Number of pages** 99+34 **Language** English

Abstract

The aim of this experimental work is to investigate the distribution coefficients ($L_X^{Cu/Wm}$) of cobalt, nickel, silver, gold and palladium in copper converting conditions between the metal phase and the white metal phase. The first part of this work is a literature review, the later part describes the experimental work and presents the data.

The experimental work investigates the distribution coefficients of the elements as functions of temperature ranging from 1250 C° to 1350 °C and sulphur dioxide partial pressures ranging from 0.01 to 1 atm in SO_2 – Ar mixtures. The experimental work consisted of the equilibration of the samples, quenching into ice cold water, grinding and polishing of the cross sections and the analysis of concentrations in both phases by EPMA. The EPMA work was carried out at the Geological Survey of Finland (GTK).

It was found that there are dependencies between the $L_X^{Cu/Wm}$ and P_{SO_2} and temperature for silver, gold, palladium and nickel. Silver was found to be more concentrated to the metal phase at 1250 °C and 1 atm $P(SO_2)$ with a value for $L_{Ag}^{Cu/Wm}$ decreases as a function of increasing temperature and decreasing $P(SO_2)$. $L_{Ni}^{Cu/Wm}$ is found to increase with increasing temperature and $P(SO_2)$. For cobalt it was found that there was a dependency between $L_X^{Cu/Wm}$ and P_{SO_2}. $L_{Co}^{Cu/Wm}$ increases as $P(SO_2)$ decreases, $L_{Co}^{Cu/Wm}$ falls from 0.85 to 0.15. The concentrations of silver in certain experiments, gold and palladium in the white metal phase fell below the detection limit of the EPMA. Both gold and palladium were found to be more concentrated to the metal phase.

Keywords Cobalt, Nickel, Silver, Gold, Palladium, Distribution coefficient, Copper converting.

List of Symbols and Abbreviations

atm = atmospheres

wt. % = weight percentage

v = valence

X = solute element

T = Temperature

t = Time

l = Litres

Me = Metal Phase, Ma = White metal phase

F = degrees of freedom

C = number of components

P = number of phases

N = Number of species

R = Number of independent reaction equilibria

S = Stoichiometric constraints of the system

$t_{\text{Special constraints}}$ = the special constraints in the system

P_{SO_2} = Partial pressure of sulphur dioxide gas

P_{O_2} = Partial pressure of oxygen gas

P_{S_2} = Partial pressure of sulphur gas

EPMA = Electron microprobe analyser

SEM = Scanning electron microscope

EDS = Energy Dispersive X-ray spectroscopy

BSD = Back scattered electrons

PPM = Parts per million

$L_x^{Cu/Wm}$ = Distribution coefficient of X between metal and white metal phases

a = Activity

γ = Activity coefficient

K = Reaction Constant

n = Number of moles, M = Molar Mass

1 Introduction

Valuable trace elements occur in many different copper bearing ores, and demand for these elements is only increasing in modern times. Understanding their thermodynamic behaviour will improve the recovery rate of these valuable trace elements from the copper material during converting operations.

The distribution coefficients of silver, gold, nickel, cobalt and palladium have been investigated by previous researchers: Asano and Ichio (1962), Asano (1965), Asano et al. (1971), Burylev (1974), Choi and Cho (1997), Eguchi et al. (1977), Kashima et al. (1978), (1980), Kho et al. (2006), Krivsky and Schuhmann (1957), Schlitt et al. (1973), Schlitt and Richards (1975), Schmiedl et al. (1977), Schuhmann (1950), Sinha et al. (1985), Yazawa (1974), (1980) and Zakeri et al. (1998). However, the effects of temperature and sulphur dioxide partial pressure have not been investigated for palladium and gold as a function of sulphur dioxide partial pressure.

This work investigates the effects of temperature and sulphur dioxide partial pressure on the distribution coefficients of cobalt, nickel, palladium, silver and gold between the immiscible liquids, metal blister copper and white metal phase, which simulate the nearly iron-free copper converting stage in the copper manufacturing process.

This work consists of a theoretical section, which is a review of literature results, an experimental section, where a description of the experimental method used is presented, and a results section, where the results of this work are presented and then compared to the results found from literature.

The experimental procedure consisted of equilibration, quenching and EPMA analysis. The metal phase consisted of pure copper with the solute elements and iron dissolved into it in order to simulate this stage of the copper converting process. Three different temperatures (1250 °C, 1300 °C and 1350 °C) and five different partial pressures of sulphur dioxide diluted with argon (0.01 atm, 0.05 atm, 0.1 atm, 0.5 atm and 1 atm) were investigated. Micrographs were made using SEM, and a phase analysis was made using EDS and EPMA.

2 Theoretical Section and Literature Review

2.1 Copper Converting Process

The converting of copper is a process where the molten matte phase is oxidised to form the so-called blister copper. The matte is a molten phase mainly comprising of Cu, Fe, and S. The trace elements are also dissolved into the matte. During the process, the converter blows air or a gas feed with higher partial pressures of O_2 to oxidise the Fe and the S from the matte phase to form a slag layer. The feed gas is blown through tuyeres into the converter. The oxidisation of this material first forms an Fe-deficient white metal, which is mostly molten Cu_2S with a low concentration of Fe. The slag is removed at this stage before further oxidation is carried out. After this, further oxidisation mostly removes the sulphur leaving behind a product known as blister copper that has low concentrations of S and O. (Schlesinger et al., 2011, pp. 127–153).

The overall converting process follows the general reaction, equation (1):

$$Cu, Fe, S_{(in\ the\ matte)} + O_{2\ (in\ gas)} + SiO_{2\ (In\ flux\ charge)} \rightarrow Cu_{(liquid)} + 2FeO \cdot SiO_{2\ (molten\ slag)} + SO_{2(\mathrm{gas})} \quad (1)$$

In the first stages of the copper converting process, the oxygen from the gas phase, which is charged into the reactor, reacts with the matte phase to form a slag on the surface of the matte phase. Iron and sulphur are oxidised in these reactions. The iron concentration is initially high but through reactions (2) and (3), the iron reacts with the O_2 and moves to the slag phase. (Schuhmann, 1950).

$$FeS + 1.5O_2 \rightarrow FeO + SO_2 \quad (2)$$

$$3FeS + 5O_2 \rightarrow Fe_3O_4 + 3SO_2 \quad (3)$$

The melting points of FeO and Fe_3O_4 are significantly higher than the reactor working temperature, 1377 °C and 1597 °C respectively. A silica-fluxing agent is added to reduce the slag melting temperature and to decrease its viscosity. White metal is the term used when the Fe in the matte has mostly been oxidised. The product that is left consists mainly of molten Cu_2S with minor impurities. The Fe content is roughly 1 %. (Schlesinger et al., 2011, pp. 127–153).

Copper matte is charged into the converter slowly, ladle by ladle, due to the physical practicalities of the process. The slag is then removed from the converter leaving only the white metal. (Schlesinger et al., 2011, pp. 127–153).

The next stage after reaction (2) and (3) is the oxidation of the white metal in order to form sulphur dioxide. Fortunately, copper does not oxidise in large amounts until there are very low concentrations of sulphur in the white metal. This means that the converting process produces a copper with very low levels of sulphur and oxygen, typically 0.001 to 0.03 % and 0.1 to 0.8 % respectively. (Schlesinger et al., 2011, pp. 127–153).

Reactions (4) and (5) are the most likely route for copper making. The oxygen available for these reactions comes from blowing oxygen on to the white. Reaction (6) is a direct route for copper making. (Schlesinger et al., 2011, pp. 127–153).

$$Cu_2S + 1.5O_2 \rightarrow Cu_2O + SO_2 \quad (4)$$

$$Cu_2S + 2Cu_2O \rightarrow 6Cu + SO_2 \quad (5)$$

$$Cu_2S + O_2 \rightarrow 2Cu + SO_2 \quad (6)$$

Reactions (2) and (3) occur when oxygen is blown into the converter during the removal of iron from the matte to form a slag phase. These reactions occur before the main oxidation of Cu_2S to Cu and SO_2. The slag forming stage is stopped when the metallic Cu appears in matte samples, which is typically 76 to 79 % Cu in matte. The end of the slag forming can also be seen in the Cu–S binary phase diagram roughly when the Cu concentration is moved to the Cu–CuS immiscible area in Figure 1. The converter flame also turns a green colour when there is Cu vapour in the converter flue gas. (Schlesinger et al., 2011, pp. 127–153).

The blowing removes S to SO_2 by oxidation, which then forms white metal from the matte. This occurs until there is roughly 19.6 wt. % of sulphur in the white metal depending on temperature. The proposed general reaction (7) is:

$$Cu_2S + vO_2 \rightarrow Cu_2S_{1-v} + vSO_2 \quad (7)$$

The v in reaction (7) signifies that not all sulphur is removed in it, which proves that this is not a stoichiometric equation. (Schlesinger et al., 2011, pp. 127–153).

Continued blowing of the white metal with the oxygen/air mixture causes a second immiscible liquid formed of molten copper to appear. This happens when more sulphur oxidises from the system. Oxidising sulphur from the system moves the system into the immiscible zone on the Cu–S binary phase diagram seen in Figure 1. When a line is traced from right to left at 1200 °C, the two-phase region begins at 19.6 wt. % sulphur in the system. This can be seen in Figure 1. The liquid copper is denser than the white metal so it physically sinks to the bottom of the converter vessel. (Chakrabarti, 1983).

Once the system has such a reduced sulphur content, typically around 1 % sulphur, the system is to the left side of the immiscible region, Figure 1. The only phase that exists is the liquid blister copper phase. Continued blowing of this last amount of S should be taken with great care, because if the system is over-oxidises, the copper would oxidise to Cu_2O in significant quantity. According to reaction (8), the oxidation of Cu occurs when there is no more S to oxidise, and before the system is mostly devoid of S, the Cu_2O can react back to liquid copper. (Schlesinger et al., 2011, pp. 127–153).

$$Cu + O_2 \rightarrow Cu_2O \tag{8}$$

After this the molten copper is poured from the converter into a ladle where it is then sent to fire refining to further decrease the remaining O_2 and S_2. (Schlesinger et al., 2011, pp. 127–153).

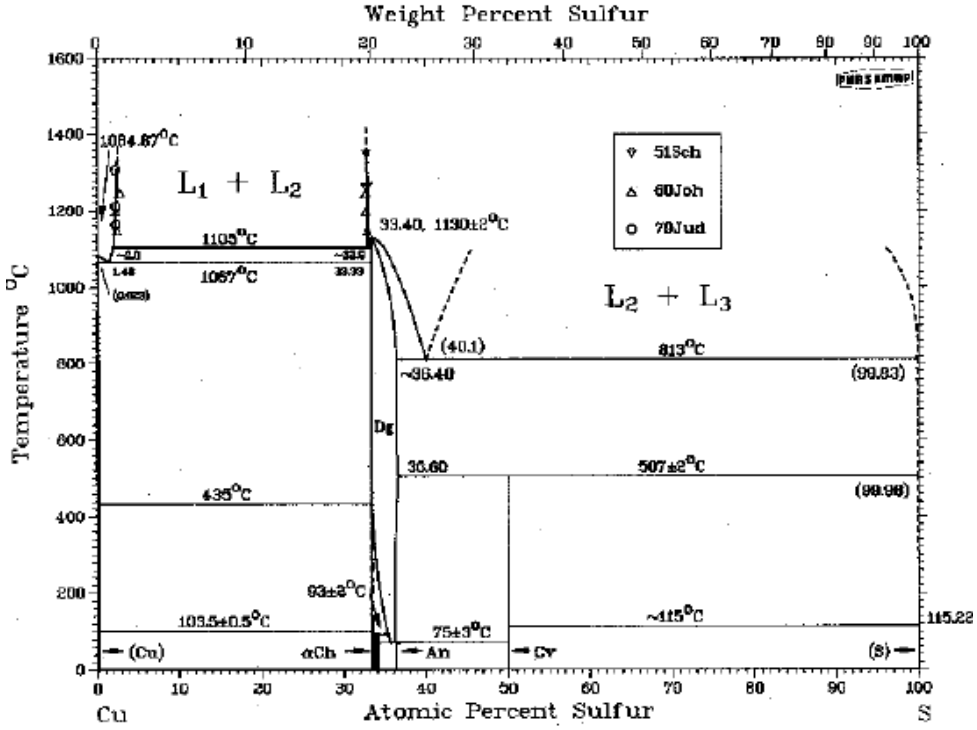

Figure 1 Cu–S binary phase diagram. (Chakrabarti, 1983).

Figure 2 shows a closer view of the immiscible region, and Figure 3 shows experimental data gathered for the miscibility gap. It can be seen from both Figure 2 and Figure 3 that increased temperatures increase the sulphur solubility in copper. (Schlesinger et al., 2011, pp. 127–153). (Chakrabarti, 1983).

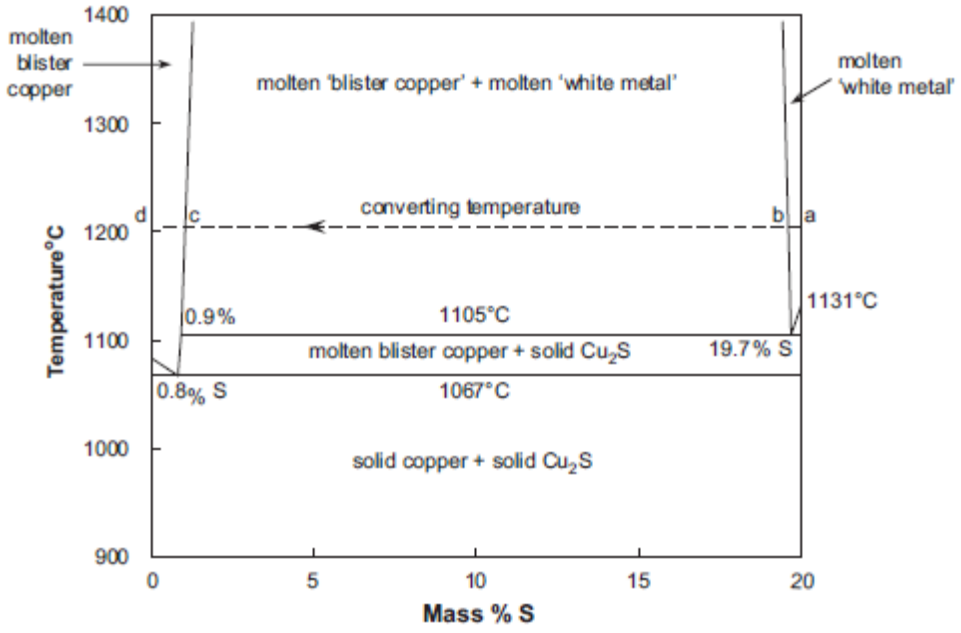

Figure 2 Immiscible region of Cu–S binary phase diagram. (Schlesinger et al., 2011, pp. 127–153).

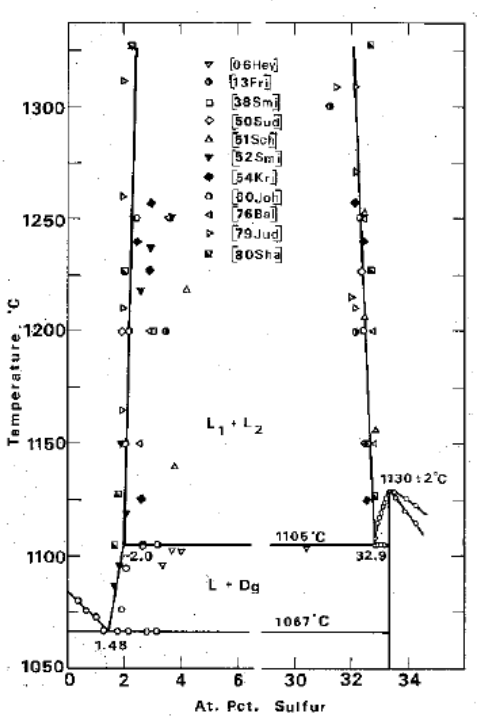

Figure 3 Collected data of the immiscible region. (Chakrabarti, 1983).

2.2 Industrial Converting Operations

Ninety percent of the world's copper matte is converted with Peirce-Smith converters . The Peirce-Smith converter is a rotatable unit as can be seen from Figure 4, which depicts the

front and side views of the unit. The rotation allows the unit to be charged, ladled and operated on with a fume hood. Oxygen enriched air is blown into the melt via 40–60 tuyeres mounted through the refractory lining, typically 0.5 m of magnesite-chrome brick. (Schlesinger et al., 2011, pp. 127–153)

The typical Peirce-Smith converter is 12 m long with a 4.5 m diameter. With these dimensions, 600 to 1000 tonnes of matte can be converted per day. Depending on the individual specifications, a converter is charged with 200 to 350 tonnes of matte per cycle. Each converter can produce 140 to 310 tonnes of blister copper per batch. The melt is blown with 650 to 750 Nm^3 per minute for the slag blowing stage, and 600 to 800 Nm^3 per minute during the copper blow. (Schlesinger et al., 2011, pp. 127–153).

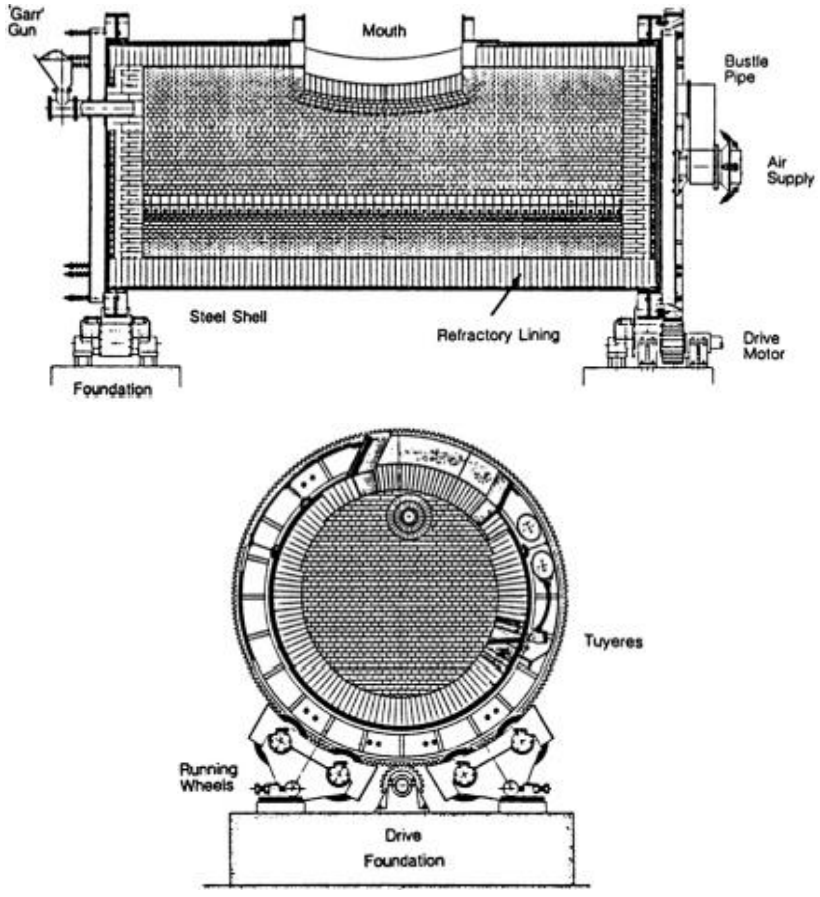

Figure 4 Front and side views of the Pierce-Smith converter. (Schlesinger et al., 2011, pp. 127–153).

A gas collection hood is placed over the mouth of the Pierce-Smith converter during the operation. The Pierce-Smith converter is not a perfect unit as it leaks gas during the charging of the feed materials and the pouring of the blister copper. The process of flue-gas collection,

which takes place during the operation of the converter and especially during the changing and pouring, can also take in atmospheric gases from the surroundings, thus diluting the SO_2 stream for sulphuric acid production. The Peirce-Smith converter is also a batch process, which limits the production capacity. (Schlesinger et al., 2011, pp. 127–153).

There are other converter units in the world that attempt to rectify the shortcomings of the Pierce-Smiths. These include the Hoboken converter, which has an improved gas collection system, siphoning flue at one end of the converter and a gooseneck design, preventing liquids from leaving the furnace. Flash converting requires solidified and crushed particulate matte feed. Flash converting utilises a small Outotec flash furnace. One of the benefits of this is that a stockpile of crushed matte can be built during the maintenance times of the converting furnace. In addition, no matte layer is formed in the flash converting furnace, but the matte layer is prevented by adjusting the O_2 input ratio to matte feed which slightly favours the formation of Cu_2O over Cu_2S. This results in a blister copper with only a 0.2 % S content. (Schlesinger et al., 2011, pp. 127–153).

The Noranda converter process is a continuous process, so there are three molten phases of copper, matte and slag always present. The three phases are tapped intermittently. This converter has submerged tuyeres which blow O_2 into the matte phase. The process is controlled by O_2 blowing, temperature and by the amount of the blister copper tapped from the furnace. (Schlesinger et al., 2011, pp. 127–153).

In addition, there is the top-blown Mitsubishi converter which uses O_2 rich air blown onto the surface of the matte via vertical lances. There are also three continuous converting processes being developed (as of 2011), which are Codelco-Chile, Ausmelt and Isaconvert. (Schlesinger et al., 2011, pp. 127–153).

2.3 The Sulphur Oxygen Potential Diagram

The diagram in Figure 5 has been produced at 1300 °C for the copper smelting process. The diagonal lines represent the overall $P(SO_2)$. The axis refers to $P(O_2)$ and $P(S_2)$ levels. The different regions depict what phase relations and chemical compositions are present. In the first stage of the copper making process, which is depicted in the diagram from points A to B as oxidation, the Cu increases from 50 to 70 % which is the smelting stage. Following further from line B to C, the copper grade increases, and when it increases to roughly 80 %,

the immiscible region occurs. This is the slag-blow stage of copper converting. Point C is the equilibrium point between Cu and Cu_2S. (Yazawa, 1974).

The copper concentration throughout the pyrometallurgical copper production is also represented in Figure 5. The figure is split into several predominance regions: FeS, Fe, matte, slag Fe_3O_4 and Cu_2O. The partial pressures of the gas species is also represented in Figure 5. $P(SO_2)$ increases towards top right corner on the diagram. $P(O_2)$ and $P(S_2)$ can be read along the axis, reading from the $P(SO_2)$ lines. The converter process follows the line on Figure 5 between B and C. The concentration of Cu increases to 70 % at point B. The line C C' shows the equilibrium between Cu and Cu_2S. Increasing the $P(O_2)$ above 0.0001 atm oxidises the Cu to Cu_2O. This means that increasing O_2 above 0.0001 atm should be avoided. (Yazawa, 1974)

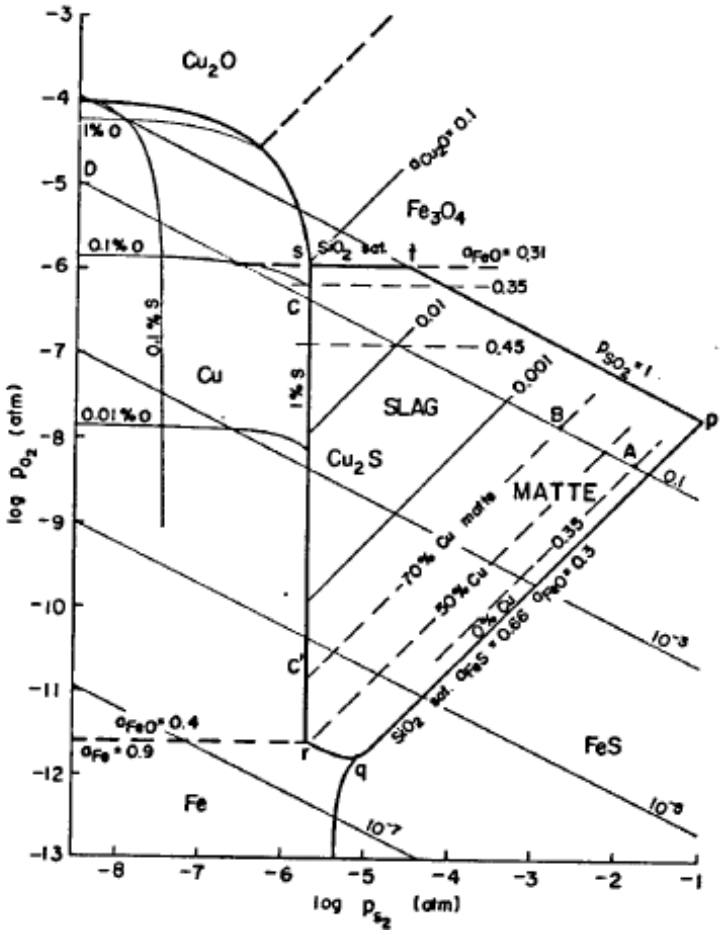

Figure 5 Yazawa diagram at 1300 °C. (Yazawa, 1974, 1980).

Figure 6 shows the estimated partial pressure of the gases SO_2, O_2 and S_2 through the entire converting from low grade matte to blister copper given by (Schuhmann, 1950). The entire

copper smelting and refining process involves a sequence of process steps that revolve around the decreasing of the sulphur activity and increasing the activity of oxygen. (Schuhmann, 1950).

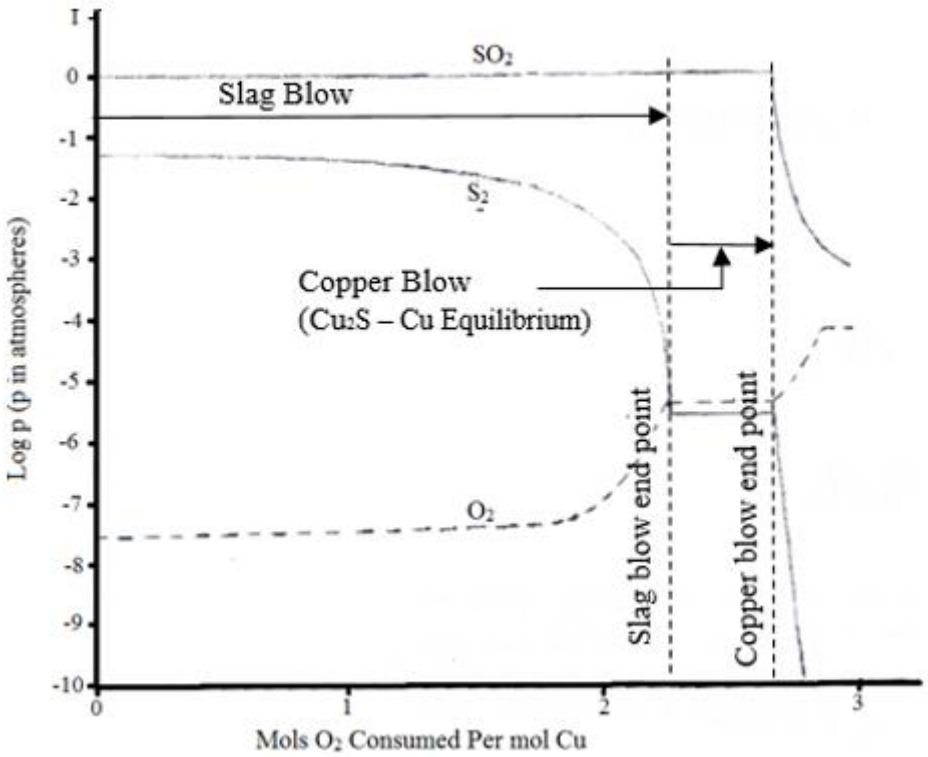

Figure 6 Equilibrium partial pressures of SO_2, O_2 and S_2 during copper converting. (Schuhmann, 1950).

The partial pressures of each of the gases are given in Figure 6 for the entire converting operation up to the point blister copper is produced. The sulphur dioxide pressure does not change, but remains SO_2 = 1 atm. The oxygen pressure increases, O_2 5.2 x10^{-8} atm to 3.4 x 10^{-6} atm, and the S_2 decreases, 10^{-2} atm, to 2.7 x 10^{-6} atm. (Schuhmann, 1950). The partial pressures presented here are the estimated equilibrium partial pressures of the prevailing gases that occur if at any point during the converting process the blowing is stopped, and the system is allowed to reach equilibrium. Continued oxidation of the copper after the copper blow end point means that there is no Cu_2S left to oxidise, so the copper would become over oxidised and form Cu_2O.

3 Thermodynamics

3.1 Distribution of Minor Elements

At equilibrium, solute elements in the systems will be distributed between both of the liquid phases at some concentration. The solute elements will also be distributed between the two liquid phases at varying amounts depending on the activity of the particular element.

Nagamori and Mackey (1978), made models for the distribution of minor elements in their paper. They analysed several different elements: Au, Ag, Bi, Sb, As, Pb, Zn, Ni, Co, Sn, Se and Te. The copper/matte distributions for these elements are simplified into three groups in Table 1.

Table 1 Distribution coefficients of different elements as a function of $P(SO_2)$ and temperature. (Nagamori and Mackey, 1978).

Model	**Elements**	**T**	**$P(O_2)$**	**$P(SO_2)$**
A	Au, Ag, Bi, Sb, As	Dependant	Independent	Independent
B	Pb, Zn, Ni, Co, Sn	Dependant	Dependant	Dependant
C	Se, Te	Dependant	Dependant	Independent

The models A, B and C in Table 1 are for estimating the distribution coefficients between copper and matte, copper and slag as well as matte and slag.

The presence of the slag phase should not affect the distribution coefficient of a solute element between the metal and matte phases. This means that the distribution coefficient of the solute element between metal and matte can occur independently of the distribution of the solute element between slag and matte, and slag and metal. (Coursol et al., 2012). Kashima et al. (1978), stat that "the distribution ratio between metal and matte does not seem to be affected by the coexisting slag components".

3.2 Distribution of Minor Elements between Metal and White Metal Phases

The distribution ratio for a minor element between metal and matte phases in the general form is as follows:

$$L_X^{Me/Wm} = \frac{(wt\ pct\ X)\ concnetration\ of\ X\ in\ the\ metal}{[wt\ pct\ X] concentration\ of\ X\ in\ the\ matte} = \frac{K''\gamma_{XS}}{\gamma_X} \quad (9)$$

Here X is the element under consideration, Me is the metal phase and Wm is the white metal phase. The curved brackets also indicate that this is referring to the metal phase, whereas the square brackets refer to the matte phase. K'' is a reaction constant and γ_{XS} and γ_X are the activity coefficients for the solute element and its sulphide form. Values of this distribution ratio tell where the particular elements will tend towards after equilibration has occurred. Values over one mean a higher percentage of the element will distribute to the metal phase, and high numbers such as 100 or more mean that there is such a large percentage of the solute element in the metal phase that there will be a very low concentration of it in the matte phase. A distribution coefficient with a value of one signifies that the element distributes evenly between both phases in terms of concentration. Values below one mean that the element will tend to the matte phase. (Yazawa, 1980).

It is stated in the paper by Asano (1965), that the weight distribution coefficient is a parameter that indicates the interaction energy between the solvent atoms and the solute atoms. If the value for the distribution ratio is smaller or larger than one, then there must be a difference in the interaction energies of the different phases. This however assumes the solute atoms are randomly distributed throughout each phase, but it could happen that these elements, which distribute randomly in one phase might then also form agglomerates in the other phase. It is therefore easier to interpret the distribution ratio and to avoid agglomerates if the atoms are present in both phases in dilute concentrations.

When the copper phase and the molten copper sulphide phase are in equilibrium, the activity of each component in each phase is thermodynamically equal. The distribution ratio of the minor elements will coincide with the reciprocal of the ratio of their activity coefficients. (Asano, 1965).

Minor elements dissolve in the metal phase in their atomic form, and to move to the matte phase the element must become ionic, and in this case, the minor element becomes sulphidic, as can be seen in equation (10) (Yazawa, 1974), (Kho, 2006), (Sinha et al., 1985).

$$vX + Cu_2S = vXS_{1/v} + Cu \quad (10)$$

The general form of the basic metal-to-metal sulphide reaction has an equilibrium constant, which can be expressed in equation (11).

$$K_1 = \frac{a_{XS_2}}{a_X P_{S_2}^{v/2}} \tag{11}$$

The distribution ratio can be expressed in equation (12), as a ratio of the activity coefficients of the solute element in the metal and the activity coefficient of the solute element as a sulphide in the white metal phase. Where γ is the activity coefficient, n_T is the total moles in each phase and K1 is the equilibrium constant in equation (11). (Kho, 2006).

$$L_X^{Metal/Matte} = \frac{(wt.\%\ Metal)}{[wt.\%\ Matte]} = \frac{K_1\ [\gamma_X](n_T)P_{S_2}^{\frac{v}{2}}}{(\gamma_{XS_2})[n_T]} \tag{12}$$

Also proposed by Kashima et al. (1978), is the overall reaction (10) that the decomposition of S from Cu_2S in the white metal phase at copper saturation is available to form sulphides with the minor alloying elements in the system, resulting in the following equilibrium reaction (13). This assumes that the solute elements exist as a singular atom in its sulphidic form, rather than multiple solute element atoms bonded together also with sulphur.

$$X + vCu_2S = XS_v + 2vCu \tag{13}$$

The reaction constant of reaction (13) is given as an approximate by the ratio of the activities of the solute element in the pure atomic form and its sulphidic form:

$$K_2 = \left(\frac{a_{Cu}^2}{a_{Cu_2S}}\right)^v \cdot \left(\frac{a_{XS_v}}{a_X}\right) \approx \frac{a_{XS_v}}{a_X} \tag{14}$$

Kashima et al. (1978), also suggest that if the low concentrations of Fe and O are neglected in the white metal phase, then the activity of the solute element in its sulphidic form can be represented with equation (15):

$$a_{XS_v} = (\gamma_{XS_v}) \cdot N_{XS_v} \approx 1.59(\gamma_{XS_v}) \cdot \frac{[X\%]}{M_x} \tag{15}$$

N_{XSv} is the molar fraction of XS_v, M_X, M_{Xs} is the molar mass of X and XS, X% is concentration of X in solution and γ_{XSv} is the activity coefficient of X in its sulphide form.

The activity of the solute element in its metallic form in the metal phase is approximately according to equation (16), but it is only valid at low concentrations of the solute element in the metal phase.

$$a_X \approx 0.64(\gamma_X) \cdot \frac{(wt.\%\ Metal)}{M_x} \tag{16}$$

Wt. % metal is the concentration of the solute element in the metal phase. γ_X is the activity coefficient of X in its metallic form in copper. In this equation γ_X is assumed to be kept constant. (Kashima et al., 1978).

Combining equations (14) (15), and (16) can then relate the distribution coefficient to the ratio of the activities coefficients of the solute element in its metallic form and its sulphidic form.

$$L_X^{Me/W} = \frac{(X\%)}{[X\%]} = \frac{2.5}{K_2} \cdot \frac{[\gamma_{XS_v}]}{(\gamma_X)} \quad (17)$$

K_2 is the equilibrium constant described in equation (14).

Kashima et al. (1978) state that the existence of Fe and O at low concentrations (slag formers) does not affect the distribution ratio between the metal and white metal phases.

3.3 Distribution of Silver between Copper and Matte

Silver is a common element to be found in copper ores (Kucha and Cichowska, 2001). Silver is therefore present during the smelting and converting of copper. Silver is a valuable by-product of the copper smelting industry-

The silver distribution in the matte and metal phases is the most researched of all the elements that are of interest in the current study. This has been studied by Kashima et al. (1978), Sinha et al. (1985), Nagamori et al. (1978), Zakeri et al. (1998), Schlitt and Richards (1975), Asano et al. (1971), Asano (1965) and Taylor (1983).

Taylor (1983) investigated the distribution coefficient of silver between metal and white metal phases at 1200 °C. The experiments consisted of 3.5 g of Cu, which contained 1 wt. % Ag and 3.5 g of Cu_2S. Alumina crucibles containing the chemical reagents were sealed into an evacuated silica ampoule. The samples were equilibrated at the working temperature from 24 to 96 hours. The samples were quenched by quickly lifting the ampoule from the furnace to a water bath. The metal and white metal phases were separated into 2–4 samples of 0.5 g each of each phase and then dissolved into aqua regia and analysed by atomic absorption spectrophotometry. Corrections were made for the interference that the dissolved Cu had on the results. The distribution ratio was found to be:

$$L_{Ag}^{metal/matte} = 2.93 \; for \; 1200 \; °C \quad (18)$$

3.3.1 Distribution Ratio of Silver, Concentration and Infinite Dilution

Figure 7 shows the distribution ratio of silver in metal phase and white metal phase at 1127 °C and 1227 °C (Sinha et al., 1985).

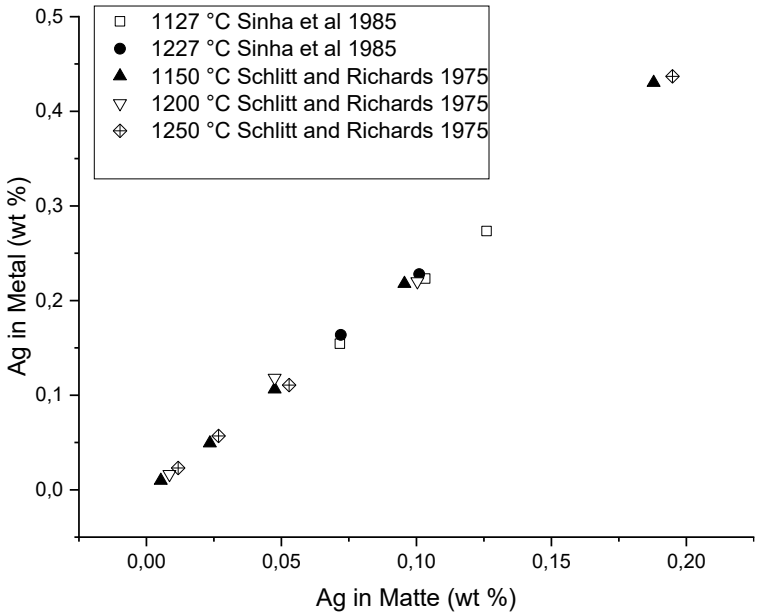

Figure 7 Distribution of silver as a function of silver concentration. (Schlitt, 1975), (Sinha et al., 1985).

The authors deduced the distribution coefficients (19) and (20) at infinite dilution.

$$L_{Ag}^{metal/matte} = 2.13\ for\ 1127\ °C \tag{19}$$

$$L_{Ag}^{metal/matte} = 2.21\ for\ 1227\ °C \tag{20}$$

Schlitt and Richards (1975), investigated the distribution of silver in the copper and white metal system. Silver in the system varied from 0.01 to 0.4 weight percentage and temperatures between 1150 and 1250 °C as well as the experimental conditions described above. Figure 8 shows the distribution ratio of silver between metal and matte phases as reported by Schlitt and Richards (1975) and reveals the distribution ratio (21) as a function of silver weight concentration.

$$L_{Ag}^{metal/matte} = 2.17\ for\ 1150\ to\ 1250\ °C \tag{21}$$

In the work by Asano et al. (1971), Asano (1965) silver distribution coefficient between liquid copper and cuprous sulphide was investigated with up to 7% of silver in the copper

phase. The data collected by Asano et al. (1971) is shown in Figure 8. The data from Figure 7 is also shown in this graph to present the agreement of the data collected.

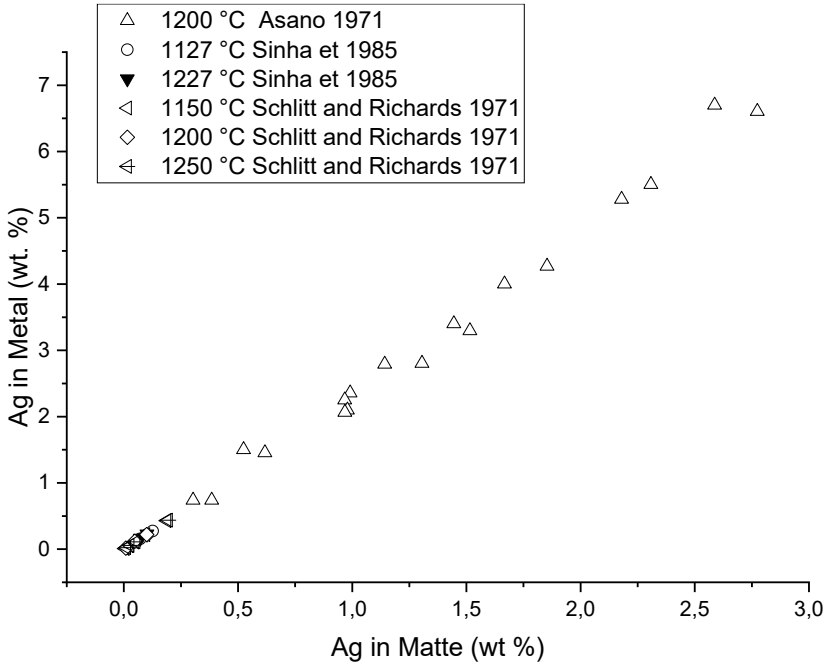

Figure 8 The distribution of silver between metal and matte phase. (Schlitt, 1975), (Sinha et al., 1985), (Asano et al., 1971).

$$L_{Ag}^{metal/matte} = 2.37\ at\ 1150\ °C \tag{22}$$

In Figure 7 and Figure 8 it can be seen that Asano et al. (1971), Schlitt and Richards (1975) and Sinha et al. (1985) also vary along with temperature. The data presented by Sinha et al. (1985) shows the greatest difference of the distribution coefficient as a result of temperature variation.

3.3.2 The Effect of Iron Concentration on the Distribution Ratio of silver

Sinha et al. (1985) also conducted experiments as a function of matte grade and found that $L_{Ag}^{metal/matte}$ increases as a function of iron content in the matte phase. In their experiments, the Fe content ranges from 0 to 12 wt % in the matte phase with temperatures from 1400 (1127 °C) to 1500 K (1227 °C). Figure 9 shows the combination effect with temperature. From this data it can be seen that the increased temperature decreases the distribution coefficient.

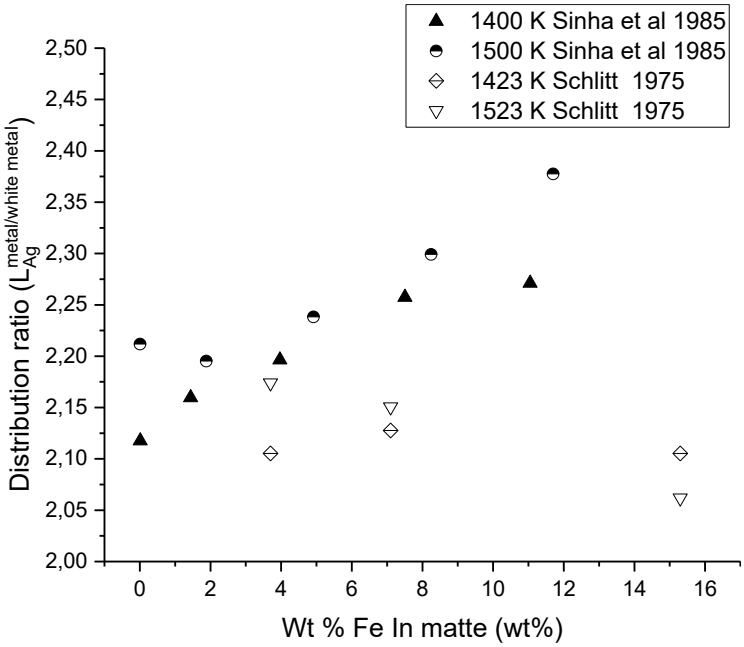

Figure 9 The distribution ratio of silver against iron content in the matte phase. (Sinha 1985), (Schlitt, 1975).

Schlitt and Richards (1975), investigated the distribution of silver in the copper-iron-sulphur system. The experiments with the copper-iron-sulphur system were conducted at 1150, 1200 and 1250 °C, with two silver concentrations (0.2 and 0.4 mass pct.) and three different calculated iron-sulphide concentrations (3.7, 7.1 and 15.3) in the matte phase. The distribution of silver was found to be 2.12 across all experiments with a standard deviation of ± 0.02. These results show that similar to silver content, iron content has practically no effect on the distribution ratio of silver. The data given is presented in Figure 8, which depicts $L_{Ag}^{metal/matte}$ vs iron concentration. It can be observed that the silver distribution coefficient is a function of the iron content. The authors state that the temperature at this range has no effect on the distribution coefficient. The calculated standard deviations can account for the observed function.

Schlitt and Richards (1975), also conducted experiments investigating the distribution ratio of silver between the metal and matte phases. Their experiments were carried out at 1150, 1200 and 1250 °C and under partial pressures of oxygen of 10^{-25} atm and 10^{-8} atm with sulphur dioxide partial pressure of 0.2. Nitrogen was used as the inert carrier gas. A fraction of this gas was bubbled through the molten/liquid components to mix the two liquids. This

also had the effect of increasing the interfacial area between the two liquids as well the gas phase. After this, the system was allowed to separate before the sampling was taken. Each phase was sampled separately at the working temperature. The purpose of this was to avoid the problems of separation of the material during cooling or solidification. Using the contemporary methods, the solidification of the samples took 10–12 seconds, which was easily enough time for the element redistribution of material from one phase to another Schlitt et al. (1973). The experiments were carried out with the use of a synthetically prepared matte phase and refined copper to simulate the metal and matte immiscible phases. The total mass of each experiment was 1 gram, which was small enough to be easily assayed in total for the measured element at the working temperature. Figure 9 shows the distribution ratio as reported by Schlitt and Richards (1975) at different temperatures.

Also Kashima et al. (1978), conducted experiments to investigate the distribution coefficient of silver between the copper phase and the matte phase. They conducted the equilibration at 1300 °C for 45 h under a SO_2-Ar gas stream of 150 ml/minute. The reported distribution coefficient (23) for low silver concentration and therefore at infinite dilution is:

$$L_{Ag}^{me/ma} = 2.4 \; for \; 1300 \; °C \tag{23}$$

3.3.3 The Effect of Sulphur Dioxide Partial pressure on the Distribution Ratio of Silver

In the paper by Kashima et al. (1978), the silver distribution between copper, white metal and slag phases were investigated with varying sulphur dioxide partial pressures. The experiments were conducted at 1300 °C in a SO_2-Ar mixture gas flow of 150 ml/minute. The concentration was analysed with a fire assay and gravimetric method, and the experiments were equilibrated for 45 h. The copper activity was kept constant at 0.85. The effects of the small amount of Fe, O and S were neglected. The distribution coefficient was plotted against copper content in the metal phase. In Figure 10 the distribution ratio is plotted against SO_2 pressure. The distribution ratio of silver between the copper and matte phases was found to increase slowly as a function of the SO_2 partial pressure.

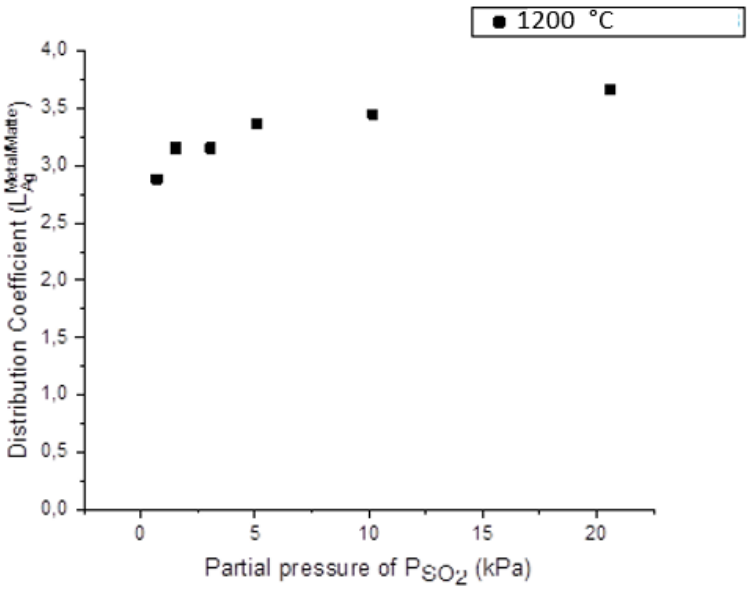

Figure 10 Ag distribution coefficient plotted against SO_2 pressure. (Kashima et al., 1978).

3.4 Distribution of Nickel in Copper and Matte

Nagamori and Mackey (1978) modelled the distribution of nickel for the continuous converting Noranda process and investigated the distribution coefficient of nickel as a function of the SO_2 partial pressure, temperature as well as the activity of magnetite in the slag.

Asano (1965) studied the basic behaviours of the distribution equilibrium of nickel between blister copper and the white metal phase. The experiments were carried out at 1200 °C. The solute elements were added at appropriate amounts to electrolytic copper and copper sulphide. The total weight of the material was 5 to 8 g. The mixture was vacuum-sealed in a quartz tube, heated for two hours and then quenched. Figure 11 shows Asano's experimental results, correlation of Ni-concentrations in the matte (white metal) and the copper alloy. The nickel distribution coefficient was reported to be 3.059.

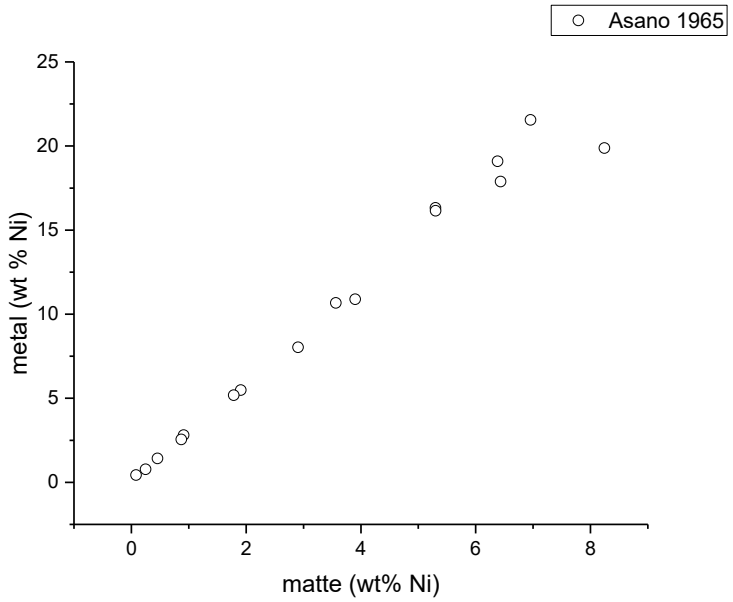

Figure 11 Concentration of nickel in metal phase vs matte phase. (Asano, 1965).

What is interesting about the smaller graph within the first graph is that it shows a correlation to the effect of temperature on the distribution ratio of nickel. It shows that between 1150 °C and 1250 °C the distribution ratio slightly decreases meaning that at the higher temperature after equilibration there will be more nickel concentrated to the matte phase than there would be at the lower temperature. However, it is concluded that the temperature dependence of the distribution coefficient is extremely small.

Asano and Ichio (1962) investigated the distribution of nickel in the copper-nickel-sulphur system as a function of nickel content. They investigated at three different temperatures 1150 °C, 1200 °C and 1250 °C and with varying nickel content of the system, from 1 % to 21 %. Figure 12 shows that with increasing nickel wt % as part of the entire system, the distribution ratio slightly decreases. However, the authors state that nickel content does not affect the distribution ratio until the system exceeds 15 to 16 % Ni. What is relevant is that the rough models for each data set predict the distribution ratio at infinite dilution. The distribution ratio ranges from 3.42 to 2.82. It also predicts that with increasing temperature the distribution coefficient value decreases.

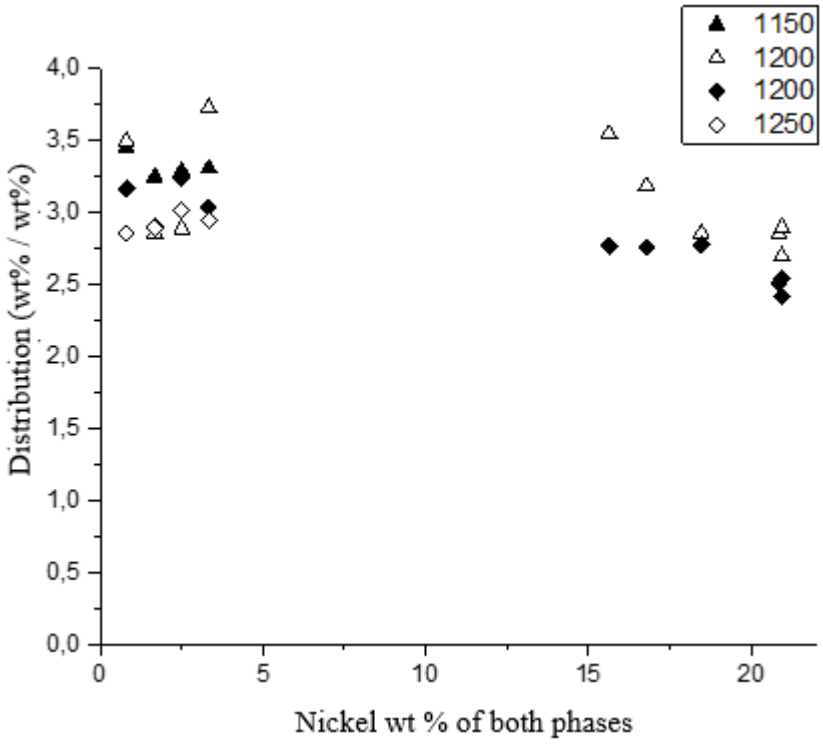

Figure 12 Calculated distribution coefficient of nickel. (Asano, 1962).

3.4.1 The Effect of Temperature on the Distribution Coefficient of Nickel between Metal and Matte Phase

Nagamori and Mackey (1978), modelled the distribution coefficient of nickel between copper and matte and reported the distribution ratio to be 3.07 at 1200 °C and decrease to 2.90 at 1250 °C.

Asano and Ichio (1962), investigated the distribution of nickel in the copper-nickel-sulphur system at three different temperatures: 1150 °C, 1200 °C and 1250 °C. In this study, the authors used 99.99 % pure electroplated copper and synthesised Cu_2S with a sulphur content of 20.07 % and a purity of 99.83 %. The nickel used was 99.98 % pure in synthesising the Ni_3S_2. The Ni_3S_2 contains 26.83 % of S. Each sample used weighed between 5 and 6 g. The samples were placed into a quartz tube under a vacuum of 0.054 Pa. The samples were kept at the measured temperature within a tolerance of ± 5 °C for two hours. Asano and Ichio (1962), determined experimentally that equilibrium was reached in 1 h, but an experiment time of two hours was used to make sure this equilibrium had been truly reached. Once the samples were taken out of the furnace, they were air-cooled. It is stated that the solidification of the sample occurred 10 to 12 seconds after it was removed from the furnace. Therefore,

the composition after the cooling is considered an indication of the distribution at liquid temperatures.

Asano and Ichio (1962), reported the distribution coefficient to decrease as a function of temperature: 3.28 at 1150 °C, 3.07 at 1200 °C and 2.93 at 1250 °C. They also give a model to predict the distribution coefficient with respect to temperature, as depicted in equations (24) and (25):

$$L_{Ni} = 7.296 - 0.0035\,T\ (1150 - 1250\ °C) \quad (24)$$

$$Log\ L_{Ni} = 1066/T - 0.2344\,T\ (1150 - 1250\ °C) \quad (25)$$

The models seem to predict the experimental results well. The authors state that because at lower concentrations of Ni the distribution ratio shows a constant behaviour depending on temperature. (Asano and Ichio, 1962).

3.4.2 The Effect of $P(SO_2)$ on the Distribution Coefficient of Nickel between Metal and Matte Phase

Nagamori and Mackey (1978) investigated the effect of partial pressure of sulphur dioxide on the distribution of nickel between metal and matte phases. The change in SO_2 partial pressure is reported to have an effect on the distribution ratio between the copper and slag phases but not the distribution between copper and matte.

Kashima et al. (1978) investigated the distribution coefficient of nickel. At 1200 °C the distribution coefficient of nickel increases slightly as $P(SO_2)$ increases from 0.007 atm to 0.1 atm. This can be seen in Figure 13. The values for the distribution coefficient as discovered by Kashima et al. (1978) range from 2.92 to 3.25 under the varying SO_2 pressure.

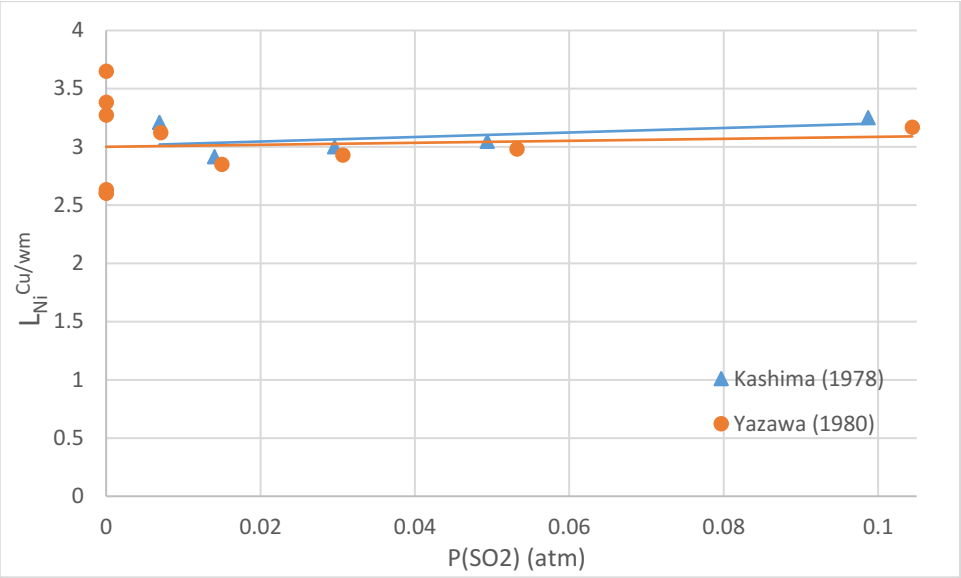

Figure 13 Nickel distribution ratio vs P(SO_2). (Kashima et al., 1978), (Yazawa, 1980).

Yazawa (1980) investigated the distribution of nickel between metal and matte against P(SO_2) between 0.1 atm and 10^{-6} atm. According to him, the distribution coefficient is independent of the partial pressure of O_2 and therefore both SO_2 and S_2. From the experimental results presented in Figure 13, the distribution ratio plotted against the P(O_2) shows possibly that as P(SO_2) increases, so does $L_{Ni}^{Cu/Wm}$. This is therefore in agreement with what was also found by (Kashima et al., 1978). In Figure 13 the average distribution coefficient of nickel is $L_{Ni}^{metal/matte} = 3.01\ for\ 1300\ °C$.

3.4.3 The Effect of Oxygen Blowing Volume on the Distribution Coefficient of Nickel between Metal and Matte Phase

Schmiedl et al. (1977) studied the distribution of nickel between copper and matte phases. The distribution ratio is reportedly ranged between 2.86 and 3.02. In their work, they reported the nickel concentration between the copper, matte and slag phases as a function of air blown in the system at 1250 °C. The experiment started with 150 g of the matte phase placed into a crucible, and air flow was introduced at a flow rate of 1 l / min. In Figure 14, it can be seen that after the initial phase the nickel content in the matte phase rises slowly. The Ni content in the blister copper phase remains high until the beginning of the first stage but then decreases at around 140 l of air blown. This corresponds with the formation of the white metal from the matte phase. The formation of the metal phase begins after 160 l of air blown. The authors go on to explain this phenomenon by reasoning that the decrease of Ni in the metal phase as well as the subsequent increase in the slag phase happened due to the

decrease in activity of ferrous sulphide, which makes the oxidation of nickel possible and therefore increases the amount of nickel in the slag phase. (Schmiedl et al., 1977)

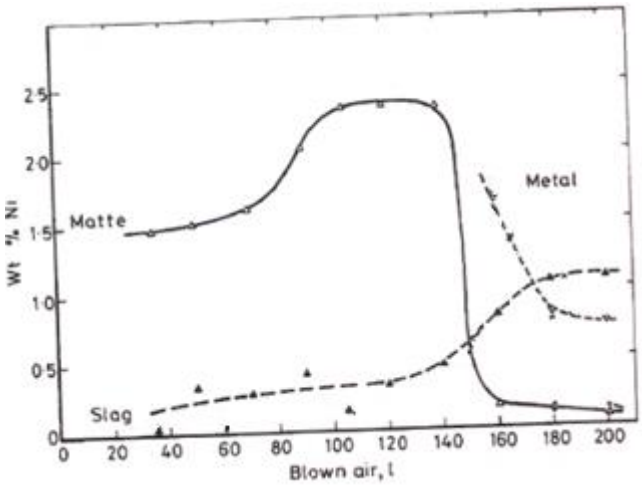

Figure 14 Ni concentration in matte, slag and metal phase in the converter process simulation as a function of air blown. (Schmiedel et al., 1977).

Figure 15 shows the distribution coefficients for the various phase relationships as a function of amount of air blown into the system. This work was designed to simulate the working conditions in a converter with laboratory scale equipment, so the equilibrium conditions change as air is blown into the system.

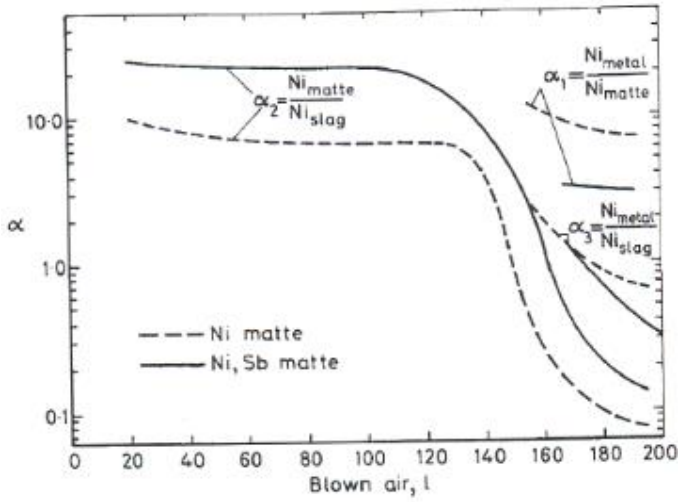

Figure 15 Distribution Coefficients as a function of air blown. (Schmiedel., 1977).

It can be concluded from the literature studies presented in this chapter that the distribution coefficients from each of the studies are in good agreement with each other. This comparison is presented in Table 2.

Table 2 $L_{Ni}^{Cu/wm}$ reported in previous studies.

Summary		
Authors	**Distribution coefficient**	**Conditions**
Nagamori and Mackey	3.07, 2.90	1200, 1250 °C, 0.161 – 0.232 $P(SO_2)$
Schmiedl, Repčák and Havlík	2.86 – 3.02	1250 °C
Kashima, Eguchi and Yazawa	2.92 – 3.25	1300 °C, 0.7 – 20 kPa $P(SO_2)$
Yazawa	3.01	
N. Asano	3.059	1200 °C, Vacuum
N. Asano and T. Ichio	3.42 – 2.82	1150 – 1250 °C

3.5 Distribution of Cobalt between Copper and Matte

Similar to the other elements being studied here, cobalt is more commonly studied for its behaviour between slag and matte or slag and metal (Choi and Cho, 1997, Kho et al., 2006). Cobalt is an element that is often found to be present in small quantities in copper bearing ores. Cobalt is especially associated with copper sulphide ores, for example the ores in Gecamines in Zaire. (Kho et al., 2006).

Asano (1965) reported the distribution ratio of cobalt to be 1.124 at 1200 °C. The experimental conditions are described in chapter 3.4 Distribution of Nickel in Copper and Matte, and the experimental results are presented in Figure 16.

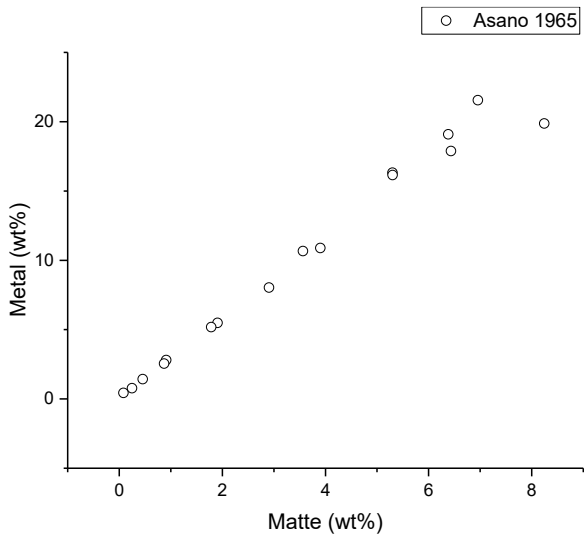

Figure 16 Concentration of cobalt in matte phase vs metal phase. (Asano, 1965).

There has been no discovery of the functional dependency of temperature on the distribution coefficient of cobalt between metal and white metal phases. (Asano, 1965).

3.5.1 Cobalt Distribution as a Function of P(SO_2)

Kashima et al. (1978) found that cobalt is distributed between the metal and matte phases in relatively equal parts during the copper converting process. Cobalt was most highly concentrated to a slag phase, when a slag phase was present. The experiments of the study were carried out at 1300 °C. The samples were allowed to equilibrate for 45 h in SO_2-Ar mixture with a flow rate of 150 ml / min. Cobalt was found to be distributed between the metal and white metal phase as the closest to unity, i.e. it was distributed equally between the white metal and metal phases.

Figure 17 shows the experimental data of Kashima et al. (1978). The trend line is added to evaluate the data presented. The authors state that the partial pressure has no effect on the distribution of cobalt through the matte and metal phases. Running the analytical results presented in their paper, it can be seen that there is a slight trend: the distribution coefficient decreases as a function of the increasing pressure of SO_2. Though the R^2 value is low, the trend line in Figure 17 reveals this direction. Perhaps the authors did not feel this was a strong enough trend to report on or there were experimental inaccuracies present in the work. What they did point out is that the majority of the cobalt tends to the slag phase.

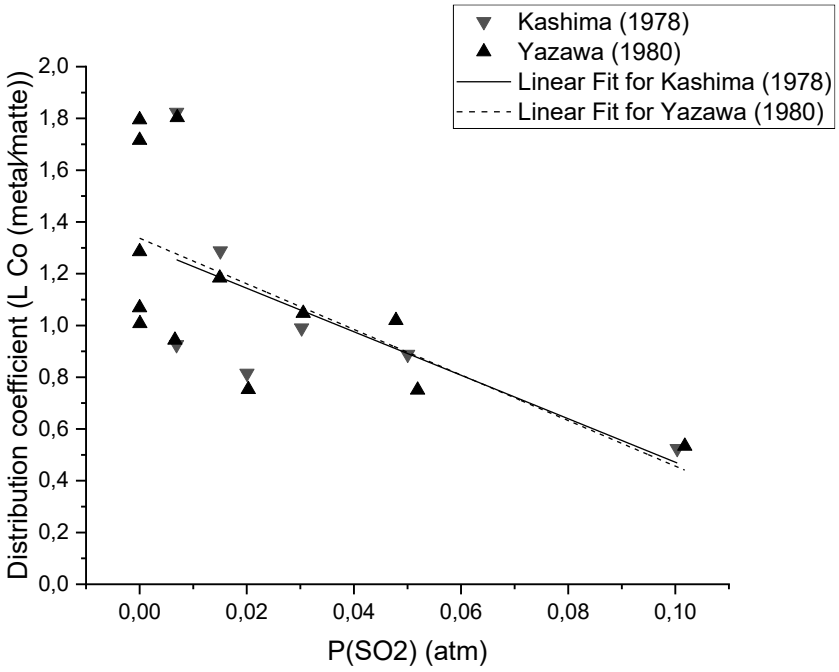

Figure 17 Distribution coefficient of cobalt as function of the partial pressure of $P(SO_2)$. (Kashima et al. 1978), (Yazawa, 1980).

Yazawa (1980) carried out experiments with varying SO_2 partial pressure at 1300 °C. The samples were equilibrated and silica crucibles were used. It should be noted that this work like that of Kashima et al. (1978), states that the trend line of the distribution ratio of cobalt against the logarithm of oxygen potential is nearly horizontal. This is explained by the derivation for the relationship of distribution coefficient in equation (9).

Figure 17 also shows data from Yazawa (1980) for the distribution coefficient of cobalt as it varies with $P(SO_2)$. The trend line of the data seems to be in disagreement with the conclusions. The distribution coefficient as expressed by (Yazawa, 1980) is given in equation (26).

$$L_{Co}^{metal/matte} = 1.14 \; for \; 1300 \; °C \tag{26}$$

The three papers by Asano (1965), Kashima et al. (1978), and Yazawa (1980) agree on the distribution ratio being close to the value of unity between the two phases ranging from 1.03 to 1.14. They are also in agreement about the fact that the sulphur dioxide partial pressure and therefore the oxygen potential have no influence on the distribution. However, the numbers presented by Kashima (1978) and Yazawa (1980) suggest that an influence might exist, but as stated already there may have been some experimental errors, the values were

within standard deviations or the researchers felt like the correlation was not strong enough to remark upon.

3.6 Distribution of Palladium between Metal and Matte Phases

There is a particularly small amount of experimental data regarding palladium distribution coefficient between metal and matte phases as well as the functional dependency of the distribution ratio on either temperature or sulphur dioxide partial pressure.

One of the few papers that does discuss the distribution coefficient of palladium between metal and matte phases is the report by Schlitt and Richards (1975) on the distribution ratio, which is presented in equation (27):

$$L_{Pd}^{metal/matte} = 166.67 \; for \; 1200 \; °C \tag{27}$$

These experiments were carried out at 1200 °C under a N_2 atmosphere. The metal and matte phases were added in equal parts with the total Pd weight percentage of 0.4. The experiments were repeated four times. The high value for $L_{Pd}^{metal/matte}$ means that the majority of the palladium collected to the metal phase and only a very small amount collected to the matte phase.

Burylev et al. (1974) investigated the distribution of platinum and palladium between metal and sulphide melt in the Cu-S and Cu-Ni-S systems. In their experiments, they used cathodic copper and synthetic Cu_2S. The samples were reacted for 1 hour at 1150 °C and 1300 °C. In total 30 g of material was used in these experiments. Alumina crucibles were used. To measure the distribution ratio the radioactive isotopes, Pd^{109} and Pt^{193} were used as tracers.

Burylev et al. (1974) propose the reaction mechanism in equation (28) for the noble metals in the Cu-S system:

$$Cu_2S + Me_{(Pd \; or \; Pt)} = MeS + 2Cu \tag{28}$$

The reaction constant is defined as the following equation (29), where N is the mole fraction.

$$K_{(a)} = \frac{a_{Pd} a_{Cu_2S}}{a_{PdS} a_{Cu}^2} = K_{Pd} \frac{N_{Cu_2S} \cdot f_{Cu_2S} \cdot f_{Pd}}{N_{Cu}^2 \cdot f_{Cu}^2 \cdot f_{PdS}} \tag{29}$$

Burylev et al. (1974) found that in the Cu-Cu_2S system the distribution coefficient of palladium changed as a function of temperature. The coefficients were found to be according

to equation (30) and (31). The palladium coefficient was found to decrease with increasing temperature.

$$L_{Pd}^{metal/matte} = 94\ for\ 1150\ °C \tag{30}$$

$$L_{Pd}^{metal/matte} = 62\ for\ 1300\ °C \tag{31}$$

At infinitely dilute solutions of these noble metals – palladium in this case – their activity coefficients are found to be constant, so they obey Henry's law for a dissolved substance at least at infinitely dilute concentrations.

Burylev et al. (1974) also investigated the palladium distribution by increasing the nickel content of the system. Nickel was introduced into the system in the form of nickel sulphide. The effect of nickel concentration of the entire system can be seen in Figure 18. It can be seen that with increasing nickel concentration, the distribution of palladium decreases meaning that the palladium becomes increasingly more concentrated to the matte phase. The nickel distribution is also presented in this figure to show that it does not change as function of nickel concentration. In the experiments, the distribution ratio of nickel was found to be 3.17 ± 0.37. With the addition of 2.79 wt. % nickel which can be seen from Figure 18, the distribution ratio of palladium is reported to be 28. The distribution coefficient of palladium falls to 18 at 11.5 wt. % nickel in the system.

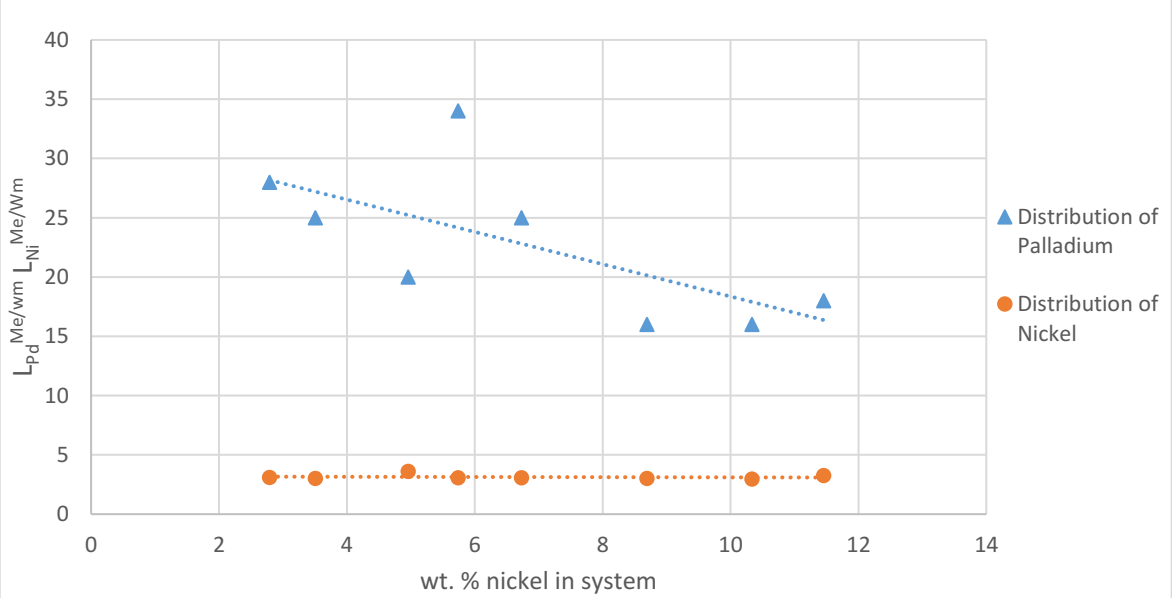

Figure 18 Palladium concentration as a function of nickel concentration. (Burylev et al., 1974).

3.7 Distribution of Gold in Metal and Matte Phases

Gold is often among the impurities of copper converting, as it is commonly found in copper bearing ores Kucha and Cichowska (2001), Schlesinger et al. (2011). Sinha, Sohn and Nagamori (1975), Schlitt and Richards (1975), Asano et al. (1971) and Asano (1965) have investigated the distribution of gold between metal and matte phases.

Schlitt and Richards (1975) conducted experiments and found the distribution coefficient of gold to be as shown in equation (32) in copper - white metal system at 1200 °C under a purified N_2 atmosphere. Gold was added as 0.4 percentage of the total system weight. The individual phases were sampled at the working temperatures.

$$L_{Au}^{metal/matte} = 125 \; for \; 1200 \; °C \tag{32}$$

Because the gold concentrations were too low for the experimental analysis technique used by Schlitt and Richards (1975), they deemed the accuracy to be questionable. For this reason, the distribution coefficient is only given to one significant figure.

With the assumption that the system is under equilibrium and the precious metal has a dilute concentration, the Raoultian activity can be related to the equilibrium constant of the reaction of the solute metal between metal and matte phases. K_{eq} is the equilibrium constant, $\gamma_{(metal)}$ is the Raoultian activity coefficient and M_{cu} is the molecular weight of the partially soluble phase.

$$K_i = K_{eq} \cdot {\gamma_{metal}}/{\gamma_{matt}} \cdot {M_{cu}}/{M_{Cu_2S}} \tag{33}$$

In the experimental work by Asano et al. (1971), the distribution of gold between liquid copper and cuprous sulphide was investigated. It was found that the distribution ratio L_{Au} was 171.5. The experimental data gathered is shown in Figure 19. The experiments were carried out at 1200 °C. Asano et al. (1971) also concluded that the distribution ratio of gold was not affected by the silver content in the metal phase up to 4.5 wt. %. In addition, silver was not affected by the gold content in the metal phase up to 1 wt. %.

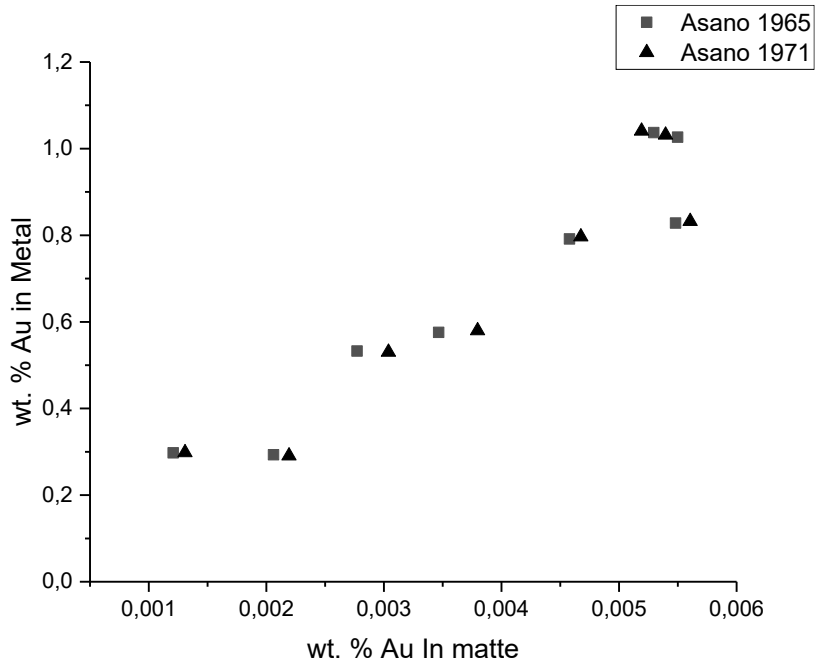

Figure 19 Concentration of Au distribution in matte phase vs metal phase. (Asano, 1965, 1971).

Asano (1965) investigated the distribution ratio of gold between liquid copper and matte phases at 1200 °C under vacuum conditions. The experimental procedure is described in chapter 3.4, and the experimental results are shown in Figure 19. Asano (1965) found the distribution ratio to be:

$$L_{Au}^{metal/matte} = 172.9 \; for \; 1200 \; °C \tag{34}$$

The distribution ratio can be seen from Figure 19, which also shows that gold distribution is not affected by gold concentration at these dilute concentrations up to about 0.01 wt. %.

3.7.1 Gold Distribution as a Function of Temperature

Sinha et al. (1985) investigated the effect of temperature on the distribution coefficient of gold between metal and white metal or matte phases. The experiments were run at 1127 °C and 1227 °C . The samples were equilibrated from 1 to 7.75 h. Elemental copper, iron, sulphur, and gold were used in the experiments each having 99.99 wt. % purity. In the experiments, 0.0022 to 0.0042 wt. % of gold was used to investigate the distribution coefficient under infinitely dilute conditions. The samples were analysed using the atomic adsorption method. After equilibration and cooling the samples were dissolved into aqua

regia at boiling temperatures for around 24 h. The authors concluded that because gold is such a noble metal, gold dissolves in its metallic state into the matte phase.

Sinha et al. (1985) plotted the concentrations of Au in the matte phase against Au concentration in the metal phase at the temperatures at 1126.85 °C and 1226.85 °C. They extrapolated the data presented in Figure 20 to infinite dilution and presented it in equations (35) and (36):

$$L_{Au}^{metal/matte} = 102 \; for \; 1126.85\,°C \tag{35}$$

$$L_{Au}^{metal/matte} = 127 \; for \; 1226.85\,°C \tag{36}$$

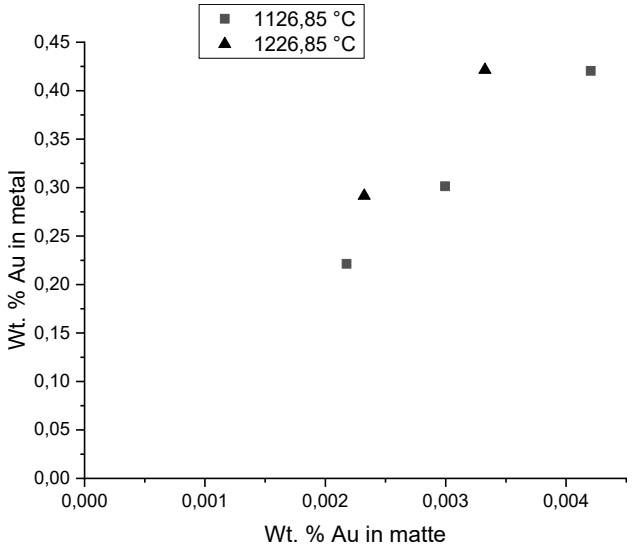

Figure 20 The distribution of gold between metal phase and iron free matte as weight percentage in metal and matte phases at different temperatures. (Sinha et al., 1985).

The distribution ratio increases as a result of the increased temperature, which is observed in Figure 20. Figure 20 also shows that the distribution coefficient is independent of gold concentration in the matte phase, and this is why the authors were able to extrapolate to infinitely dilute solution and produce the values above.

Sinha et al. (1985) calculated the activity coefficients for gold in the copper saturated matte phase – this is shown in equation (37) under the conditions of the temperature range of 1126.85 °C to 1226.85 °C, gold wt. %. in the matte phase of less than 0.0042 and iron wt. %. in the matte phase of less than 11.

$$log\gamma_{Au_{(mate,liquid)}} = -3310/T + 3.15 \quad (37)$$

Sinha et al. (1985) state that the activity coefficient for gold in the matte phase was independent of the iron concentration in the matte phase. According to them, the activity coefficient is not known for higher temperatures.

3.7.2 Gold Distribution as a Function of Iron Concentration

Sinha et al. (1985) also investigated the functional dependency of iron concentration on the distribution coefficient of gold. Figure 21 shows that temperature increases the distribution coefficient for gold, as well as the fact that increasing iron content in the matte phase decreases the distribution coefficient of gold. The high value for the distribution coefficient in all cases means that the gold is highly concentrated to the liquid metal phase.

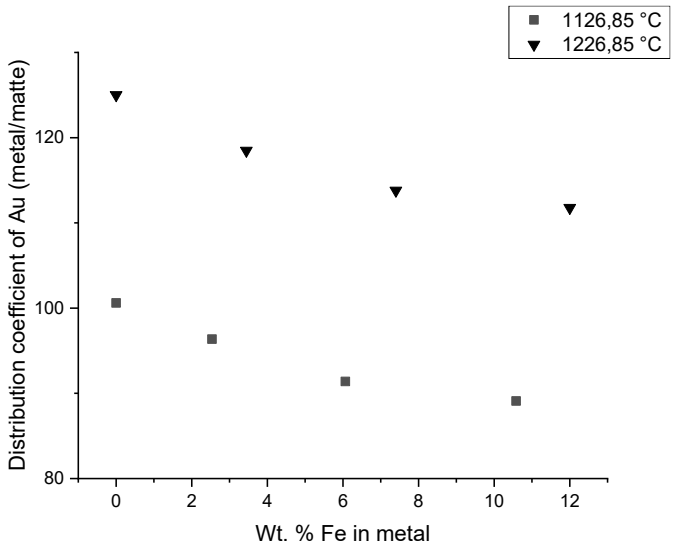

Figure 21 The effects of iron content in matte on the distribution ratio of gold between metal and matte phases. (Sinha et al., 1985).

Table 3 Reported distribution coefficient of Au according to author

Author	Reported L_{Au}	Notes
Sinha et al.	102, 127	1127, 1227 °C
Schlitt and Richards	125	1200 °C
Asano et al.	171.5	1200 °C
Asano	172.9	1200 °C

Based on the distribution coefficients for gold presented in Table 3, it can be concluded that gold is highly concentrated to the metal phase.

3.8 Distribution of Iron between Liquid Copper and Matte

Asano (1965) investigated the distribution of iron. It was reported that the distribution coefficient is 0.201 at 1200 °C, and the experimental results can be seen in Figure 22.

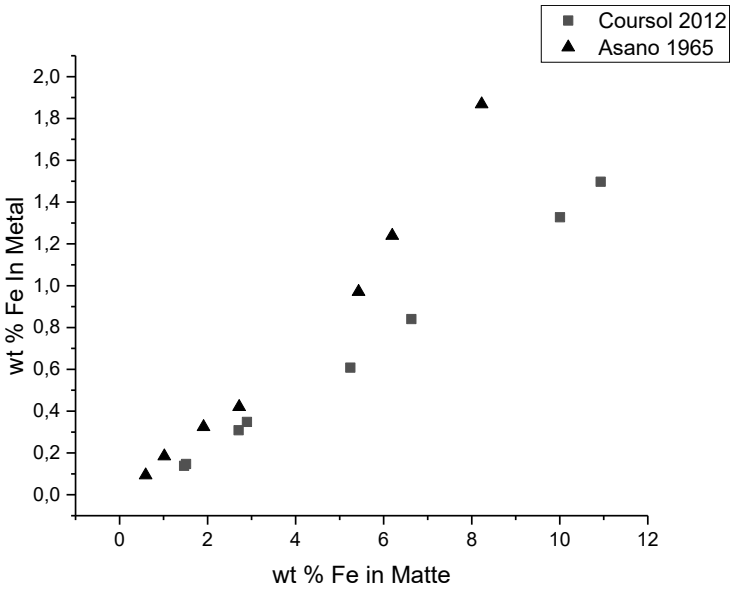

Figure 22 Concentration of Fe distribution in matte phase vs metal phase. (Coursol, 2012), (Asano, 1965).

Coursol et al. (2012) also investigated the iron distribution as a function of concentration of Fe in the Cu-Fe-S system, and also these experimental results are shown in Figure 22. The distribution ratio was found to be in the range of 0.1 to 0.14 at 1200 °C.

3.9 Iron Distribution as a Function of Temperature

In the work of thermodynamics of the Cu-Fe-S system at matte smelting temperatures by Krivsky and Schuhmann (1957), the distribution of iron between liquid matte and liquid metal was observed in equilibrium conditions. The authors investigated the equilibria of the system from 1150 °C to 1350 °C, for which the data is presented in Figure 23. The materials used in these experiments are described as highly pure. Additionally, an Armco sleeve which is a very low C pure iron, was used to ensure the saturation of iron in the system. In addition,

iron sulphide was prepared. The $P(SO_2)$ is fixed with the mixtures of H_2S and H_2 by the reaction $H_2 + \frac{1}{2}S_2 \leftrightarrow H_2S$. This gas mixture was bubbled through the liquid Cu-Fe-S matte.

The gases were analysed before and after passing through the matte, and the entrance gas was altered until both inlet and outlet gases were at the same composition. This was maintained for several hours. Once the equilibrium was reached, samples were taken by inserting a borosilicate glass tube (vycor tube) into the matte. Each liquid phase was sampled, but the tube was sealed before being inserted into the liquid. The end of the tube was broken off against the bottom of the crucible while being submerged into the liquid. The authors normalised the data from an average of 99.7 %, so this was not perceived to add significant error. The ratios reported by the authors are the ratios of "equivalents to iron to the total cation equivalents". E_{Fe} equals 1 in stoichiometric FeS, and E_S also equals 1 in FeS. Therefore, E_{Fe} is the mole ratio FeS. This according to the authors was a more convenient way to calculate the correlations in the liquid matte. The equation given is as follows. (Krivsky and Schuhmann, 1957).

$$E_{Fe} = \frac{n_{Fe}}{n_{Fe} + \frac{n_{Cu}}{2}} \tag{38}$$

Temperatures for the experiments ranged from 1150 to 1350 °C. It can be observed from Figure 23 that increasing the temperature of the system has the effect of increasing the distribution coefficient of Fe between the metal and matte phases.

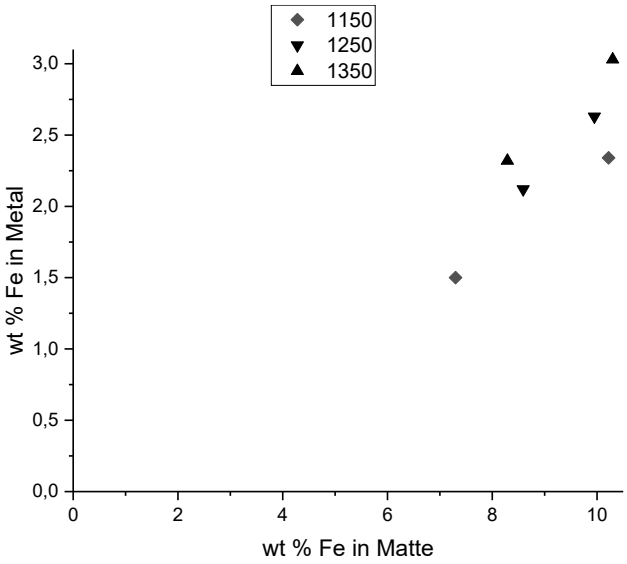

Figure 23 Concentration of Fe distribution in matte phase vs metal phase as a function of temperature. (Krivsky and Schuhmann, 1957).

The distribution ratios from Figure 23 are calculated from the data presented by Krivsky and Schumann (1957), and shown in equations (39), (40) and (41).

$$L_{Fe}^{me/ma} = 0.221 \; for \; 1150 \; °C \tag{39}$$

$$L_{Fe}^{me/ma} = 0.255 \; for \; 1200 \; °C \tag{40}$$

$$L_{Fe}^{me/ma} = 0.302 \; for \; 1250 \; °C \tag{41}$$

It is visible that after equilibration the majority of the Fe should collect to the matte phase and that this coefficient is slightly affected by increasing temperatures.

Nagamori and Mackey (1978) cite the work by Krivsky and Schuhmann (1957) in their paper and report that at 1200 °C and 1250 °C the distribution of iron is 0.178 and 0.183 respectively. This is relatively close to the results that they had published. It also states that the distribution coefficient has a slight dependency on temperature of the system.

4 Methodology

4.1 Procedure

In this chapter the methodology, equipment set up and special consideration made for these experiments are presented and described. The distribution of solute elements between molten copper and molten copper sulphide is investigated as a function of temperature and partial pressure of sulphur dioxide. The solute elements investigated in these experiments are cobalt, nickel, silver, gold and palladium. In these experiments, the samples were made from equal parts of copper doped with solute elements and synthetic copper sulphide. The samples were equilibrated in the vertical resistance furnace under different temperatures and SO_2 partial pressures. The samples were then quenched into a bath of 0 °C water in a matter of seconds, and after that the samples were mounted into epoxy resin and a cross-section in the samples was made that reveals both phases. These samples were analysed with an electron probe microanalyser (EPMA) in order to get results that are more reliable for those solute elements with low concentrations in certain phases.

In this work, rapid quenching was utilized. Small samples (~ 0.2 g) were quenched into ice-cold water, the small sample size and the ice-cold water should mean that the samples are rapidly quenched. Other researchers Arvamaa (2015), Choi and Cho (1997), Zakeri (1998), Eguchi and Yazawa (1977), have utilised water quenching. The quenching rate used is faster than in many of the previous studies where many samples only utilise air-cooling Kho (2006), Takeda (1997), Schmiedl (1977), Schlitt et al. (1973). Another method for sampling is taking the samples while the sample is still molten (Schlitt and Richards, 1975), (Krivsky and Schuhmann, 1957). The zirconia crucibles utilized in these experiments are open from the top, and this should also allow for a faster quenching. The combination of the drop into the ice-cold quenching media, the small sample size and openness of the crucible should allow for a rapid and more even quenching across the sample material.

This work investigates the second stage of the converting process, where sulphur oxidation from the copper sulphide begins. In industrial processes, there remains roughly 1 % of iron in solution in sulphide matte during the second stage of converting. In this work, iron is added as a solute element to better simulate these conditions.

4.2 Experimental Considerations

Distributions of cobalt, nickel, silver, gold and palladium between copper and copper sulphide are investigated in this work. The distribution coefficients are investigated as a function of temperature, 1250 °C, 1300 °C and 1350 °C, as well as a function of sulphur dioxide partial pressure, 0.01, 0.05, 0.1, 0.5 and 1 atm . The controlled atmosphere of sulphur dioxide was diluted with argon to achieve the desired partial pressure of the reactant gas.

The solute elements were introduced into the system as pure metals and were dissolved into the copper phase prior to the experiments.

The experimental process consisted of three main steps: equilibration and quenching, grinding and polishing (sample preparations of cross sections), EPMA analysis and calculations.

Stabilized zirconia (ZrO_2) (Degussa, Germany) crucibles were used, as they were not expected to react with samples.

Rapid quenching into a bath of 0 °C water was used to preserve the composition of the phases that exists while the sample is being held at the equilibrium conditions of the specific temperature and gas atmosphere. The polished cross sections of the samples are analysed first with a Leo 1450 (Carl Zeiss Microscopy GmbH, Jena, Germany) scanning electron microscope with an Oxford Instruments X-Max 50 mm^2 energy dispersive spectrometer (EDS) (Oxford instruments, Abingdon, UK) and back scattered electron detection (BSD) to observe the micro structure and to determine suitable areas for analysis. The concentration of the solute elements was examined using a Cameca SX100 microprobe (Cameca SAS, France) (EPMA) equipped with five wavelength dispersive spectrometers (WDS). The distribution coefficients for the solute elements were calculated from these results.

4.3 Experimental Apparatus

This section describes the furnace, atmosphere control system and measurement systems of the experimental apparatus. Figure 24 is a diagram of the furnace and Figure 25 is a photograph of the actual apparatus. The experiments in this work were carried out in high temperature conditions (1250–1350 °C).

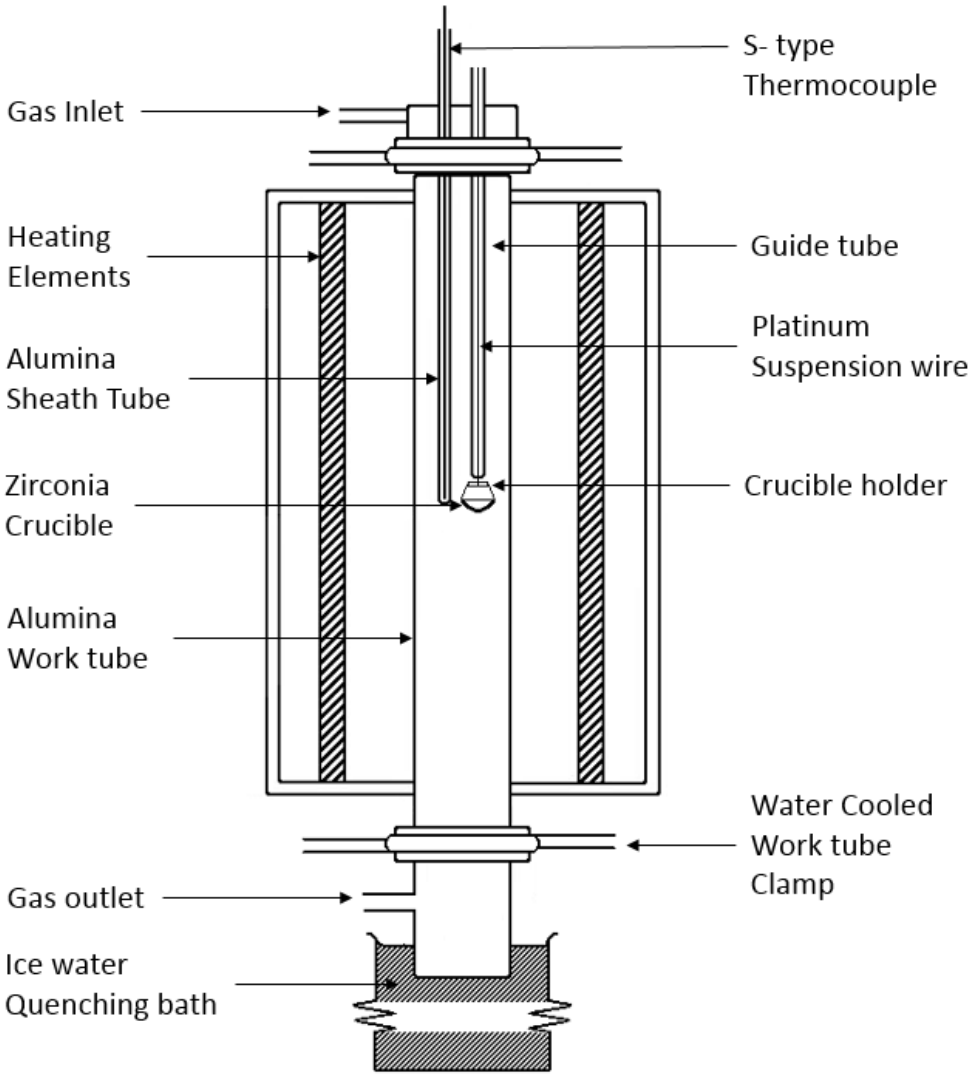

Figure 24 Diagram of a test furnace used in experimental series.

During each of the experiments the sample is drawn into the isothermal zone within the work tube, which is next to the measuring point of the thermocouple. In Figure 24 the position of the sample during the equilibrations is marked by the location of the zirconia crucible.

The SO_2-Ar gas mixture enters the work tube through a gas inlet at the top of the work tube which can be seen in Figure 24. The gas mixture passes the sample in the work tube, and the gas mixture exits the work tube at the gas outlet point at its base.

In this study, a Lenton PTF 15/50/450 (Lenton, Hope, UK) was used to heat the samples. The apparatus has a maximum heating temperature of 1500 °C and a maximum power delivery of 5.0 kW. The work tube was a gas impermeable alumina tube (38/45/1100 mm, Friatec, Mannheim, Germany). The furnace was heated by silicon carbide rod elements that

are mounted parallel to the work tube. This furnace has three heating zones, which provide a longer uniform temperature zone. In this case, the uniform temperature zone was measured to be roughly 100 mm. The Lenton thermal design company states that the temperature variation in the uniform zone is typically within ± 5 °C with a large portion of the uniform zone within ± 1 °C (Lenton 2017). The furnace temperature was controlled by three Eurotherm 3216 PID temperature controllers (Eurotherm, Ashburn, USA), which had separate controllers. The temperature was measured with a calibrated S-type thermocouple (100% Pt / 90 % Pt -10 % Rh) (0.5 mm diameter, Johnson Matthey, UK) which measures the uniform zone inside the work tube next to the sample. The temperature signal from the thermocouple was monitored with a Keithley 2010 multimeter, (Keithley instruments, Ohio, USA), the cold junction (room temperature) was measured with a Pt100 resistance thermometer (SKS-Group, Finland) connected to a Keithley 2000 multimeter (Keithley instruments, Ohio, USA). The furnace was controlled by the on-board PID and thermometer.

The samples were suspended in the sample holder with platinum wire that runs through the guide tube from the top of the furnace to the isothermal zone.

The sulphur dioxide (99.98 vol. %, AGA) and argon (99.999 vol. %, AGA) gases were controlled with digital mass flow controllers (DFC) (Aalborg, USA). The argon was controlled with DFC 26 with a range of 0–500 ml / min, the SO_2 is controlled by model DFC 26 with a range of 0–500 ml / min for high partial pressures and a DFC 26 with a range of 0–100 ml / min for low partial pressures of SO_2. The accuracy of the flow controllers was ± 1 % of the full range of mass flow for each of the controllers. For this reason the smaller range mass flow controller was chosen for the lower partial pressures of SO_2. The pressure of each gas before the DFCs was set to an over pressure of 1.38 atm as recommended (Aalborg, USA). The two gases were mixed together in the gas-mixer before entering the work tube, which can be seen in. The DFCs were controlled with DFC control terminal program. Before each experiment, the gas mixture was stabilised in the work tube for 15 minutes prior to the sample entering the uniform temperature zone.

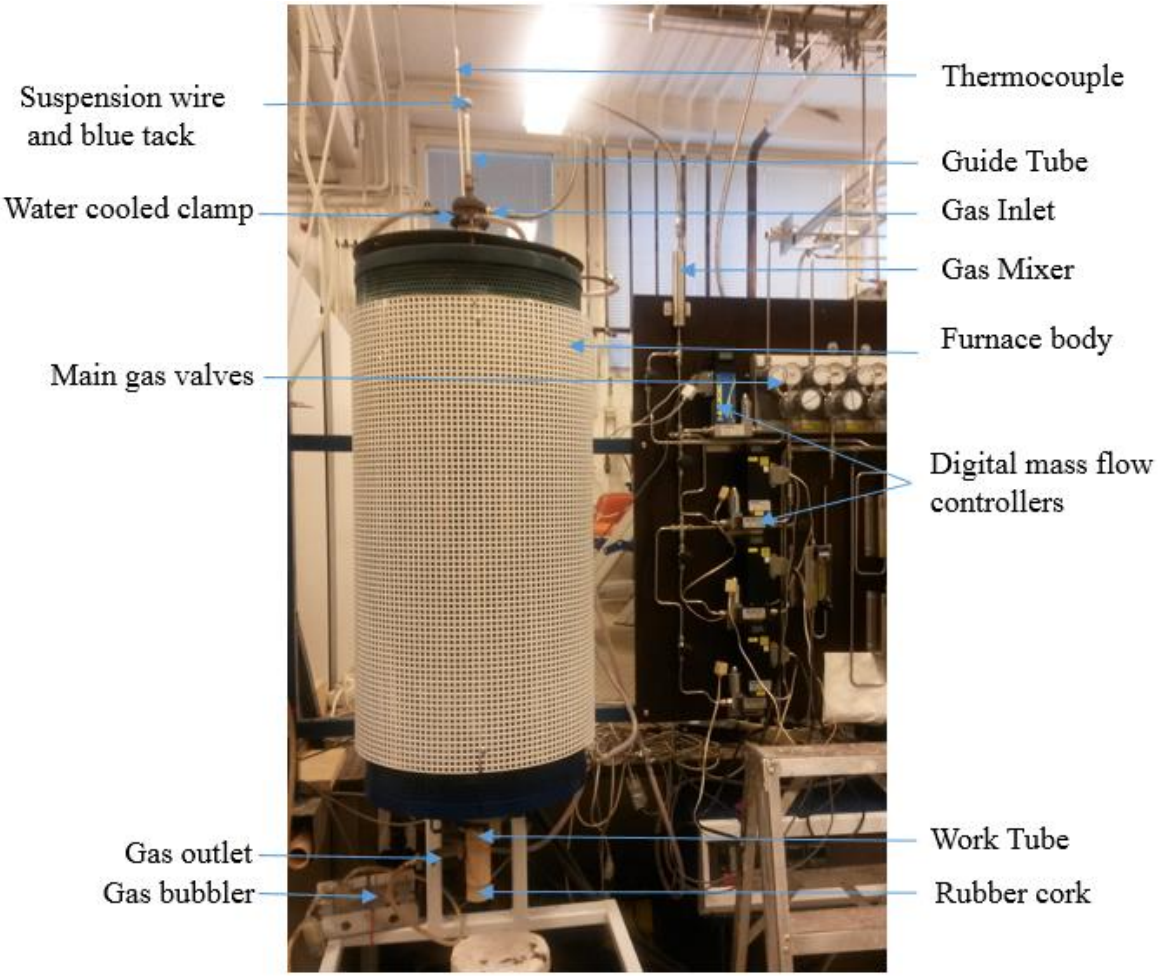

Figure 25 Photograph of the test furnace and gas mixing system.

The reactant gas passes the sample and is exhausted through the bottom of the work tube, and the exhaust gas is passed through a set of two bubblers. These act as a way to indicate that the reactant gas is passing through the work tube as well as not allowing the atmospheric gases back in to the base of the work tube. Also, a glass chamber filled with ceramic particles which is designed to precipitate elemental sulphur from the exhaust gases.

4.4 Sample Preparation

The quenched samples were mounted into ⌀ 25 mm epoxy resin buttons and prepared with the traditional metallographic method. Cross sections of the sample pieces were made by grinding away material until a suitable area that exposes both of the phases was found. The grinding was carried out with a grinding machine (Stuers, Denmark, seen in Figure 26) with sandpapers (Mirka, Finland) with grades of 240, 400, 800 and 1500 grits.

Figure 26 Struers grinding table.

After grinding with the finest grit sand paper, the samples were polished with 3 µm and finally with 1 µm diamond spray (Dp Spray M; Struers, Denmark) and lubricated with Dp lubricant blue on a polishing machine (Struers, Denmark, seen in Figure 27). An optical microscope was used to check if the polishing had removed the scratch marks created by the grinding process.

Figure 27 Struers polishing machine.

Once the phases had been opened up and the polishing was deemed sufficient, the samples were cleaned in an ultrasonic cleaner with ethanol. The samples were then coated with carbon so that the surface of the epoxy could conduct to the sample surface for the SEM-EDS and the EPMA. The apparatus used to coat the samples with carbon was a carbon coating machine (Leica EM SCD050, Austria, seen in Figure 28).

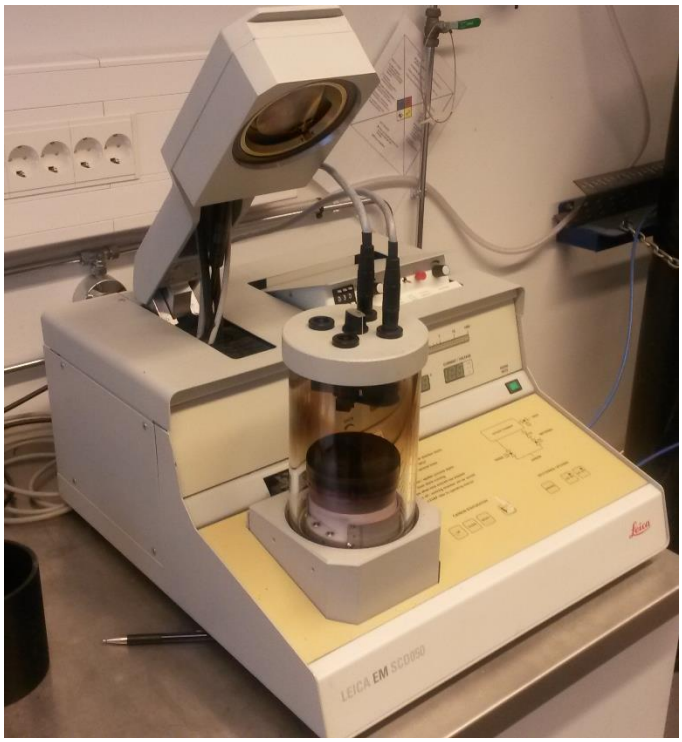

Figure 28 Leica carbon coating machine.

4.5 Sample Analysis

The samples were initially analysed with a SEM to find suitable areas in the cross section for analysis. The solute elements of interest in this study are at concentrations below the SEM EDS detection limit, for this reason, the EPMA is utilised.

4.6 Experimental

In this section, the chemical and materials used in these experiments are reported. The preparation of the master alloy from which the copper phase for all the experiment is taken from is described and the preparation of the samples and crucibles is described. The prepared samples were placed in to the crucible and lifted to the isothermal zone.

4.6.1 Reagent Chemicals and Materials

All of the samples were prepared from 0.1 g of the master alloy and 0.1 g of copper sulphide. The master alloy contains the solute elements dissolved in solution prior to the experiments. The main solute elements were prepared at 1 wt. % of the master alloy each. The iron was prepared at 0.25 wt. % of the master alloy. The materials were weighed and prepared in the

laboratory to these concentrations. The weights of each element are presented in Table 4. Each of the solute elements were added in their metallic form in various powdered grades.

Table 4 Master alloy components.

Copper metal			
Element	**Weight**	**wt. %**	**Notes**
Cu	4.7297	99.999 %	Alfa Aesar, (Germany) Copper shot
Cu	0.0076	99.9 %	Alfa Aesar, Copper powder <1000 ppm O_2
Co	0.0505	99.99 %	Koch-light laboratories (UK), Cobalt sponge
Ni	0.0509	99.996 %	Alfa Aesar, Nickel powder
Ag	0.0502	99.99 %	Alfa Aesar, Silver Powder
Au	0.0498	99.95 %	Alfa Aesar, Gold Sponge
Pd	0.0499	99.9 %	Alfa Aesar, Palladium Powder
Fe	0.0129	99.99 %	Alfa Aesar, Iron powder

The copper sulphide that forms the second immiscible phase at the elevated temperatures was added to each sample. Each sample was aimed to have about 0.1 g of the copper sulphide, Table 5.

Table 5 White metal components.

White metal phase			
Chemical	**Weight**	**wt. %**	**Notes**
Cu_2S	0.1 g per sample	99.5 %	Alfa Aesar (Germany), powder

The atmospheres of the gases used in these experiments were created using a mixture of the two gases shown in Table 6. The gases were pre-mixed at the set partial pressures before entering the work tube, and the immiscible liquids were equilibrated at the fixed $P(SO_2)$.

Table 6 Gas components.

Gases Used		
Chemical	**Vol. %**	**Notes**
SO_2	99.98 %	AGA (Finland)
Ar	99.999 %	AGA

There were low amounts of impurities in the argon gas, less than 2 ppm O_2, less than 3 ppm H_2O, less than 5 ppm N_2 and less than 0.2 ppm of hydrocarbons (C_nH_m). AGA (2017).

4.7 Master Alloy Preparation

The master alloy forms the metal phase which is present in all experiments. The master alloy was prepared with the components presented in Table 4. The materials were weighed with a semi-microbalance (Mettler-Toledso, UK). The aim of using the master alloy in this experimental series is to ensure that the material in each experiment would be as homogenous as possible across all experiments.

The weighed solute elements were pelletised using the method described in chapter 4.4 sample preparation. The pellet was combined with the copper shot in a pre-cleaned pure silica glass ampoule. The ampoule tube was then heated with an oxygen/hydrogen blowtorch on the open end to form a neck of sorts and after this allowed to cool. The open ampoule end was connected to a vacuum pump. The vacuum pump applied a pressure of 3-4 $x10^{-2}$ mbar to the ampoule, and the atmosphere in the ampoule was then replaced with argon. The gas atmosphere within the ampoule was vacuumed and charged with argon four times. The remaining atmosphere should be at a low pressure in the ampoule should then be almost entirely argon. This ensured that the gas atmosphere in the ampoule was entirely inert and the pressure exerted by the expanding gas atmosphere minimised as the ampoule was held at the working temperature.

The next step was to reheat the neck of the ampoule gently with a blowtorch. Once the ampoule material began to melt, the over pressure of the outside atmosphere forced the neck of the ampoule closed, thus sealing the ampoule. The ampoule was then suspended with a Kanthal D wire to the hot zone of a vertical tube furnace (Lenton LTF 16/-/450, Lenton, UK, seen in Figure 29) that can be rotated about its hot zone.


Figure 29 Tiltable vertical tube furnace.

Kanthal wire was affixed to the ampoule and both ends of the furnace so that the ampoule would change position within the furnace during its rotation. Alumina wool was placed at both ends of the furnace to aid in heating the ampoule evenly.

The master alloy was homogenised in the ampoule for 120 hours at 1200 °C. The furnace was rotated twice, once at 66 hours past and then again at 90 hours past. After the 120 hours had passed, the ampoule was quenched into ice water. The ampoule was then broken, and the master alloy removed. A small piece from the top and the bottom of the main master alloy lump was removed as well as one of the droplet pieces. They were prepared for and analysed with the SEM-EDS, in the same metallographic manor as described in chapter 4.4.

The SEM-EDS revealed that the master alloy had been homogenised. Table 7 shows the average values for the solute elements in the master alloy. The averages were taken from four large areas from each of the sample surface areas. The values are presented as a weight percentage of the total mass of the sample.

Table 7 SEM-EDS results for master alloy composition.

Master Alloy	**wt. %**				
	Co	**Ni**	**Pd**	**Ag**	**Au**
Site 1	1.05	0.95	0.91	1.06	0.93
Site 2	0.84	0.97	0.97	1.05	1.09
Site 3	0.93	1.02	0.94	1	0.83

The inside of the ampoule had adsorbed some material to the inside surface. The contact with the main liquid metal alloy at the base of the ampoule had a copper like colour, whereas the rest of the ampoule (aka the gas phase) had a silvery colour. This could actually be silver adsorbed onto the surface of the silicate glass. The silver should have the highest volatility of all the components within the alloy, so there must have been silver in the gas phase within the ampoule, and during the quenching the silver in the gas phase solidified to the inside surface of the ampoule.

4.8 Reaction Gas

One of the variables in this series of experiments is the partial pressure of SO_2 in the gas phase of the system. In this study, the partial pressure of SO_2 was controlled by diluting it with Ar gas. It is assumed that the gases are perfectly mixed prior to entering the work tube.

The $P(SO_2)$ is fixed from the concentration in the gas phase (Ar + SO_2). The $P(S_2)$ is fixed from the metal - white metal equilibrium equation (42). The $P(O_2)$ is fixed because of the fixed $P(SO_2)$ which is fixed by the $P(S_2)$ from the liquid phases, according to equation (42) and equation (43).

$$2Cu_{(l)} + \frac{1}{2}S_{2(g)} \leftrightarrow Cu_2S_{(l)} \tag{42}$$

There was some amount of decomposition of SO_2 at these elevated temperatures of the experiments (1250 °C to 1350 °C) and partial pressures of O_2 and S_2. This means that the $P(O_2)$ is also regulated by the basic reaction (43). If only the gas phase was present, the equilibrium constant of the decomposition SO_2 would be as stated in equation (44) (Schuhmann, 1950).

$$1/2\,S_2 + O_2 = SO_2 \tag{43}$$

$$K3 = \frac{P_{SO_2}}{P_{O_2} P_{S_2}^{1/2}} = 1.8 \times 10^8 at\ 1300\ °C \quad (44)$$

The decomposition P(SO_2) increases along with the temperature. At 1250 °C P(O_2) = 5 x 10^{-9} at 1300 °C P(O_2) = 10^{-9} and at 1350 °C P(O_2) = 5 x 10^{-8}. These values are roughly estimated from the Ellingham diagram. In all cases the partial pressure for O_2 is low and the majority of the gas will remain SO_2, but when the condensed phases (Cu and Cu_2S) are present, this affects the reaction (43) because of the fixes P(S_2) from reaction (42).

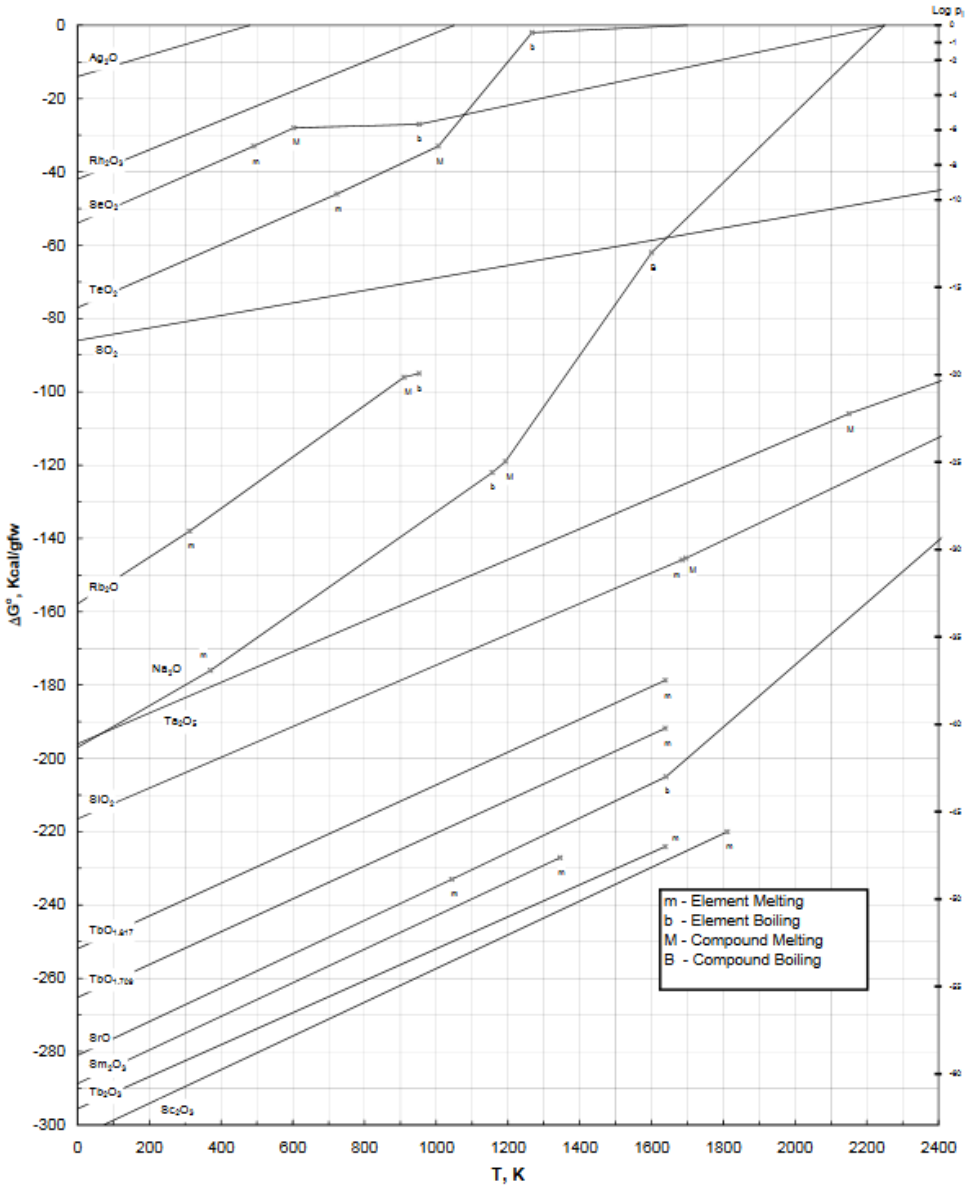

Figure 30 Ellingham diagram. (Howard, 2006).

The gas atmosphere is comprised of the gas species in equation (45).

$$P_{S_2} + P_{O_2} + P_{SO_2} = P_{total} - P_{Ar} \quad (45)$$

P_{total} is roughly equal to 1 atm. The lower $P(SO_2)$ also means that $P(O_2)$ will also be lower and that $P(S_2)$ will also be fixed, but mostly $P(S_2)$ is fixed by the Cu-Cu_2S.

Eguchi and Yazawa (1977) state that if the SO_2 partial pressure is at a fixed temperature, all the equilibria of Cu content in matte, sulphur content in matte etc. can be determined.

Eguchi and Yazawa (1977) state that the partial pressure of S_2 gas is roughly fixed despite the partial pressure of SO_2 in the reaction gas. The S_2 gas was then fixed by the dissociation copper sulphide to copper in the sulphidic phase according to equation (46). This is because the ratio of the actives of a^2_{Cu} and a_{Cu2S} are approximately equal to one when the two phases exist in contact.

$$2Cu_2S_{(liquid)} = 4Cu_{(liquid)} + S_{2(gas)} \quad (46)$$

The equilibrium constant for this reaction is approximately equal to the partial pressure of S_2; $k1 \fallingdotseq PS_2$.

The oxygen partial pressure is directly proportional to the sulphur dioxide partial pressure when using equation (47). The SO_2 from the gas phase reacts with the copper from the metal phase, the $P(O_2)$ is a product of this reaction. (Eguchi and Yazawa, 1977).

$$2Cu_{(liquid)} + SO_{2(gas)} = Cu_2S_{(liquid)} + O_{2(gas)} \quad (47)$$

The equilibrium constant KO_2 for the reaction in equation (47) is equal to the partial pressure of oxygen over the partial pressure of sulphur dioxide.

$$kO_2 \fallingdotseq \frac{PO_2}{PSO_2} \quad (48)$$

The S_2 and O_2 partial pressures derived from the above equations (47) and (48) may be different from the partial pressures derived by the dissociation of the plain SO_2 Ar mixture. (Eguchi and Yazawa 1977).

4.9 Master Alloy Sample Preparation

Once the master alloy was taken from the ampoule it was prepared in such a way that small pieces of it could be removed in a reliable way. The size of each sample was 100 mg each from the master alloy. The master alloy was cut to smaller pieces with a pair of cutters, but before that was possible, the alloy had to be flattened to make it easier to work with. The

master alloy was flattened with 20 tonnes of force with a hydraulic press. This flattened piece was then cut into five separate pieces using a hammer and chisel to make a deep grove that could be bent and finally torn apart with pliers. After this these five smaller pieces were all separately placed between the same two pieces of steel in the same hydraulic press and pressed with 20 tonnes of force. This then yielded five thin pieces of the master alloy that could be easily cut with a pair of cutters.

4.9.1 Sample Pellet Preparation

The master alloy and the powdered copper sulphide were combined together in a pellet. Both components were weighed prior to the combination with a micro mass balance. The components were placed into a 4 mm iso axial pellet-pressing tool and the press placed into a hydraulic press (Compac, Denmark). After this the pellets were subjected to 39.8 MPa of pressure, and the samples were weighed again. The presses are presented in Figure 31. The left side of the figure shows a cross section of the pellet mould, and the right side shows the hydraulic press.

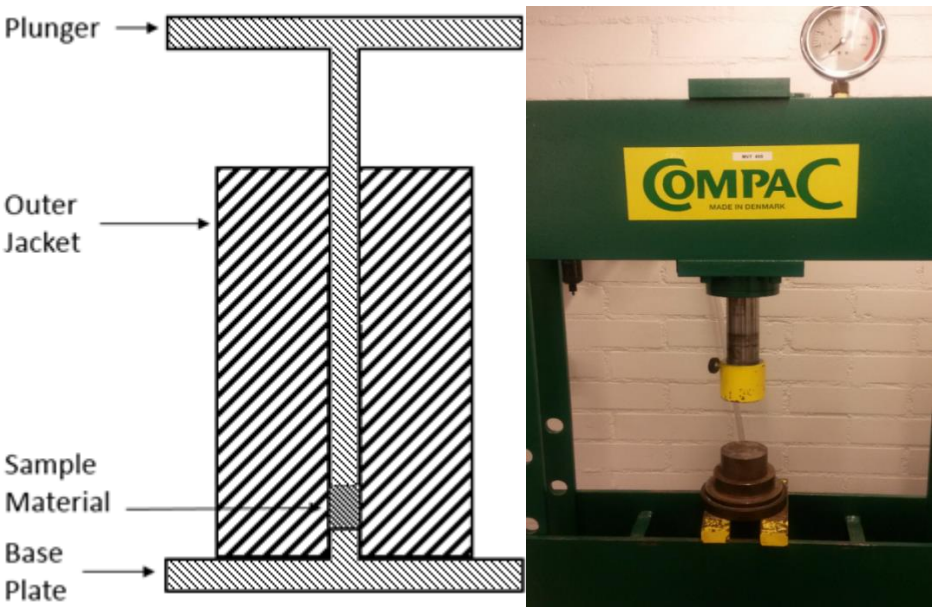

Figure 31 Cross section of the pellet mould and photograph of the hydraulic press.

The crucibles used in these experiments are made of CaO-stabilised zirconia and Hf-stabilised zirconia. The crucibles were cut to shape using a diamond-cutting wheel and cleaned using a diamond drill bit.

4.10 Degrees of Freedom

The Gibbs phase rule can be applied to this complex system with reactive components to determine the degrees of freedom. Equation (49) is used to determine the degrees of freedom of the system. (Y. K. Rao 1984, p. 516 & 519), (D. R. Gaskell 2008).

$$F = C - P + 2 - t_{special\ constraints} \tag{49}$$

Here F is the degrees or freedom, C is the number of components and P is the number of phases and $t_{special\ constraints}$ is the number of special constraints. The elements present in these experiments will react with one another, so this means there will be a number of different reaction equilibria, R, as well as stoichiometric constraints, S, in the system. The phase rule can be modified to accommodate for the reaction equilibria by modifying the number of components, C, by equation 50. (Y. K. Rao 1984, p. 516 & 519), (D. R. Gaskell 2008).

$$C = N - R - S \tag{50}$$

In this equation, N is the number of species contained in the system. So if we consider equations (43) and (46), the species are S_2, O_2, SO_2, Cu, Cu_2S plus the Ar present, which means N = 6. From equation (46) it can also see that the number of reaction equilibria = 1. There are three phases that exist in equilibrium with each other in this system, the two immiscible liquid phases; named the metal and white metal and a gas phase. So, P = 3. The partial pressure of SO_2 is fixed with Ar so there is 1 stoichiometric constraint. There is also the special constraint of 1 atm in the system and temperature is also fixed, giving t = 3. Therefore C = 6 - 1 - 1 = 4 and F = 4 – 3 + 2 – 3 = 0.

There are a number of different solute elements within the immiscible liquid phases (Fe, Co, Ni, Ag, Au and Pd). However, in this work the consideration is that there is no interaction between these solute elements. Theoretically, there are interactions between these elements (Johnson 1984). These are not considered for the sake of simplicity and because each of the solute elements are in low concentration (around 1 % by wt. of the total mass). Each solute element adds 1 degree of freedom to the system as there is a separate reaction equilibrium for each solute element which increases R by 1 following the general reaction for solute elements in equation (10), therefore increasing the degrees of freedom for each additional solute element by 1. This is measured by the distribution of the solute element between the two immiscible liquid phases according to equation (9).

4.11 Implementation

4.11.1 Equilibration Series

A series of equilibration time experiments were made to establish at which point equilibrium has been reached in this system. Equilibrium is a state of the system where the derivative of Gibbs free energy and the extent of reaction at constant temperature and pressure is equal to zero. The total of the chemical potentials for all reactants and productions are equal to one another. The change that is observed in the time equilibration series is the distribution of the solute elements Co, Ni, Ag and Cu and S between the metallic copper and white metal. In order to find the equilibrium point for the distribution of these solute elements, a number of experiments were made with varying time. Using the data acquired from this series, the time taken to reach the equilibrium point can be determined.

Five different times were investigated in this series: 1, 2, 4, 8 and 16 hours. The temperature of 1250 °C and the sulphur dioxide partial pressure of 0.01 atm were used. These conditions were chosen because it was assumed these experimental conditions will be the slowest to equilibrate.

The samples were prepared with the same grinding and polishing method as the main series of experiments described in chapter 4.4 to yield cross sections of both phases. The equilibration time series were analysed with SEM-EDS. Only Co, Ni, Ag, Cu and S were chosen to analyse with the SEM-EDS because they should be found in both phases at a suitably large concentrations for the SEM-EDS to detect. The elements with a large or small distribution ratio will be in low concentration in a certain phase, and thus the results gained for these elements will not be reliable. The SEM-EDS is not as sensitive as the EPMA. The two time-series made are presented in.

Table 8 Equilibration time series 1 and 2 distribution ratios.

Equilibration Time Series Distribution ratios, Series 1					
t (h)	**Co**	**Ni**	**Ag**	**Cu**	**S**
1	0.74	5.59	2.78	1.20	0.03
2	0.66	3.44	2.07	1.20	0.06
4	0.65	6.95	2.31	1.21	0.04
8	0.55	3.08	2.03	1.22	0.03

Series 2					
t (h)	**Co**	**Ni**	**Ag**	**Cu**	**S**
1	0.77	2.90	2.50	1.21	0.01
2	0.54	4.27	2.70	1.21	0.02
4	0.65	4.32	1.52	1.21	0.02
8	0.81	3.65	1.53	1.21	0.01
16	0.65	3.73	1.30	1.22	0.03

With examination of the data from the first series, it was deemed necessary to repeat the equilibration time series. Especially the distribution of nickel at 4 hours gives an unpredicted spike, which can be seen in Figure 32. The second series gives a more stable distribution ratio compared with time.

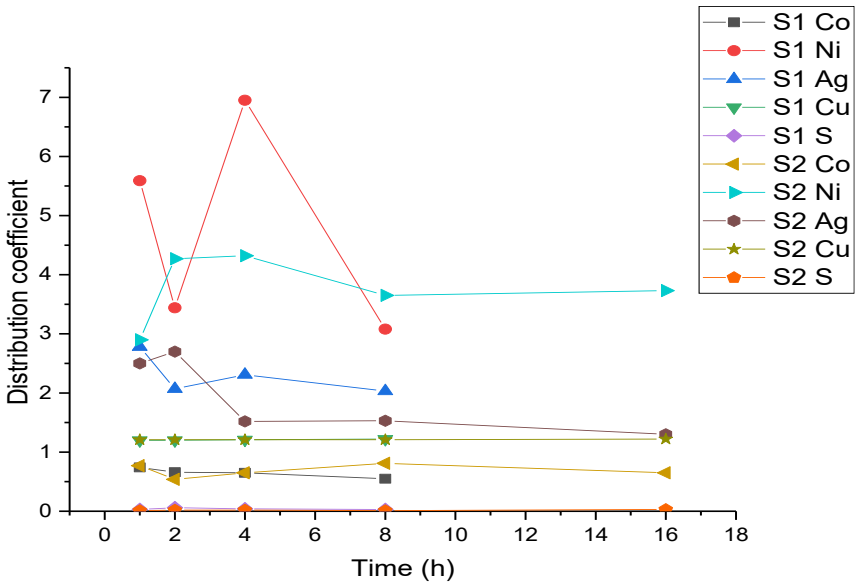

Figure 32 Distribution ratio of Co, Ni, Ag, Cu and S as a function of time, series 1 and 2.

To acquire more reliable results for the distribution ratio of these solute elements, the two series were combined. The data is presented in Table 9.

Table 9 Equilibrium time series data.

	Equilibrium Time Series Distribution ratio (Cu wt.% / Cu_2S wt.%)				
t (h)	**Co**	**Ni**	**Ag**	**Cu**	**S**
1	0.71	4.29	3.46	1.21	0.01
2	0.58	4.38	2.59	1.21	0.03
4	0.74	5.22	1.90	1.21	0.05
8	0.69	3.72	2.29	1.21	0.01
16	0.65	4.43	1.17	1.22	0.02

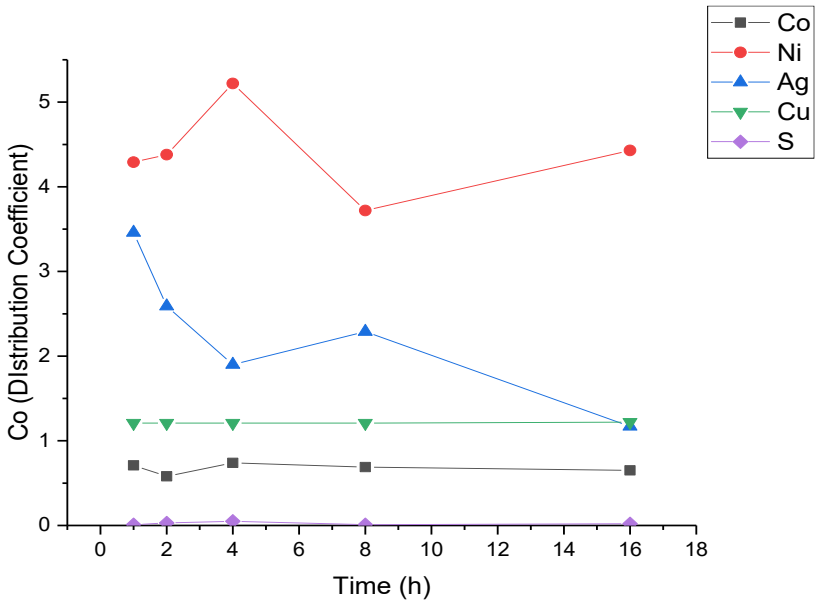

Figure 33 Distribution ratio of Co, Ni, Ag, Cu and S as a function of time.

From the combined graph (Figure 33), it was decided that 16 h was suitable to achieve equilibration for these experiments. $L_{Ag}^{Cu/wm}$ continued to decrease after 8 h. Ag in both phases vaporizes, the vaporization of Ag also factored into the decision as longer equilibrations would mean that concentrations of Ag in both phases would drop to undetectable levels. The distribution coefficients of copper and sulphur remains unchanged from 1 to 16 hours. The distribution coefficient for cobalt also appears to reach the equilibrium by 4 hours, and nickel would seem to reach its equilibrium by 8 hours. This is not immediately obvious from looking at the combined series figure, but observing the second series supports this assessment. The silver distribution coefficient in the system

seems to continue to fall after the 8-hour point. Therefore, the silver distribution ratio change dictated the choice of the 16 h equilibration time.

The SEM-EDS detection limit is based on whether the concentration peaks corresponding to the element in question can be significantly determined from the background fluctuations. The detection limit is also generally taken when the elemental concentration peak is three times the background count. In PPM this is in the range of 1000 to 3000 PPM. This detection limit can be the reason to some of the results collected here.

4.12 Practicalities

One series of experiments was carried out at each temperature and partial pressure. A second series of experiments was carried out that only consisted of the extrema points from the first series plus a mid-point. This can be seen in Figure 34.

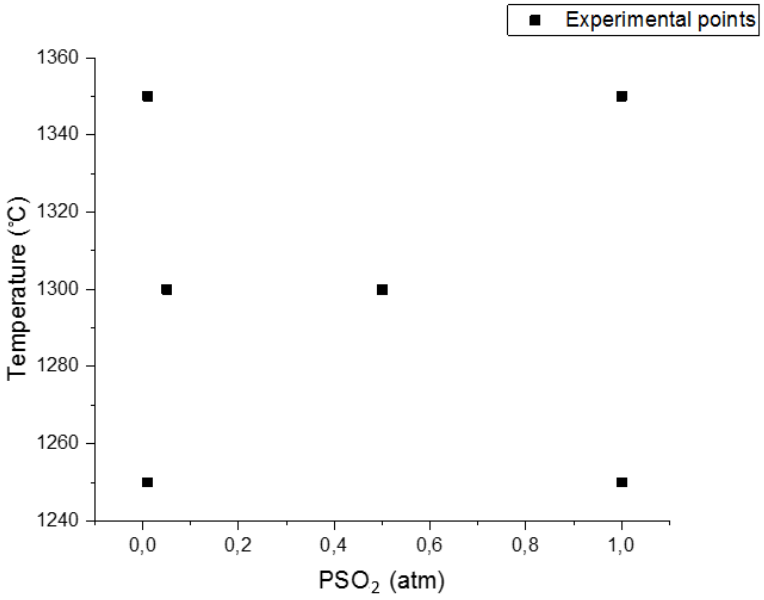

Figure 34 Representation second series of experiments.

The test apparatus was first prepared before each of the equilibration series of experiments. Between each experiment the exhaust gas pipes were checked for blockages, which could cause problems later on during the experiment as they can blow out another section of the gas path meaning that the reaction gas would not pass the sample.

The pre-weighed sample materials were placed into cut and cleaned crucible cups. The samples were made up of 0.1 g of the master alloy and 0.1 g of Cu_2S. The crucible cups were made from zirconia and cut to size with a diamond edged cutting wheel. The inside surface

of the crucible cup was cleaned with a diamond tip drill bit by eroding the outer most layer. This was done to ensure that there were no contaminate materials entering the test environment.

The sample and the crucible were loaded into a wire basket that was built specifically to hold the crucible in the work tube. The sample, the crucible and the holder are presented in Figure 35.

In the Cu-S system there are two immiscible liquid phases in contact with each other. These phases are also in contact with a solid phase, which is the crucible material. It is assumed that no reactions take place between the crucible material and the liquid phases.

Figure 35 Sample, crucible and holder prior to experimentation.

The holder was constructed from platinum, because it will remain solid and unreactive at the working the temperatures. The suspension wire was lowered to the bottom of the work tube. A hook was made in the end of the suspension wire so that the holder could be attached to it. A small alumina tube was made to separate the platinum basket wire and the platinum suspension wire as it was possible for the two wires to sinter together at the elevated temperatures of the experiments. This small tube can be seen in Figure 35, It is constructed and placed where it is because it means that the suspension wire and the wire that the wire

holder is made from cannot come into contact and sinter together once in the hot zone of the furnace.

The sample in the holder was raised into the cold zone within the work tube by carefully pulling the suspension wire, and then the work tube was sealed with a rubber bung. Next the gas atmosphere of the specific partial pressure of sulphur dioxide was stabilized within the work tube for roughly 15 minutes. It was possible to observe through the bubble lock if the reactant gas was passing through the work tube. After the gas atmosphere had been stabilised, the sample was raised to the hot zone.

After 16 hours, the samples were quenched into ice-cold water. The quenching media was prepared from an ice and water mixture, which was blended together. This mixture was placed into a plunge bath which was suspended around the base of the work tube so that the end of it was fully submerged in the quenching media. The rubber cork was then removed, because it keeps the reactant gas atmosphere and the atmosphere outside the system separate. After 16 hours the suspension wire was pulled from the top of the furnace, which forced the hook to uncurl. The sample and crucible were dropped through the work tube and rapidly quenched into the quenching media below. The work tubes atmosphere was then replaced with argon, which took roughly 15 minutes.

4.13 Sample Analysis

After the quenching of the sample, the samples were dried in atmospheric conditions. The samples were set into epoxy and cross sections of the samples were made. They revealed both phases so that they both could be analysed with SEM-EDS and EPMA. The polishing quality was checked with an optical microscope to see if the artefacts of the grinding and polishing process had been suitably removed from the surface of the samples.

The samples were initially examined under the SEM-EDS, which was used to find suitable areas on the sample surface in both of the phases. Eight points were analysed from each phase on each sample by the EPMA, giving a total of 16 examination points per sample. The largest spot size was chosen for the EPMA wherever possible to give results that are more representative of the phase being analysed. However, a smaller spot size was used when these areas on the samples surface had an increased density of the larger inclusions with the aim to give a more representative analysis. The inclusions of one phase in the other are assumed to be artefacts occurring during quenching.

The raw data as received by the EPMA is available in appendix 2, and the analysing conditions for the EPMA measurements are displayed in Table 10. The beam diameter is smaller at some certain points in certain samples in order to avoid inclusions and improve the accuracy of the results for those points.

Table 10 EPMA conditions

Phase	**Acceleration voltage**	**Beam Current**	**Beam Diameter**
Cu	20 kV	60 nA	20–100 µm
Cu_2S	20 kV	60 nA	20–100 µm

Table 11 and Table 12 show the estimated detection limits for the EPMA for each of the elements measured in each phase. The values given are the average from both sets of experiments. The concentration value in ppm for each element given in Table 11 and Table 12 is the lowest level at which each element can be called a reliable measurement. As long as the concentration in the phase is above this value, the measurement is considered reliable.

Table 11 Detection limits of the EPMA in the Cu phase

Detection limit for each phase (ppm)									
Element	**Cu**	**S**	**O**	**Fe**	**Co**	**Ni**	**Pd**	**Ag**	**Au**
Cu	347	147	1061	176	178	260	171	355	553
Cu_2S	335	147	1248	182	187	257	171	347	534

5 Results

In this chapter, the results acquired from the EPMA are presented in graphs as functions of temperature and sulphur dioxide partial pressure and as functions of both. The trends of these graphs are then discussed. The distribution coefficients presented in this chapter are taken from normalized compositions of both metal and white metal phases. The raw data is available in appendix 2.

5.1 Microstructure / Micrographs

First micrographs were made for each sample. Figure 36 is an example micrograph of a sample at 1350 °C and at 0.1 atm P(SO_2). The metal phase appears the lightest in colour. The white metal phase is identified, as it appears darker in colour than the white metal phase.

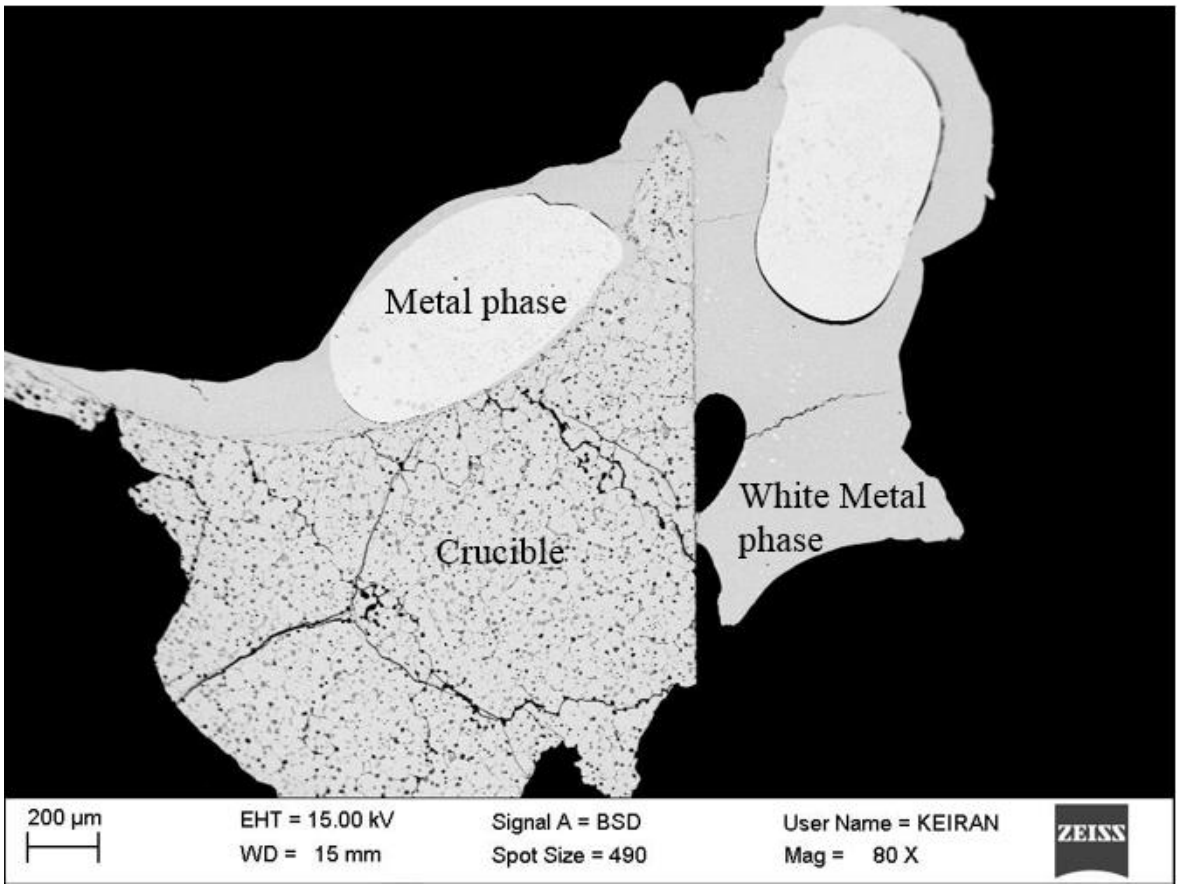

Figure 36 SEM micrograph of a sample at 1350 C and 0.1 atm P(SO_2), showing metal phase (lightest in colour), white metal phase (darker grey areas) and the crucible material (area with cracks and pit marks).

The crucible material is easily recognisable by its cracked and pitted surface. Suitable locations were determined by SEM-BSD imaging for the EPMA analysis to give a more representative data of the composition of each phase were to be taken from between the larger inclusions. Both phases seem to have many inclusions of the other phase. An example of these larger inclusions can be seen in Figure 36. This may also be an artefact of the quenching.

5.2 Solute Elements in the Metal – White Metal System

The distribution coefficient of the solute elements was calculated from the average composition values as reported by the EPMA analysis from each phase within one sample. The raw data and the calculated averages as well as the distribution coefficients are presented in appendix 2. The calculations for the distribution coefficients were made using equation (51).

$$L_X^{metal/white\ metal} = \frac{(Wt\%\overline{X})}{[Wt\%\overline{X}]} \tag{51}$$

In the above equation X stands for each individual solute element (Co, Ni, Pd, Ag, Au and Fe), and wt. % for weight percentage.

Error bars were calculated based on the standard deviations and mean values for each variable at each experimental point (52).

$$\frac{\Delta L_x}{L_x} = \left(\frac{\Delta x}{\overline{x}}\right) + \left[\frac{\Delta x}{\overline{x}}\right] \tag{52}$$

Equation (52) was used to calculate the error for the distribution coefficient. Δx is the standard deviation for the element, and $\overline{x}$ is the average value for the wt. % of the element. The error calculations are included in appendix 2.

5.3 Detection Limits for the Solute Elements Distribution Coefficient

Some of the distribution coefficients reported in this work are limited by the detection limitation of the EPMA. Though articles site a higher distribution coefficient than what is reported in this work, the EPMA limitations were used to calculate the distribution coefficient. Therefore the reported distribution coefficients will be lower than in previous articles for certain elements. The distribution coefficient limitation has been given as a detection limit range. When the reported EPMA results are below the detection limit, the

EPMA detection limit is given in place of the EPMA results, and the EPMA detection limit is used in the calculations for the distribution coefficients for those results below the EPMA detection limit.

The Co and Ni concentrations in both phases were above the detection limits for the EPMA. Ag had minimum concentrations below the detection limits of the EPMA, and the Pd minimum value in the Cu_2S phase was below the detection limits. The concentration results from EPMA of Au in the Cu_2S phase were below the detection limit.

5.4 Solute Element Distribution Coefficients

In the next few sub-chapters the results from the EPMA are presented and the distribution ratios are calculated and presented, and the trends these results are shown.

5.5 Cobalt Distribution Coefficient between Metal and White Metal Phases

Cobalt shows a dependence on sulphur dioxide partial pressure. In Figure 37 it can be seen that the wt. % of Co in the metal phase decreases as the $P(SO_2)$ increases, decreasing from 0.4 wt. % at 0.01 atm $P(SO_2)$ to a range of 0.08 to 0.12 wt. % at 1 atm $P(SO_2)$. The error bars (based on the standard deviations) do not disagree with the $P(SO_2)$ trend, except at 1300 °C and 1 atm $P(SO_2)$.

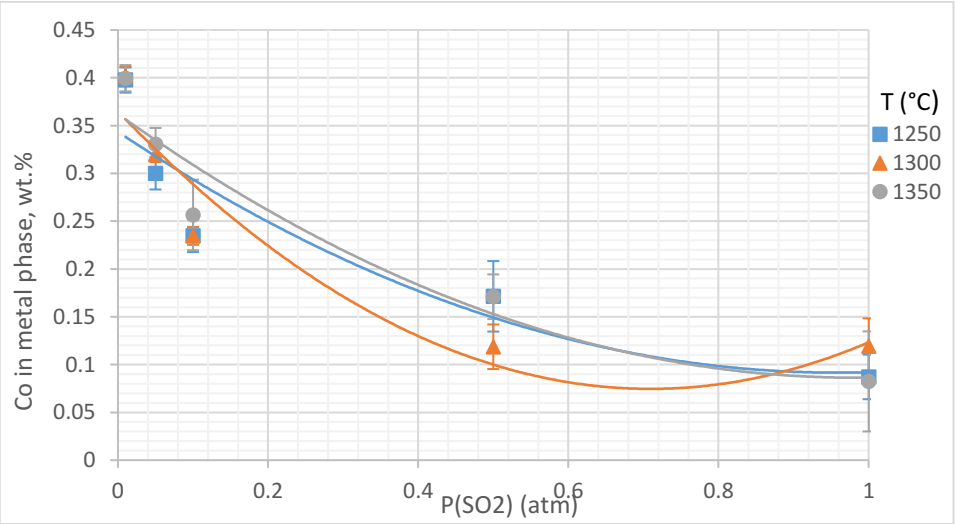

Figure 37 Concentration of Co in the metal phase, wt. % as function of $P(SO_2)$ at 1250 °C, 1300 °C and 1350 °C.

The wt. % of Co in the white metal phase in Figure 38 increases with increasing $P(SO_2)$, rising from a range of 0.46 wt. % at 0 $P(SO_2)$ at 1250 °C and 1300 °C to a range of 0.55 to 0.57 at 1 atm $P(SO_2)$. The concentration however falls at 1350 °C from 0.51 wt. % at 0.01 atm $P(SO_2)$ to 0.3 wt. % at 1 atm $P(SO_2)$. The concentration fall at 1350 °C affects $L_{Co}^{Cu/wm}$ as the concentrations in the metal phase fall as a function of $P(SO_2)$ at all temperatures, as can be seen in Figure 37. This fall at 1350 °C could also be due to the volatility of Co. The standard deviation at 0.5 atm $P(SO_2)$ and 1350 °C is very large. It can be seen from the error bars that increasing the temperature decreases the Co in the white metal phase, but also that $P(SO_2)$ could have no effect in the white metal phase.

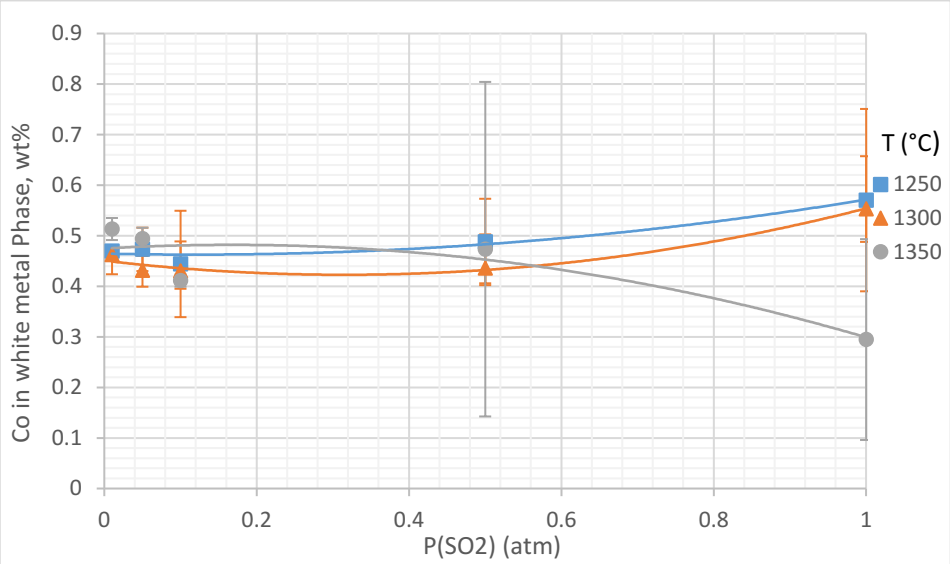

Figure 38 Concentration of Co in the white metal phase, wt% as function of $P(SO_2)$ at 1250 °C, 1300 °C and 1350 °C.

From Figure 39 it can be seen that higher cobalt distribution coefficient is affected by the sulphur dioxide partial pressure. The coefficient increases with decreasing $P(SO_2)$. At 0.01 atm $P(SO_2)$ the distribution ratio is in the range of 0.77 to 0.86 wt. % compared to 1 atm $P(SO_2)$, which is in the range of 0.15 to 0.27 wt. %. The temperature appears to have little or no effect on the distribution coefficient. At high $P(SO_2)$ (from 1 atm to 0.1 atm) the distribution coefficient increases as a function of temperature, while at lower $P(SO_2)$ (from 0.01 to 0.05 atm) the distribution coefficient decreases as a function of temperature. Error bars in Figure 39 do not seem to disprove the $P(SO_2)$ trend, whereas error bars can cover any perceived trend as a function of temperature.

In all experiments cobalt is more concentrated to the white metal phase, which is proven across Figure 37 to Figure 40. The distribution coefficient of Co approaches unity closer to the lower $P(SO_2)$.

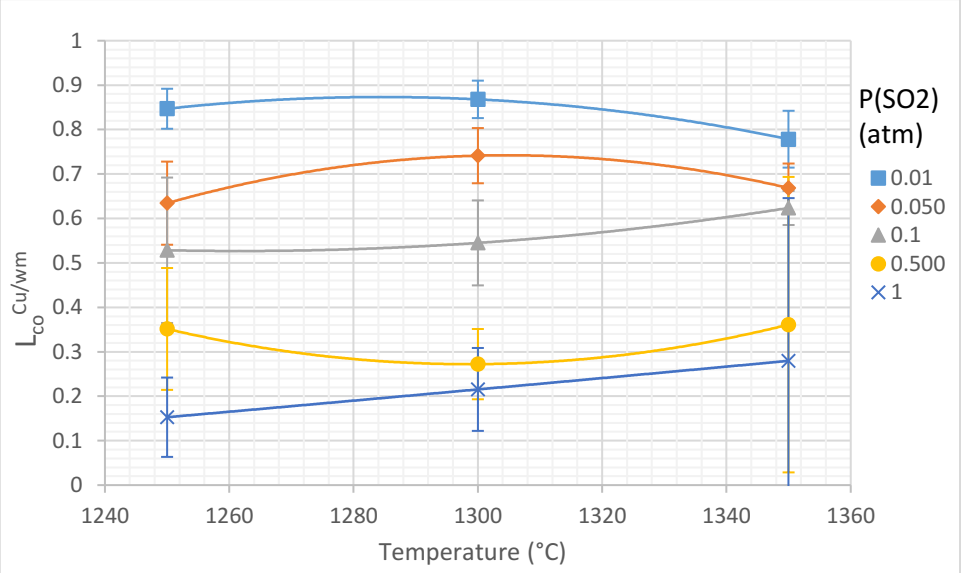

Figure 39 Distribution coefficient of Co as a function of temperature

In Figure 40, the $P(SO_2)$ effects can be seen. The distribution coefficient decreasing as $P(SO_2)$ increases. The temperature effects are not easily determined from this figure.

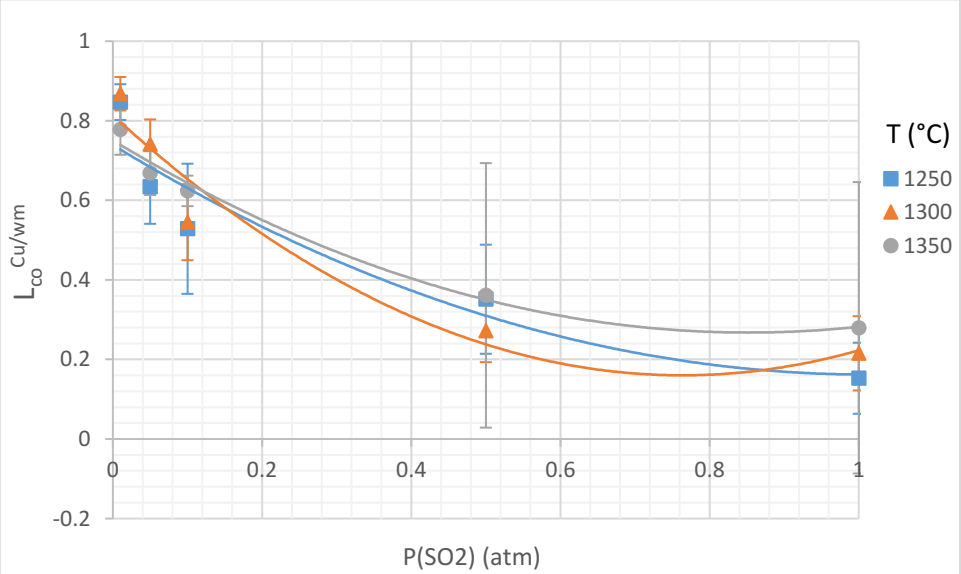

Figure 40 Distribution coefficient of Co as a function of $P(SO_2)$

The combined effects of temperature and $P(SO_2)$ are presented in Figure 41. The contour plots show that $P(SO_2)$ has a larger effect than temperature, the distribution coefficient

increases with increasing $P(SO_2)$ and that it approaches unity at 0.01 atm $P(SO_2)$. The right side of Figure 41 shows the repetition series of experiments, and it can be seen that the data is in agreement with the main series experiments as the cobalt distribution is higher at lower $P(SO_2)$ similarly.

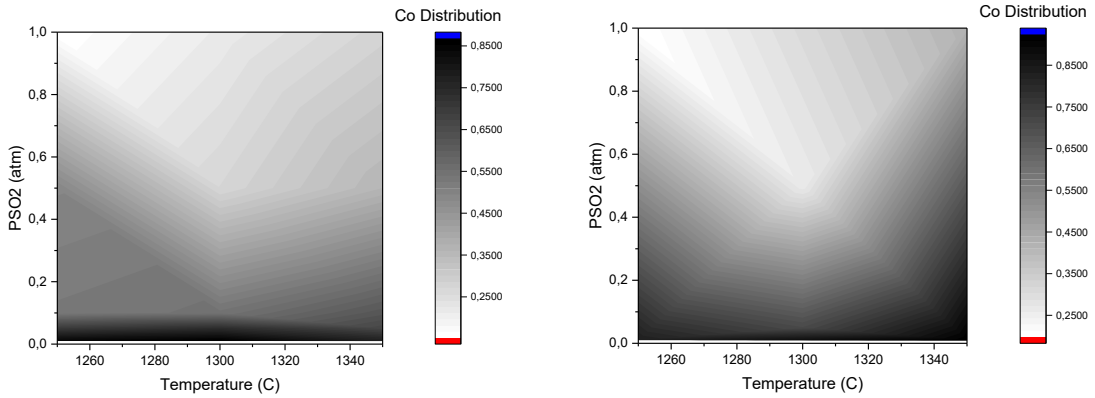

Figure 41 Contour plot of Co distribution coefficient as function of $P(SO_2)$ and temperature, main series left, repetition series right.

5.6 Nickel Distribution Coefficient between Metal and White Metal Phases

The distribution coefficient of Ni between metal and white metal is dependent on both temperature and $P(SO_2)$.

As can be seen in Figure 42, the Ni concentration in the metal phase drops as a function of $P(SO_2)$, falling from a range of 0.69 to 0.72 wt. % at 0.01 atm $P(SO_2)$ to a range of 0.55 to 0.63 wt. % at 1 atm $P(SO_2)$. The temperature effects are also visible in this figure, but they appear to be compounded with the effects of $P(SO_2)$. At low $P(SO_2)$, the concentration increases as the temperature increases. At high $P(SO_2)$, decreasing the temperature increases the concentration. The error bars shown in the graph appear not to disagree with the Ni trend as a function of $P(SO_2)$. At 1 atm it appears that the error bars do not disagree with the trend that increasing temperature decreases Ni concentration in the metal phase. Below 0.5 atm $P(SO_2)$, the error bars could account for the flipped temperature trend, which could mean that across all partial pressures of SO_2 increasing temperature decreases Ni concentration in the metal phase.

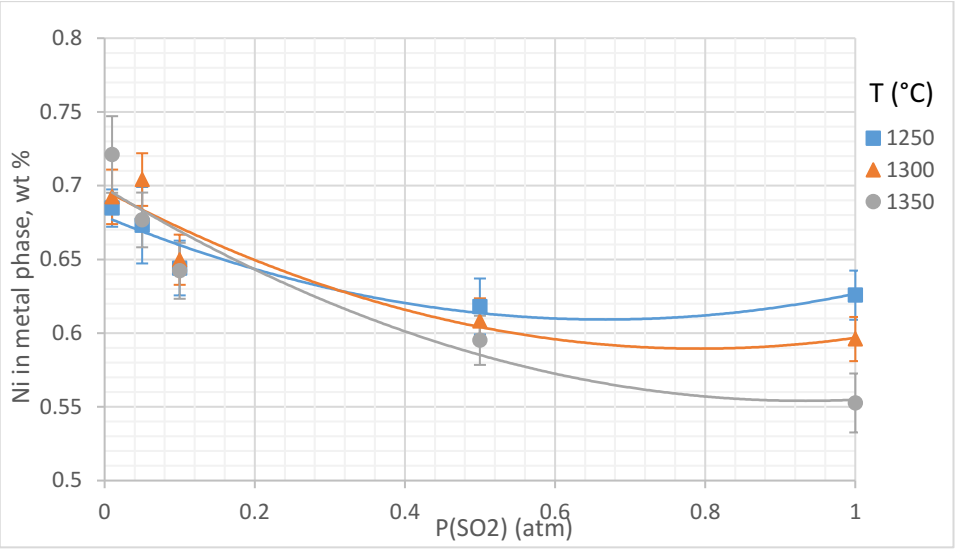

Figure 42 Concentration of Ni in the Cu Phase, wt. % as function of $P(SO_2)$ at 1250 °C, 1300 °C, 1350 °C.

Figure 43 shows the wt. % of nickel in the white metal phase. The behaviour of the wt. % of Ni in the white metal depends on both the temperature and $P(SO_2)$. At 1250 °C the wt. % of Ni reaches an equilibrium of around 0.3 by 0.1 atm $P(SO_2)$, at 1300 °C the wt. % of Ni increases as a function of $P(SO_2)$. At 1350 °C the wt. % increases initially from 0.195 to 0.319 from 0.01 to 0.1 atm $P(SO_2)$, but after this the wt. % decreases 0.105 wt. % at 1 atm $P(SO_2)$. The error bars show that the concentration of Ni in the white metal phase decreases with increasing temperature across all partial pressures of SO_2.

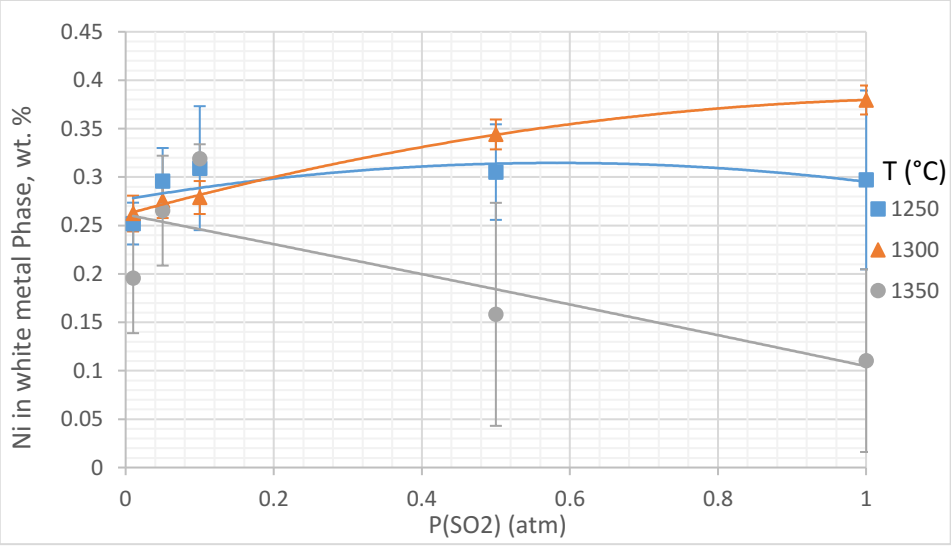

Figure 43 Concentration of Ni in the white metal Phase, wt. % as function of $P(SO_2)$ at 1250 °C, 1300 °C and 1350 °C.

The Ni concentration in the white metal phase at 1350 °C from 0.5 to 1 atm $P(SO_2)$ is exceptionally low. This could be due to vaporisation of Ni at this elevated temperature.

The results for the nickel distribution coefficient are presented here. The results show a dependence on sulphur dioxide partial pressure as well as a dependence on temperature. In all experiments nickel is more concentrated to the metal phase.

In Figure 44, the distribution coefficient is shown as a function of temperature. The figure shows that the spread of the distribution coefficient values increases as the temperature increases, 0.7 range at 1250 °C to 3.17 at 1350 C. This could be due to the compounding effects of $P(SO_2)$ but it is not obviously observed from this figure. What can be seen is that at 1250 °C the distribution ratio at 0.01 atm $P(SO_2)$ is 2.7, which decreases with increasing $P(SO_2)$ to 2.0 at 1 atm $P(SO_2)$. At 1350 °C the highest distribution coefficient is 5.17 at 1 atm $P(SO_2)$, which decreases to 2.01 at 0.1 atm $P(SO_2)$. The error bar at 1350 °C show that the increase of $L_{Ni}^{Cu/wm}$ at 0.1 to 1 atm could be caused by the wide standard deviations of the points.

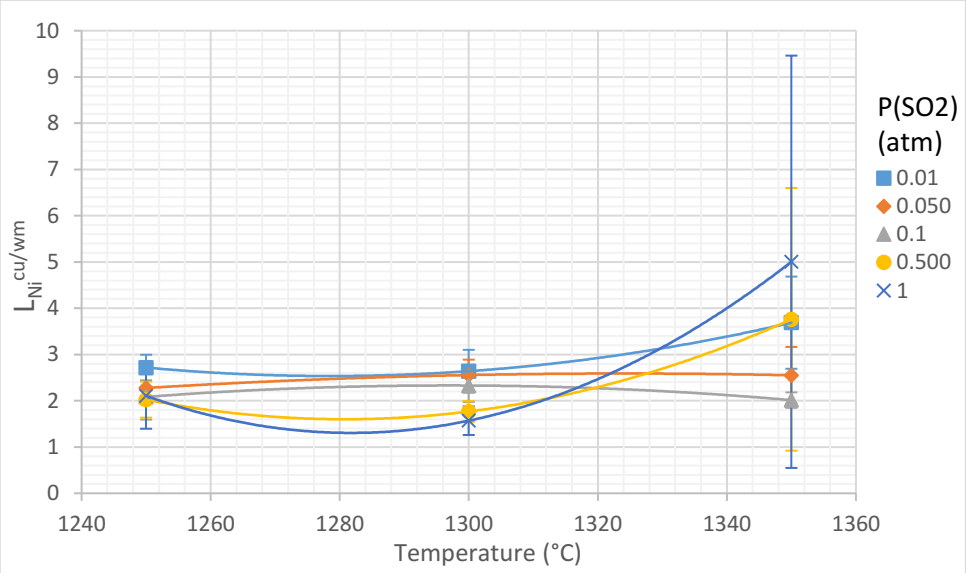

Figure 44 Distribution coefficient of Ni as a function of temperature

Figure 45 shows the functional dependency of temperature on the distribution coefficient of nickel. It can be seen that 1350 °C has the highest distribution only after 0.1 atm $P(SO_2)$ where the distribution coefficient increases rapidly. At 1250 °C and 1300 °C, the distribution coefficient appears to decrease with increasing $P(SO_2)$. The comparatively large increase of $L_{Ni}^{Cu/wm}$ at 1350 °C could also be due to the wide standard deviations at 0.5 and 1 atm $P(SO_2)$.

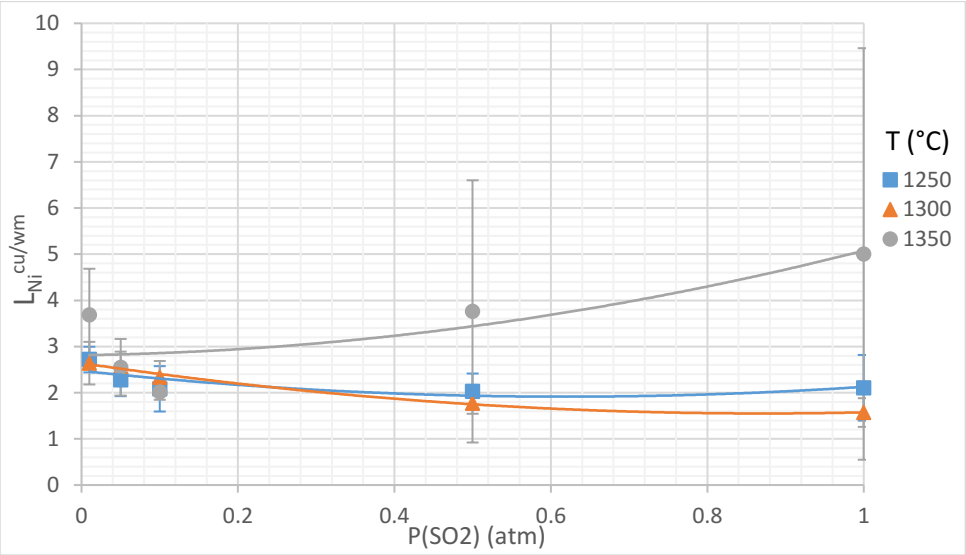

Figure 45 Distribution coefficient of Ni as a function of $P(SO_2)$

The combined effects of temperature and $P(SO_2)$ can be seen from Figure 46. The contour plots show that nickel has the highest distribution coefficient at 1350 °C and 1 atm $P(SO_2)$ and decreasing across in both x and y directions to 1250 °C and to 0.01 atm $P(SO_2)$, which has the lowest distribution ratio. There is a second peak at 1350 °C and 0.01 atm $P(SO_2)$, but this is probably due to experimental error. The right side of the figure shows the repetition series of experiments and reveals that this second set of data is in agreement with the main series experiments as the nickel distribution is higher at the higher $P(SO_2)$ and temperature similarly.

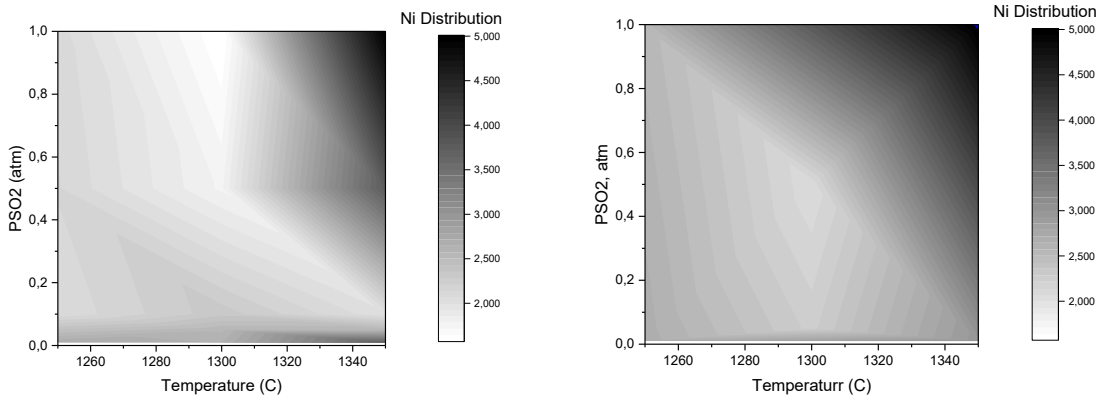

Figure 46 Contour plot of Ni distribution coefficient as function of $P(SO_2)$ and temperature, main series left, repetition series right

5.7 Palladium Distribution Coefficient between Metal and White Metal Phases

In this section, distribution of palladium between metal and white metal phases is described. Palladium distribution between metal and white metal phases is affected by $P(SO_2)$. Palladium in all experiments is more concentrated to the metal phase despite the conditions of the temperature and $P(SO_2)$.

The Figure 47 shows the Pd concentration in the metal phase. At 1250 °C the concentration decreases as a function of $P(SO_2)$. However, at 1300 °C and 1350 °C, the concentration increases between 0.5 and 1 atm $P(SO_2)$. Figure 47 also shows that the concentration of Pd in the metal phase is affected by temperature. Increasing the temperature decreases the concentration of Pd in the metal phase. The concentration is 0.89 wt. % at 0.01 atm $P(SO_2)$ for 1250 °C to 1350 °C. At 1350 °C the concentration falls to 0.65 wt. % at 1 atm $P(SO_2)$. At 1300 °C the concentration of Pd in the metal phase falls to a minimum point of 0.76 wt. % at 0.5 atm $P(SO_2)$. At 1350 °C, the concentration of Pd falls to a value of 0.83 wt. % at 0.1 atm $P(SO_2)$, but the concentration increases again to 0.94 wt. % at 1 atm $P(SO_2)$.

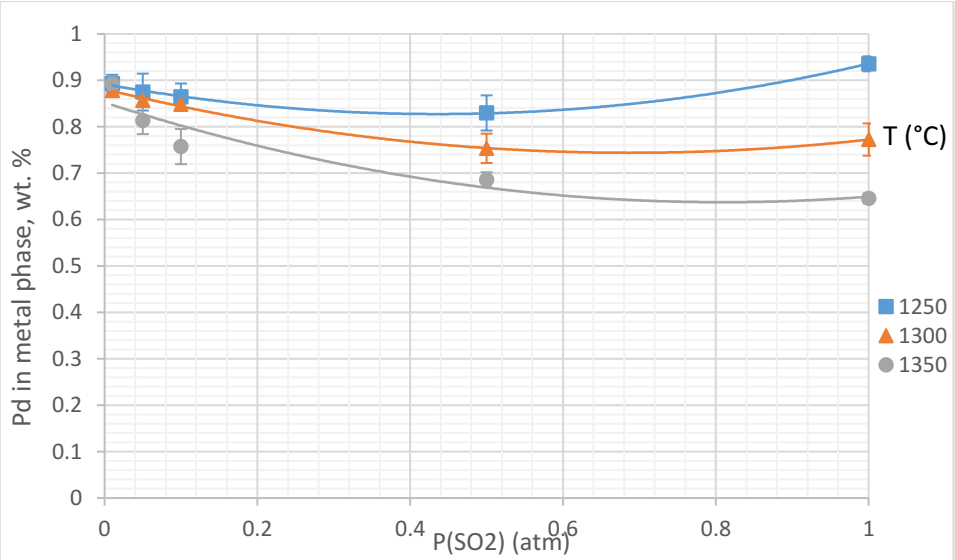

Figure 47 Concentration of Pd in the metal phase wt. % as function of $P(SO_2)$ at 1250 °C, 1300 °C and 1350 °C

Figure 48 shows the wt. % of Pd in the white metal phase. It can be seen that the wt. % of Pd is higher at the lower concentrations of $P(SO_2)$ (0.01 to 0.1 atm) ranging from 0.012 to 0.023 at 0.01 to 0.1 atm $P(SO_2)$ the wt. % ranges from 0.03 to 0.017. At 0.5 atm and 1 atm $P(SO_2)$, the wt. % is lower, with a range of 0.0017 to 0.005 at 1 atm $P(SO_2)$. The detection limit value is 0.0171 wt. % which is marked by the black line across the graph. Many of the values here reach that limit. The actual concentration as reported by EPMA are presented on the graph as 1250* °C, 1300* °C and 1350 * °C. As most of these values fall below the detection limit, they are not considered reliable. Error bars have been added to the results though as most results are below the EPMA detection, no trends can be seen.

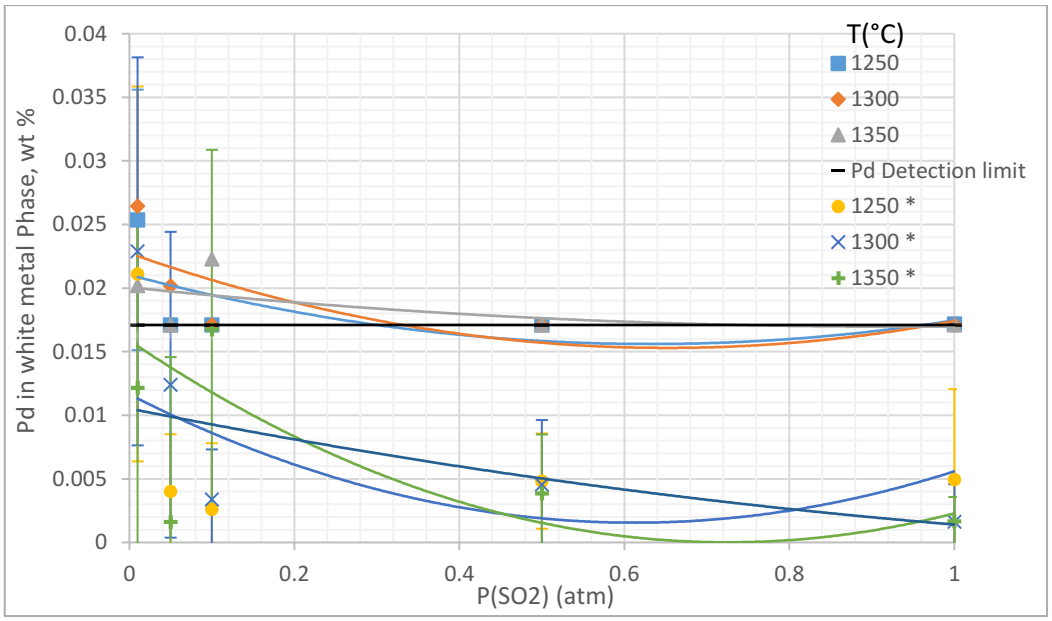

Figure 48 Concentration of Pd in the white metal phase, wt. % as function of $P(SO_2)$ at 1250 °C, 1300 °C, 1350 °C

In Figure 49, the distribution coefficient is shown as a function of temperature. The results for Pd distribution show a dependency on $P(SO_2)$ and a dependency on temperature. The distribution coefficient ranges from 33 to 55. The distribution coefficient appears to decrease as a temperature increases; however, at the lower $P(SO_2)$ of 0.01 and 0.05 atm, the distribution coefficient increases again after 1300 °C. Error bars on the figure show that the trends could be misrepresented, but they still show that there could be a clearer dependence on $P(SO_2)$.

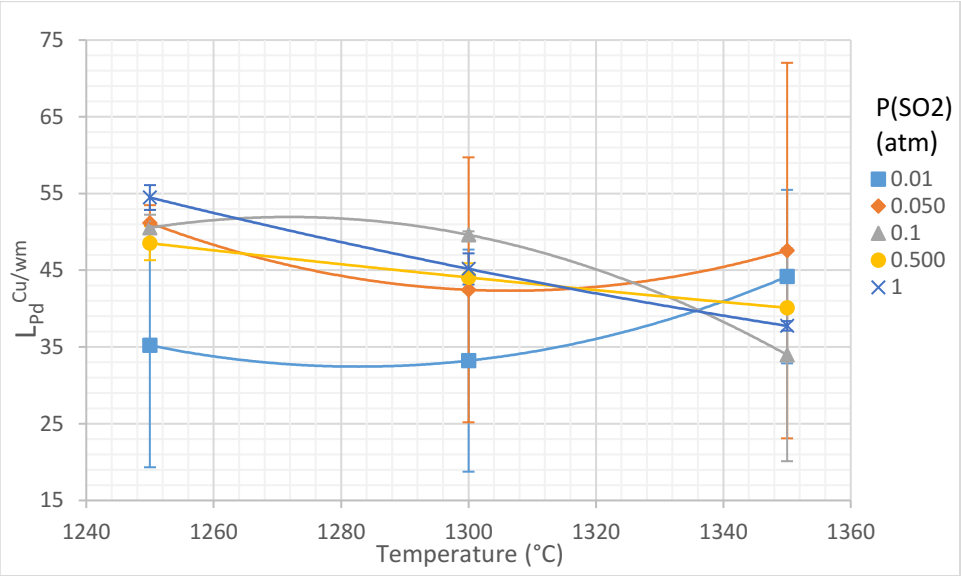

Figure 49 Distribution coefficient of Pd as a function of temperature

In Figure 50 the palladium distribution coefficient can be seen to be affected by $P(SO_2)$. At 1250 °C and 1300 °C the distribution coefficient increases with the increase of the $P(SO_2)$. However, at 1350 °C the distribution of Pd decreases with increasing $P(SO_2)$. At 0.01 atm $P(SO_2)$ the distribution coefficient is highest at 1350 °C. The standard deviations for results between 0.01 and 0.1 atm $P(SO_2)$ are larger than those at 0.5 to 1 atm. This uncertainty could mean that $L_{Pd}^{Cu/wm}$ is only a function of temperature and not $P(SO_2)$.

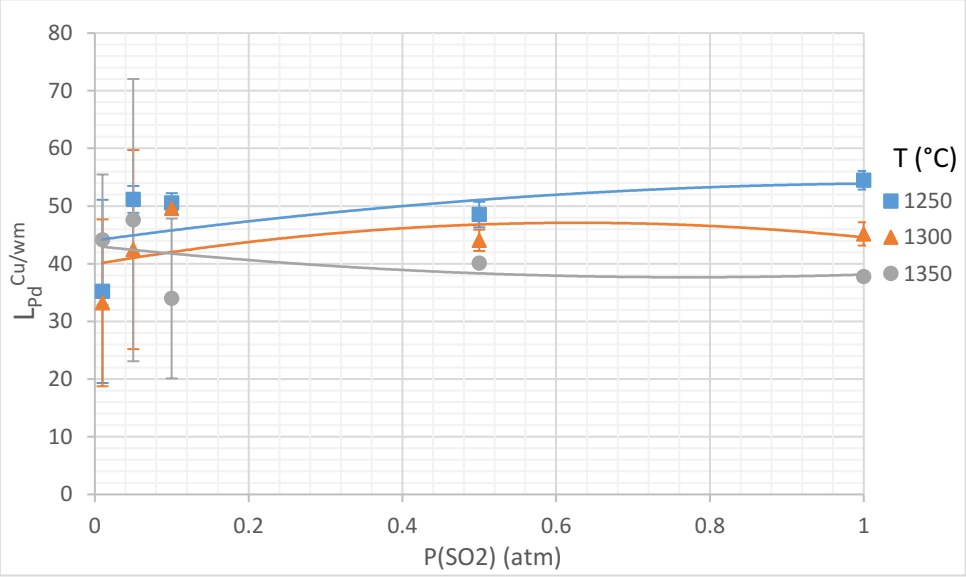

Figure 50 Distribution coefficient of Pd as a function of $P(SO_2)$

Figure 51 shows the combined effects of $P(SO_2)$ and temperature on the palladium distribution coefficient. The left side shows the main series of experiments. The palladium

is most highly concentrated to the metal phase at 1250 °C to 1300 °C and between 1 atm and 0.1 atm $P(SO_2)$ with a ratio of 54.5 to 45. Both temperature and $P(SO_2)$ seem to have an effect on the distribution coefficient. The highest concentration appears in the top right of the graph. However, there is another peak of higher distribution coefficients that runs through the centre of the graph. The right side of Figure 51 is the repetitious series of experiments. It can be seen that the highest concentration is at 1 atm $P(SO_2)$ with a distribution ratio ranging from 53.5 to 47.2. The repetitious series is in agreement with the main series of experiments, and the partial pressure of sulphur dioxide effects the distribution coefficient. Temperature has no effect on the distribution coefficient. The highest concentration to the metal phase is at 1 atm $P(SO_2)$ and the lowest distribution coefficient is at 0.01 atm (47.2 to 36.9).

The anomalous results at 0.05 to 0.1 atm $P(SO_2)$ peak does not appear in the repetitious series.

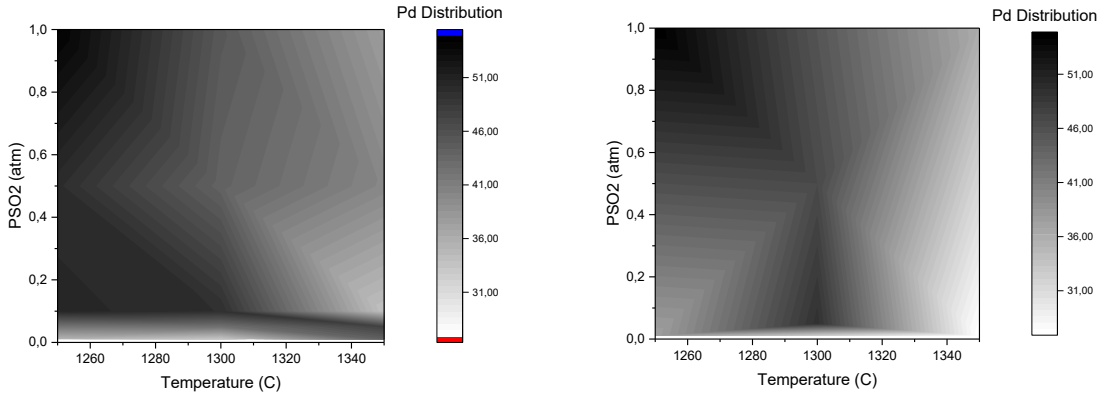

Figure 51 Contour plot of Pd distribution coefficient as function of $P(SO_2)$ and temperature, main series left, repetition series right

5.8 Silver Distribution Coefficient between Metal and White Metal Phases

The results show both a dependency on sulphur dioxide partial pressure as well temperature on the distribution coefficient. The distribution coefficient ranges from 0.144 to 3.3.

Ag is the most volatile element under those being investigated. The concentrations of silver in both phases decrease as temperature increases. Figure 52 shows the concentration of silver

in the metal phase. In this figure, the effect of temperature can be seen. At 1250 °C and 1300 °C the concentration increases as the $P(SO_2)$ increases.

However, at 1350 °C the concentration values are at the threshold or below the EPMA detection limit. The concentration values below 0.1 atm $P(SO_2)$ fall below the detection limit, and the values above 0.1 atm $P(SO_2)$ are close to the detection limit. This means that these values are less reliable than those reported at 1250 °C and 1300 °C. The vaporisation of Ag becomes more apparent and more problematic at 1350 °C. The standard deviations appear not to disagree with the temperature dependency, but those values at 1350 °C close to or at the detection limit are obscured by the detection limit.

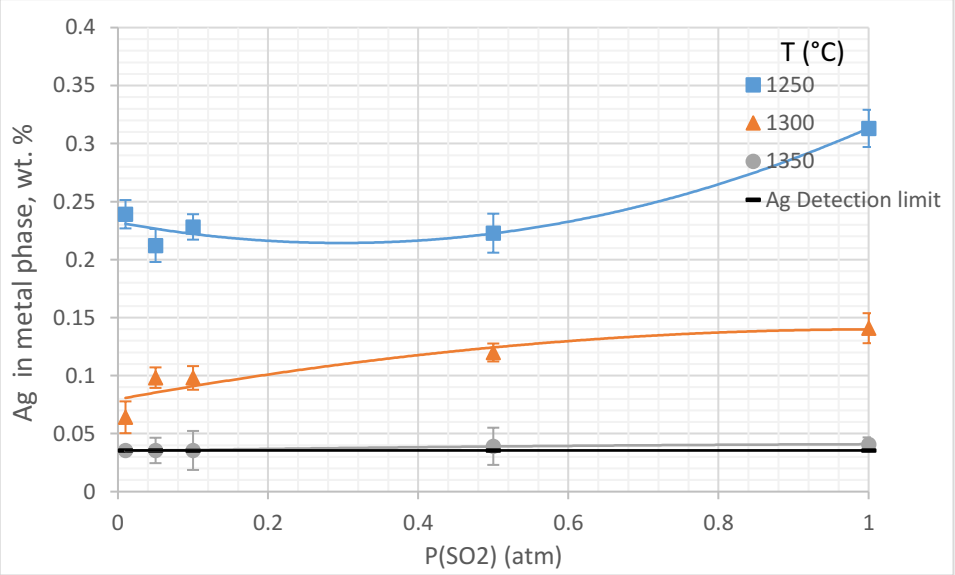

Figure 52 Concentration of Ag in the metal phase, wt. % as function of $P(SO_2)$ at 1250 °C, 1300 °C, 1350 °C

The wt. % concentration of silver in the white metal phase is shown in Figure 53. Again, the effects of temperature on the wt. % of silver in the phase are prevalent. The concentration decreases as temperature increases. At 1250 °C, the concentration also decreases with increasing $P(SO_2)$. However, at 1300 °C and 1350 °C the concentration increases with increasing P (SO_2). The concentration values at 1350 °C are close to the detection limit, but still above it, though the error estimation calculations at 0.01 to 0.1 atm $P(SO_2)$ fall below the detection limit. The standard deviation at 1 atm and 1250 °C to 1300 °C could be the explanation to the apparent $P(SO_2)$ dependency at 1 atm.

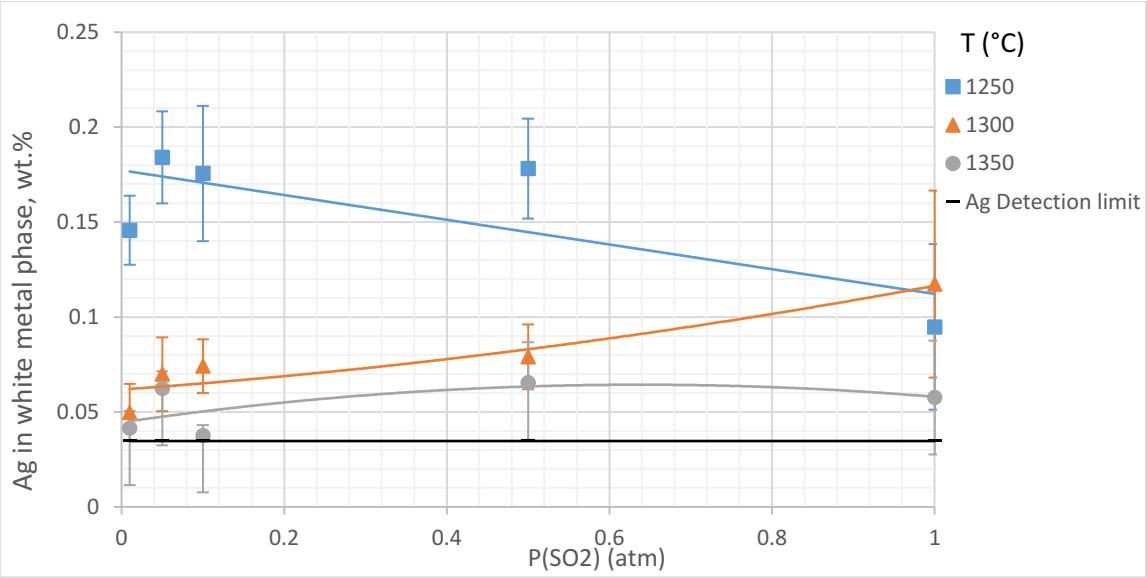

Figure 53 Concentration of Ag in the white metal phase, wt. % as function of $P(SO_2)$ at 1250 °C, 1300 °C and 1350 °C

In Figure 54, the distribution coefficient of silver is shown as a function of temperature. The distribution of Ag decreases as a function of increasing temperature. The distribution coefficient decreases from a range of 1.25 to 3.3 at 1250 °C to a range of 0.59 to 0.95 at 1350 °C. At 1250 °C and 1300 °C, Ag is more concentrated to the metal phase. At 0.01 atm $P(SO_2)$ and 1250 °C there is a large peak. However, at each different $P(SO_2)$, the distribution falls below 1 and is more concentrated to the white metal phase between 1300 and °C 1350 °C. The error bars on this graph show that the $L_{Ag}^{Cu/Wm}$ is more clearly dependant on $P(SO_2)$, but the overall temperature dependency does not seem to be contradicted by the error bars.

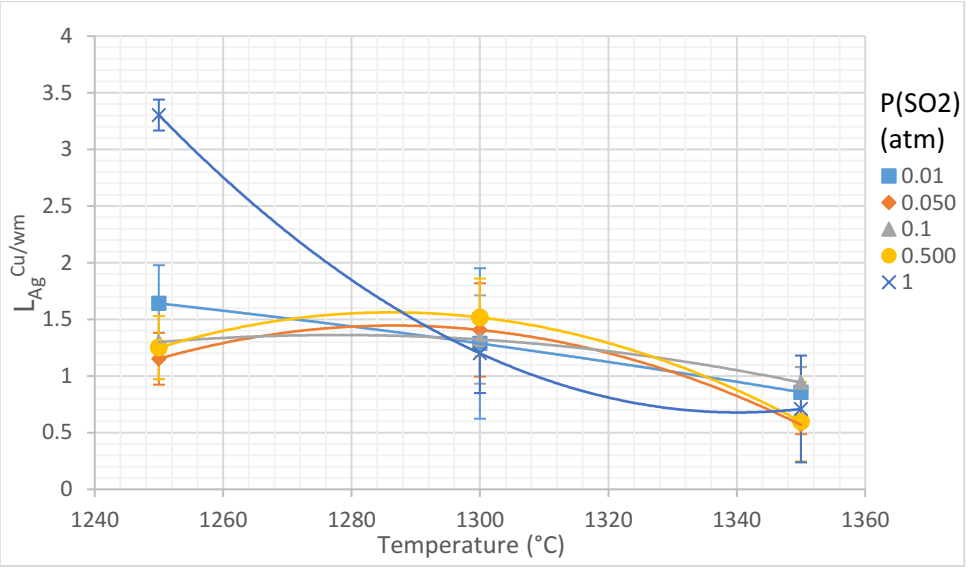

Figure 54 Distribution coefficient of Ag as a function of temperature

When looking at Figure 55, the effects of $P(SO_2)$ on Ag distribution coefficient can be seen. At 1250 °C the distribution and 1 atm $P(SO_2)$ has the highest tendency to the metal phase, and at 1250 °C the distribution coefficient decreases with decreasing $P(SO_2)$. The effect of $P(SO_2)$ is less evident at 1300 °C and 1250 °C, as it seems that at these temperatures the $P(SO_2)$ has no meaningful effect on the distribution coefficient at 1300 °C and 1250 °C. The error bars show that increasing temperature decreases $L_{Ag}^{Cu/Wm}$ across all partial pressures of SO_2. The error bars can also show that $P(SO_2)$ has no effect on $L_{Ag}^{Cu/Wm}$.

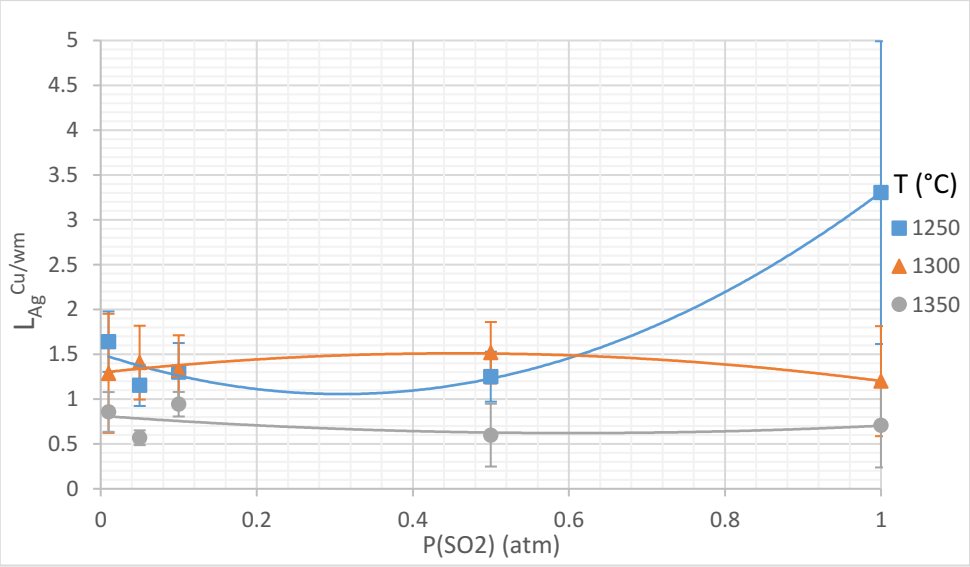

Figure 55 Distribution coefficient of Ag as a function of $P(SO_2)$

Figure 56 show the combined effects of $P(SO_2)$ and temperature on the silver distribution coefficient in contour plots. The left side of Figure 56 shows that the silver is most highly concentrated to the metal phase at 1250 °C and 1 atm $P(SO_2)$ with a ratio of 3.3. The coefficient decreases as the $P(SO_2)$ is held constant but the temperature is increased to 1350 °C to 0.71, also if the temperature is kept constant at 1250 °C and the $P(SO_2)$ is decreased the ratio also decreases to 1.64. It also appears that the general trend for the coefficient is to decrease to its minimum point of 0.72 at the lower right of the figure at 1350 °C and 0.01 atm $P(SO_2)$.

The right side of Figure 56 shows the repetitious series of experiments. It can be seen that the highest concentration is to 1250 °C and 1 atm $P(SO_2)$ of 2.3. The repetitious series is somewhat in agreement with the main series of experiments, as the highest concentration and lower concentration are under the same conditions as the main series. The difference between the two figures is that in the repetition series the highest distribution coefficient is located at 1250 °C and 0.01 to 1 atm $P(SO_2)$ and therefor shows no dependency on $P(SO_2)$.

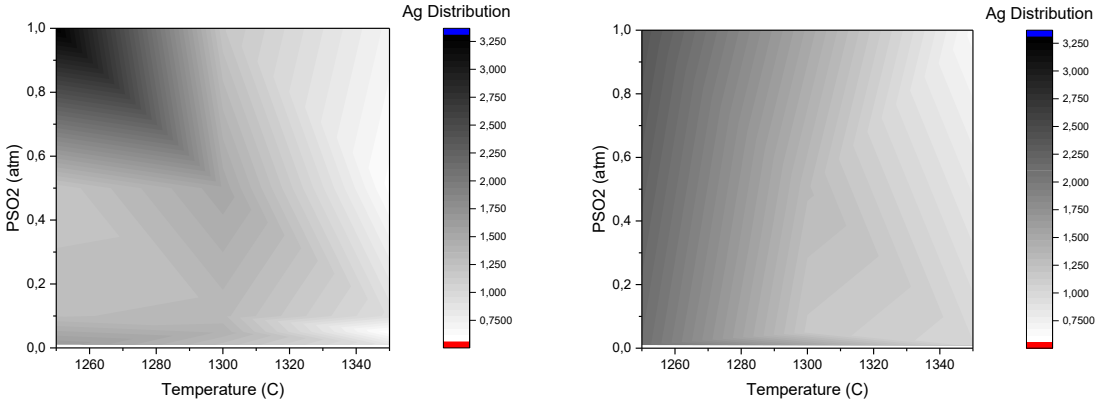

Figure 56 Contour plot of Ag distribution coefficient as function of $P(SO_2)$ and Temperature, main series left, repetition series right

5.9 Gold Distribution Coefficient between Metal and White Metal Phases

The experimental results of the distribution coefficient show both a dependency on sulphur dioxide partial pressure as well as temperature. In all experiments gold is more concentrated to the metal phase, and the distribution coefficient ranges from 10.5 to 15.6.

Figure 57 shows the concentration of Au in the metal phase as well as the effect of temperature and $P(SO_2)$. It can also be seen that increasing the $P(SO_2)$ decreases the wt. % of Au in the metal phase at 1350 °C. At 1250 °C and 1300 °C, the concentration of Au decreases as the $P(SO_2)$ increases between 0.01 and 0.5 atm. From 0.5 to 1 atm $P(SO_2)$ the concentration of Au increases again. At 1250 °C the concentration at 0.5 atm $P(SO_2)$ is 0.712 wt. %, and this increases to 0.833 wt. % at 1 atm. At 1300 °C the concentration at 0.5 atm is 0.645 wt. %, and this increases to 0.660 at 1 atm. It can be observed that this increase of Au concentration from 0.5 atm to 1 atm $P(SO_2)$ seems to increase with decreasing temperature.

At 0.01 atm $P(SO_2)$, the concentration range of gold in the metal phase is 0.79 to 0.82 wt. %, and at 1 atm $P(SO_2)$ the range expands to 0.54 at 1350 °C and to 0.83 at 1250 °C. The error bars in this figure appear not to contradict with the Au concentration trends in the metal phase.

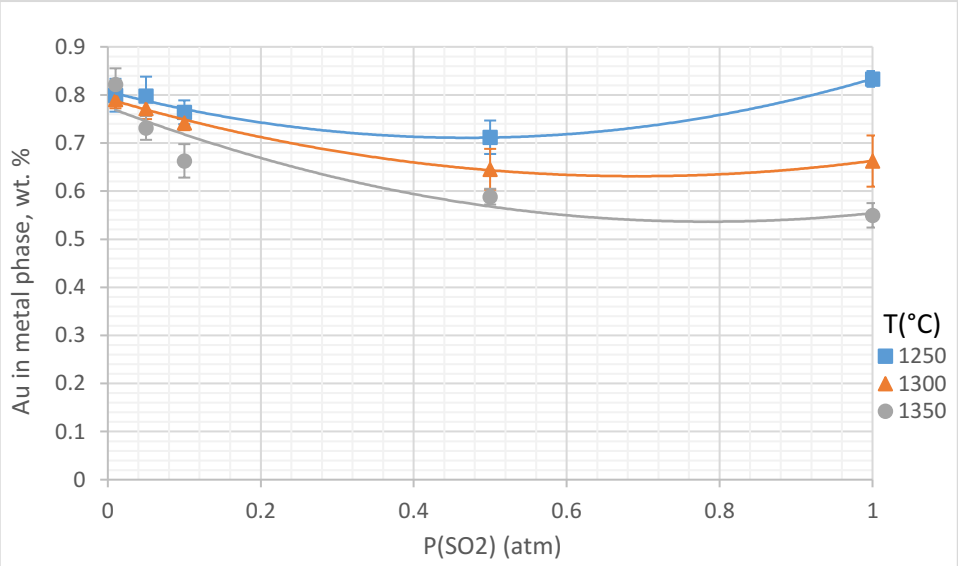

Figure 57 Concentration of Au in metal phase, wt. % as function of $P(SO_2)$ at 1250 °C, 1300 °C and 1350 °C

The concentration of gold in the white metal phase is shown in Figure 58. The concentration of gold in this phase is much lower than in the metal phase, and all data points are below the detection limit. The actual reported EPMA results are shown in this graph which are noted as 1250 * °C, 1300 * °C and 1350 * °C, and as can be seen from the graph these results are below the detection limit. Therefore, this data is not considered reliable, and the detection

limit is used to calculate the distribution coefficient in Figure 59 and Figure 60. Error bars for the EPMA values below the detection limit also show no trend.

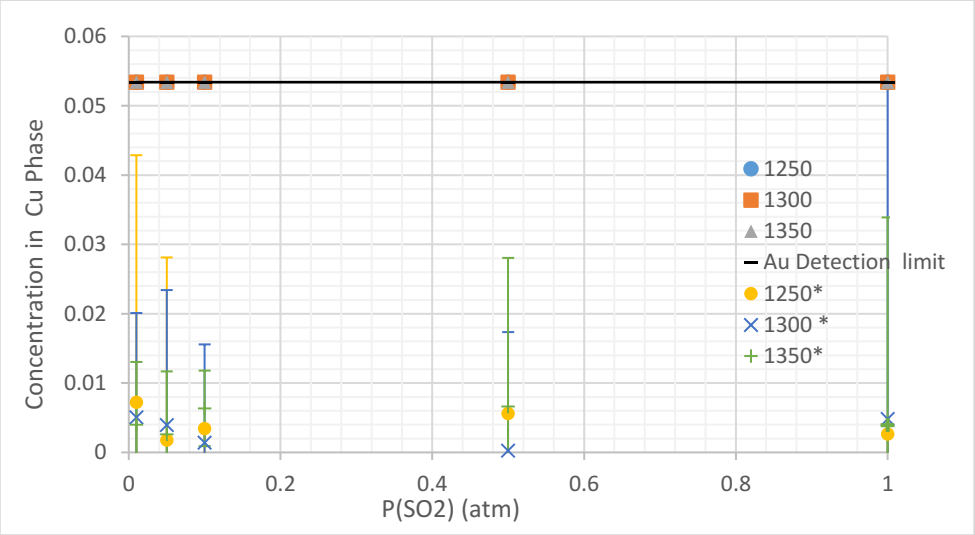

Figure 58 Concentration of Au in white metal phase, wt. % as function of $P(SO_2)$ at 1250 °C, 1300 °C and 1350 °C

In Figure 59, the distribution coefficient of Au is shown as a function of temperature. The figure suggests that temperature has a functional influence on the distribution coefficient of Au. The figure suggests that as temperature increases the distribution ratio decreases. Between 1 and 0.05 atm the distribution coefficient decreases. However, at 0.01 atm the distribution coefficient increases with increasing temperature.

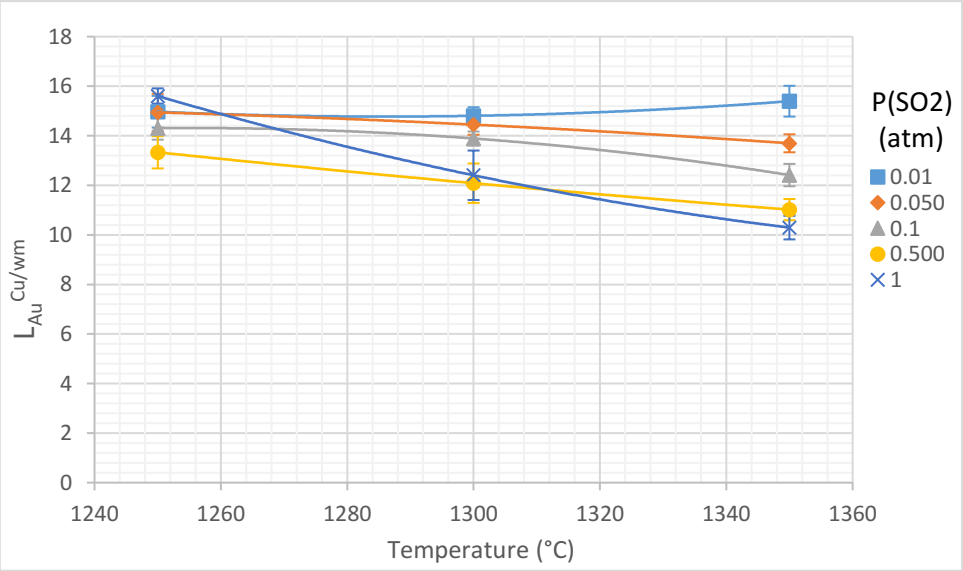

Figure 59 Distribution coefficient of Au as a function of temperature

The error bars in Figure 59 are artificially small, as $L_{Au}^{Cu/wm}$ is calculated using the EPMA detection limits, so what is being represented in this graph is the behaviour of the Au concentration in the metal phase.

Figure 60 presents the distribution coefficient of Au as a function of $P(SO_2)$. At 1300 °C and 1350 °C, the distribution coefficient decreases as the partial pressure of sulphur dioxide increases. However, at 1250 °C the distribution ratio increases as $P(SO_2)$ increases. Due to the calculation method of $L_{Au}^{Cu/Wm}$, this figure also only shows the Au concentration in the metal phase behaviours. This also means that in order to accurately calculate $L_{Au}^{Cu/Wm}$, a more reliable method needs to be implemented for measuring the accuracy of Au concentration in the white metal phase.

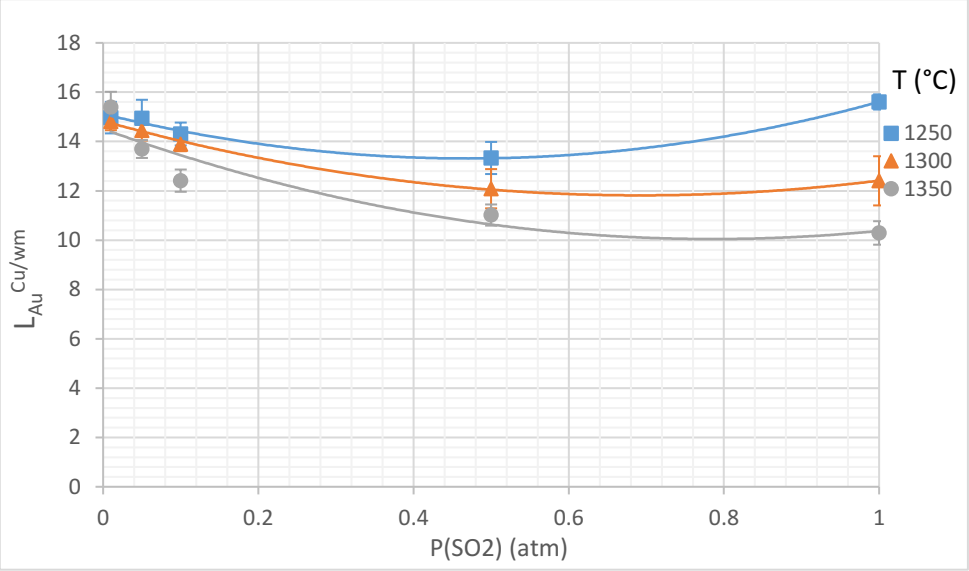

Figure 60 Distribution coefficient of Au as a function of $P(SO_2)$

The graphs shown in Figure 61, the right side and the left side show the combined effects of $P(SO_2)$ and temperature on the gold distribution coefficient. The figure shows that both temperature and $P(SO_2)$ effect the distribution ratio. Gold is most highly concentrated to the metal phase at low $P(SO_2)$ and low temperature with a ratio of 15. There is also a secondary peak at high $P(SO_2)$ and low temperature. The right side of Figure 61 presents the repetitious series of experiments. It appears that the highest distribution coefficient is at low $P(SO_2)$ and low temperature, and the distribution ratio decreases to its lowest point of 9.9 at 1350 °C and 1 atm $P(SO_2)$. The two graphs appear to be somewhat in agreement with one another, except that the main series values at low temperature and 0.1 atm to 0.5 atm are unexpectedly low.

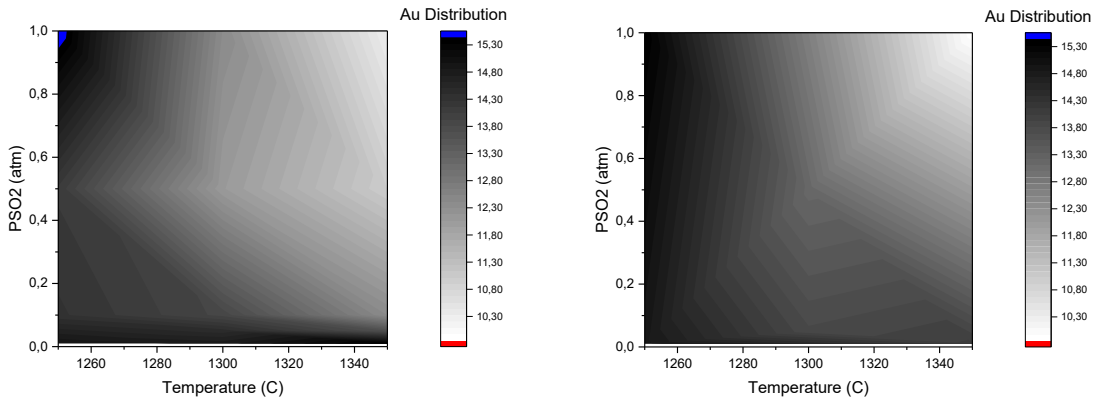

Figure 61 Contour plot of Au Distribution coefficient as function of $P(SO_2)$ and temperature, main series left, repetition series right.

5.10 Non-metallic Distribution in the System

The amount of oxygen dissolved into the system is functionally linked to the $P(SO_2)$. It can be seen from Figure 62 that as the $P(SO_2)$ increases so does the wt. % of O increase. At 0.01 atm $P(SO_2)$, the wt. % ranges from 0.29 to 0.43 in the metal phase, increasing at 1 atm $P(SO_2)$ with a wt. % of 0.56 to 0.82. The wt. % of O should also increase with the increasing temperature, though this is not represented in the graph.

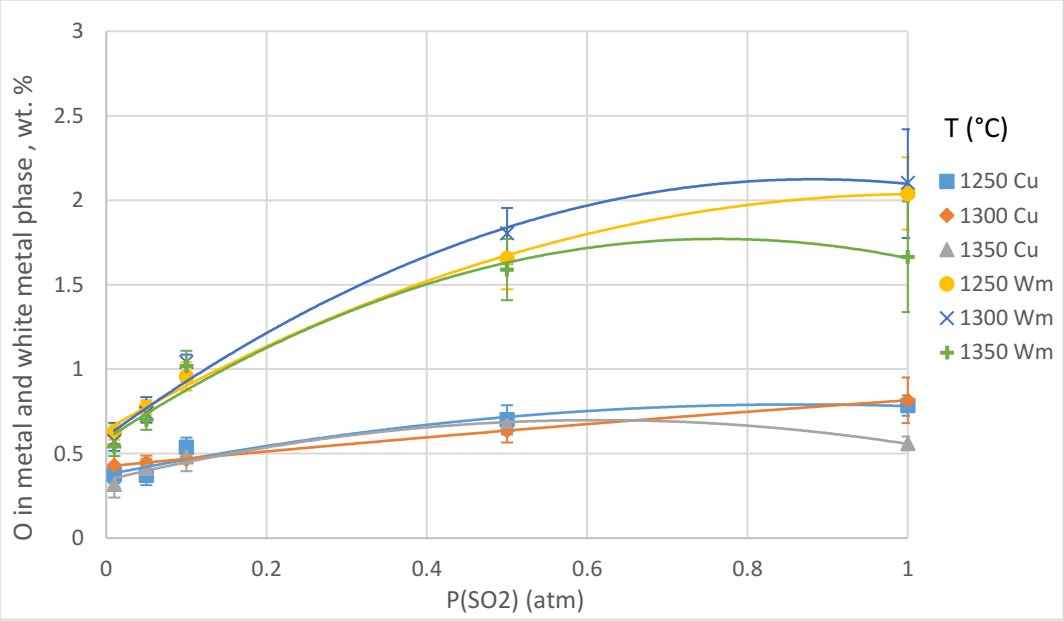

Figure 62 Concentration of O in metal and white metal phase as a function of $P(SO_2)$, wt. % as function of $P(SO_2)$ at 1250 °C, 1300 °C and 1350 °C.

The wt % of O in the white metal phase also increases as the $P(SO_2)$ increases, starting at between 0.53 and 0.58 at 0.01 atm $P(SO_2)$, and increasing to between 1.67 to 2.10 at 1 atm. It also appears from Figure 62 and Figure 63 that temperature has no effect on the wt. % of O in either phase, though theoretically the O wt. % should increase slightly as a function of temperature.

The distribution coefficient of O between metal and white metal phase decreases as a function of $P(SO_2)$. At 0.01 atm $P(SO_2)$, the distribution is between 0.55 to 0.75, and at 1 atm $P(SO_2)$ the distribution is between 0.34 to 0.39. There does not appear to be any affect from temperature on the distribution of O. The error bars in Figure 63 show a large variation, and they are large enough to account for a more linear relationship between $P(SO_2)$ and $L_O^{Cu/Wm}$.

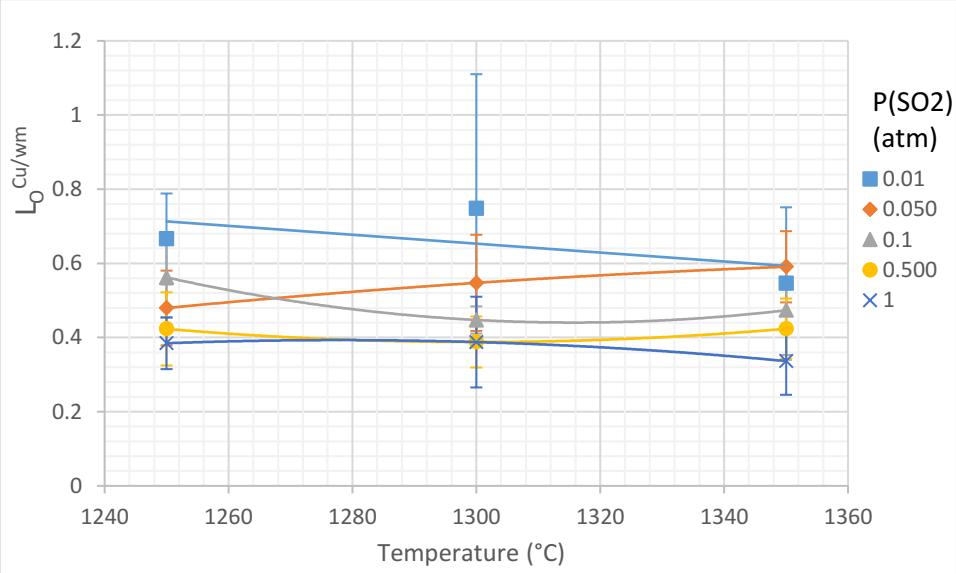

Figure 63 Distribution coefficient of O between metal and white metal.

The contour plots are formed of temperature and $P(SO_2)$ on each axis, and the grey scale on the side of the lot represents the distribution coefficient of O. The contour plot confirms what has been shown in the left-hand side of Figure 64, which is that the O distribution is only dependant on the $P(SO_2)$ and approaches unity at higher partial pressures of sulphur dioxide and thus has a higher distribution coefficient. The right side of Figure 64 shows the contour plot of the repetitious series of experiments. It shows that there is good agreement as to the trend of oxygen distribution between the metal and white metal phases.

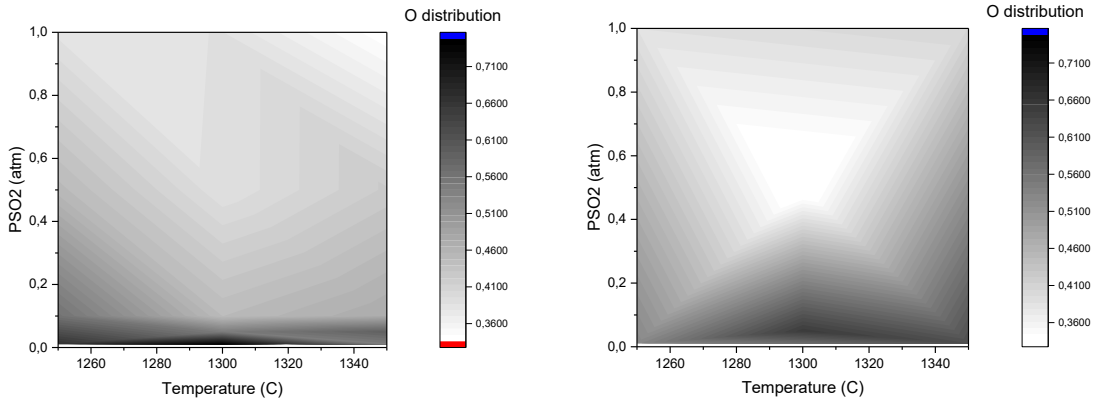

Figure 64 contour plot of O distribution coefficient as function of $P(SO_2)$ and temperature, main series left, repetition series right

It can be seen from Figure 65 that sulphur also distributes between both phases. Sulphur wt. % decreases in the white metal phase as $P(SO_2)$ increases to 1 atm, decreasing from 19.9 wt. % of S at 0.01 atm $P(SO_2)$ to 17.7 wt. %. Also, the wt. % of sulphur decreases in the metal phase as the $P(SO_2)$ is increased at 1250 °C and 1350 °C, but this trend is reversed at 1300 °C. These trends may be only due to experimental error or the standard deviation of the experimental results.

Figure 65 shows that the distribution coefficient decreases as the temperature increases. The distribution decreases from a range of 0.102 to 0.053 at 1250 °C to a range of 0.0746 to 0.0458 at 1350 °C. Standard deviations in the white metal phase are small, but those in the metal phase are larger, so it could suggest that there is a small temperature dependency of S concentration in the metal phase.

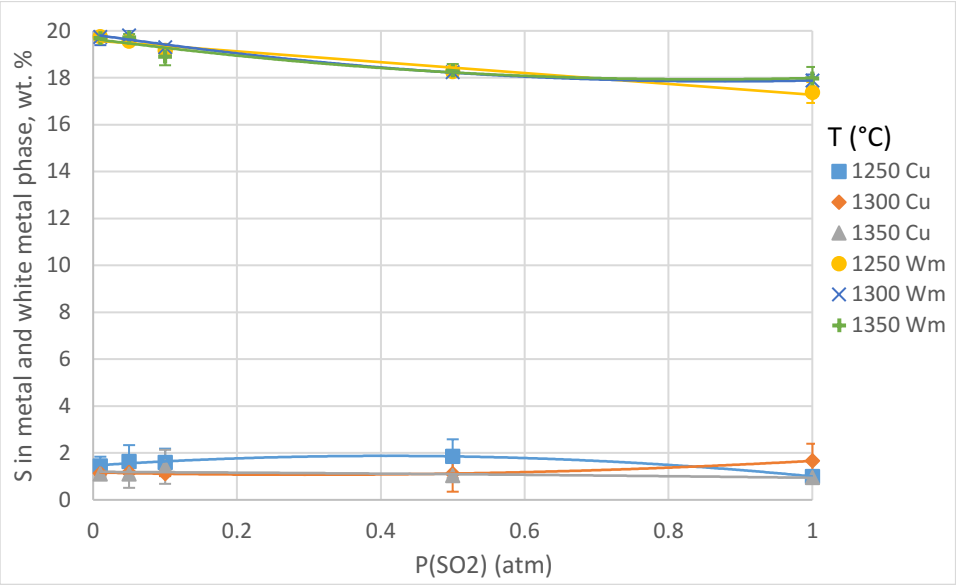

Figure 65 concentrations of S in metal and white metal as a function of $P(SO_2)$.

The $L_s^{Cu/wm}$ appears to be a function temperature, decreasing as temperature approaches 1350 °C atm. It also appears that as $P(SO_2)$ approaches 1 atm, the $L_s^{Cu/wm}$ decreases. These trends appear to be only contradicted by the trend line that follows the 1 atm $P(SO_2)$ line, but this abnormality falls within the error bars.

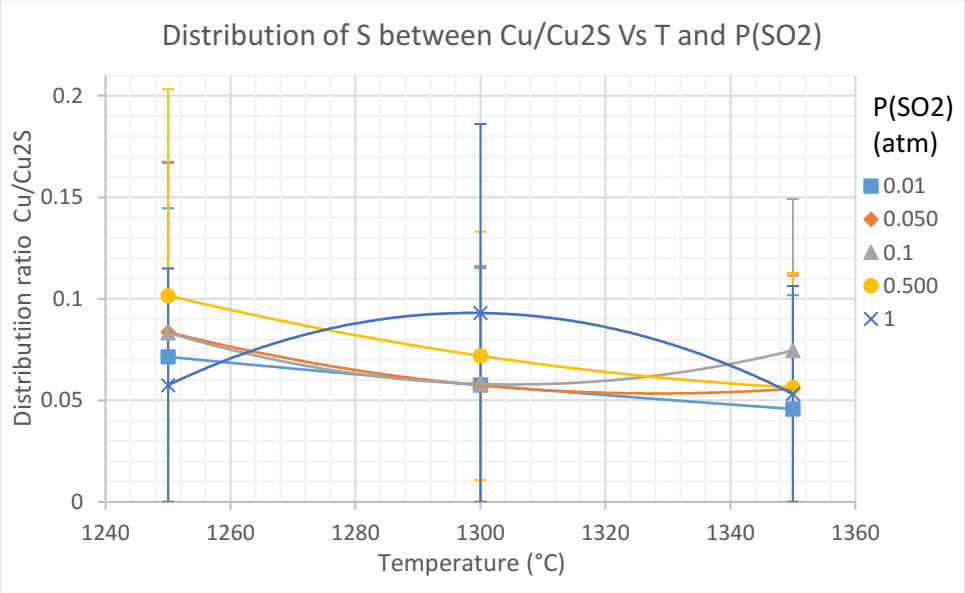

Figure 66 Distribution coefficient of S as a function of temperature

It can be seen from the contour plot on the left side of Figure 67, that the highest distribution coefficient appears to be at low temperature and low $P(SO_2)$ as well as a data point at 1300 °C and 1 atm $P(SO_2)$. The repetition series, shown on the right, presents a lower distribution

coefficient than the main series. It can be seen – though not clearly – that the largest distribution coefficient occurs at low temperature.

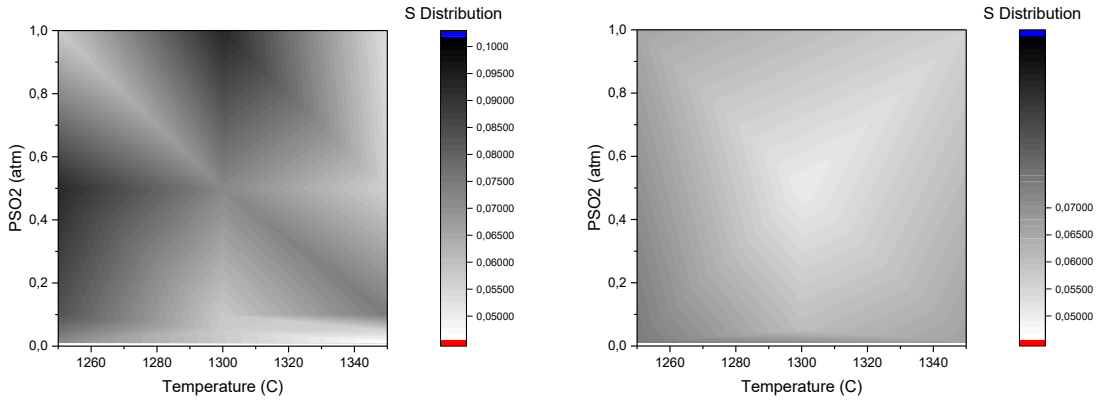

Figure 67 Contour plot of S distribution coefficient as function of $P(SO_2)$ and temperature, main series left, repetition series right

5.11 Copper and Iron Distribution in the System

The EPMA results show that both the sulphur dioxide partial pressure and the temperature have an effect on the distribution coefficient of the copper between the metal and white metal phases. Figure 68 shows the concentration of Cu in both phases, ranging from 94.8 to 96.6 in the metal phase and 78.5 to 79.8 in the white metal phase. Increased temperature increases the concentration of Cu in the metal phase. The $P(SO_2)$ effects cannot be seen in the metal phase from this figure. It appears that in the white metal phase the concentration of Cu increases between 0.01 to 0.1 atm $P(SO_2)$, from 78.5 to 79.5 wt. %. Error bars in both phases do not appear to disagree.

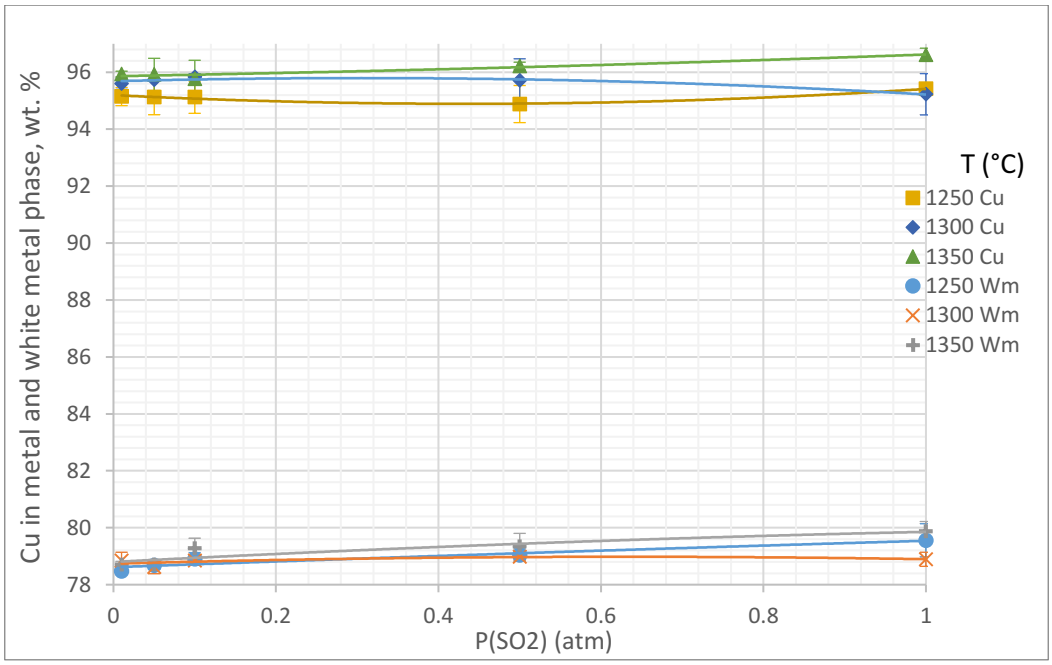

Figure 68 Concentrations of Cu in metal and white metal phase.

Increasing the $P(SO_2)$ decreases the distribution coefficient of Cu. This is observed from Figure 69. It can also be noted that the distribution coefficient increases as temperature increases from 1250 °C to 1350 °C across all partial pressures. The distribution across all measured points ranges from 1.199 to 1.219, so the difference is quite small, but as the concentrations are very high and well above the detection limits for the EPMA these can be thought to be good results and the trend is quite clear. Error bars for $L_{Cu}^{Cu/wm}$ are comparatively large, and this could therefore explain the disordered sequence of the trend lines for $P(SO_2)$. Hence it could be so that $L_{Cu}^{Cu/wm}$ is both dependant on temperature and $P(SO_2)$ in an orderly way.

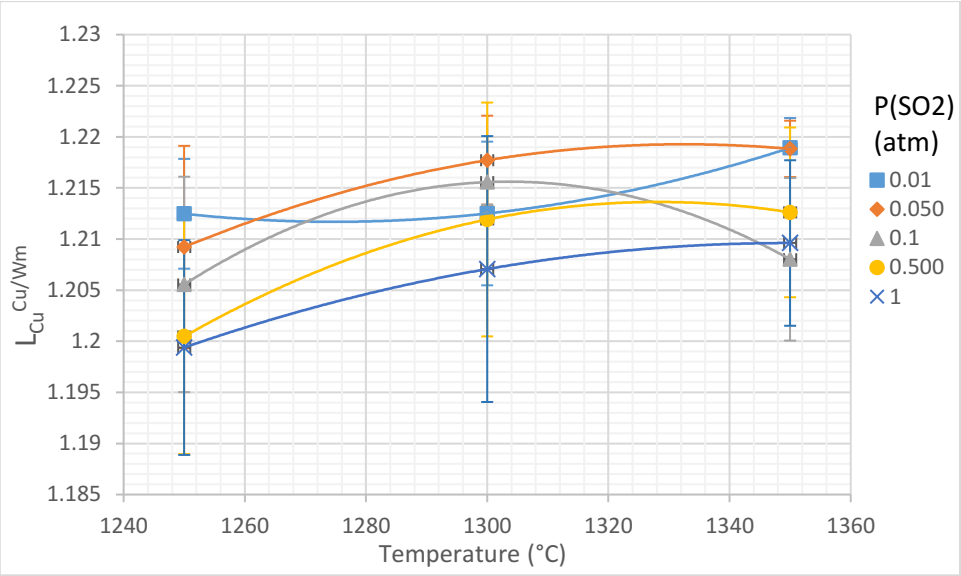

Figure 69 Distribution coefficient of Cu between the metal and white metal phases as a function of temperature and $P(SO_2)$.

The contour plots give a better understanding to the behaviour of the Cu between the metal and white metal phases. Cu is more concentrated to the metal phase at high temperature and low $P(SO_2)$ and concentrated less to the metal phase at low temperature and high $P(SO_2)$, as can be seen from the left side of Figure 70. The right side of this figure shows the second series of experiments. It presents some disagreement to where the highest concentration to the metal phase lies, as it shows that it is in the centre of the graph, but the low concentration point is in the same point and the range of the distribution coefficient 1.199 to 1.219.

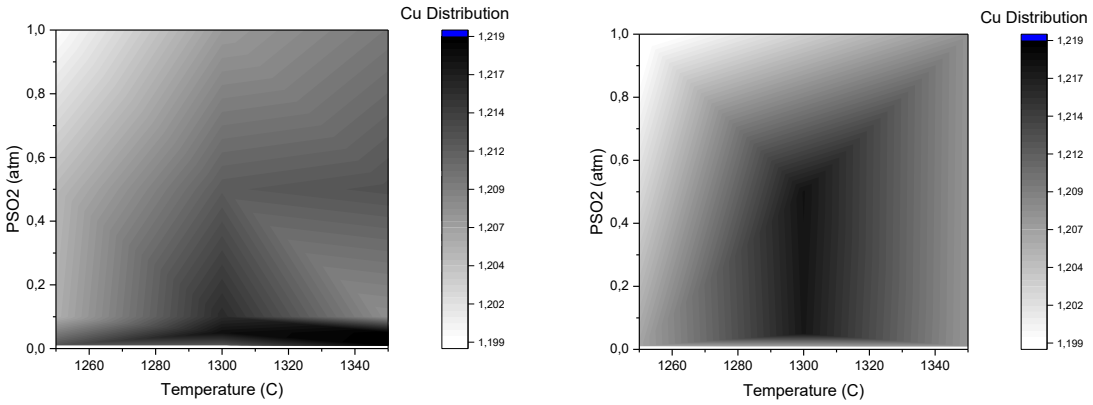

Figure 70 Contour plot of Cu distribution coefficient as a function of $P(SO_2)$ and temperature, main series left, repetition series right.

The results gathered by the EPMA show that the temperature and the $P(SO_2)$ potentially have an effect on the iron distribution coefficient between the metal and white metal phases. The concentrations are low, so the trends in the data are hard to see.

Figure 71 shows the concentration of Fe in the metal and white metal phases. Fe is more highly concentrated to the white metal phase across all experimental conditions. Concentrations of Fe in the metal phase fall below the EPMA detection limits, and in this case the distribution coefficients gathered for Fe are also unreliable and not representative of the actual Fe distribution coefficients. The error bars for Fe in the metal phase are not included, as all the data falls below the EPMA detection limit. The error bars for 1350 °C are also omitted because the standard deviation is so large it obscures the rest of the data in the figure.

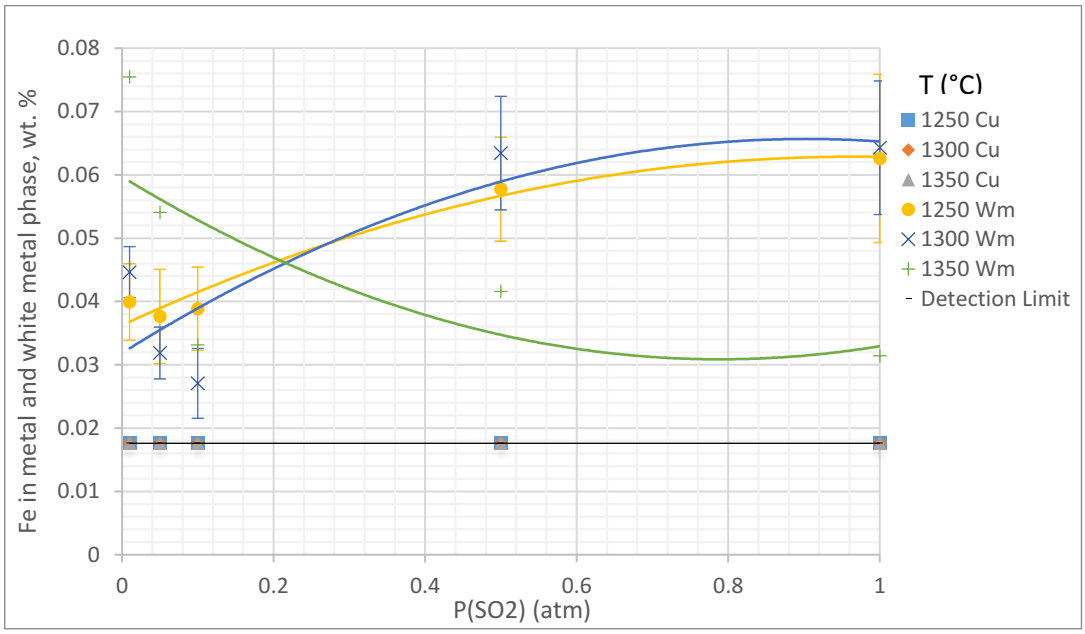

Figure 71 Fe concentrations in metal and white metal

According to Krivsky and Schuhmann (1957), increasing temperature increases the value for the iron distribution coefficient. This is opposite to the trend found in Figure 72. However, this discovered trend was probably caused by some anomalous results as the concentration of Fe in this study was very low. The distribution coefficient of iron is found to range between 0.199 at 0.01 atm $P(SO_2)$ and 1250 °C and 0.037 at 0.5 atm $P(SO_2)$ and 1300 °C. This means that the iron tends to the white metal phase in all situations.

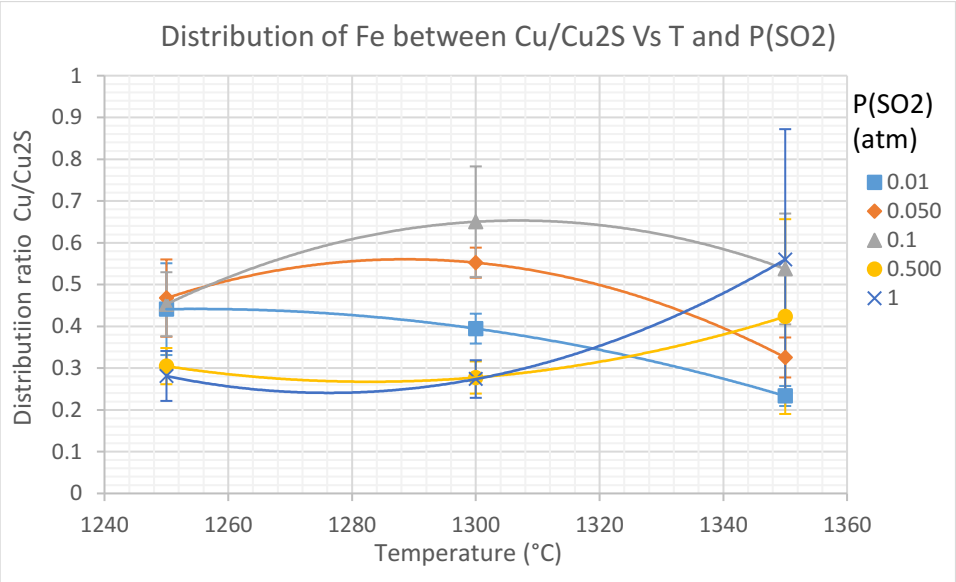

Figure 72 Fe distribution coefficient between metal and white as a function of temperature and P(SO_2).

The contour plots in Figure 73 show the Fe distribution coefficients with the variations of temperature and P(SO_2). The left side of the figure shows a higher ratio to the metal phase at lower P(SO_2), but it seems to show no trend as a function of temperature. The repetition series shown on the right side of the figure shows no trend for the distribution coefficient, with peaks showing at low P(SO_2) and high P(SO_2) and at low and high temperatures. The contour plot shows a lower concentration in the centre of the graph.

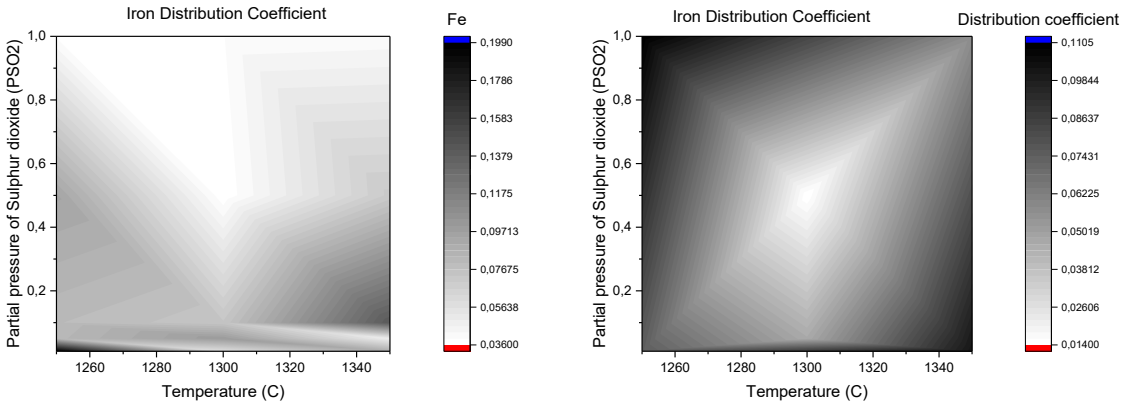

Figure 73 Contour plot of Fe distribution coefficient as a function of P(SO_2) and temperature, main series left, repetition series right.

6 Discussion

The distribution coefficient of the solute elements examined in this study all seem to experience functional dependence on either temperature or $P(SO_2)$ or both. This chapter attempts to compare the data collected in this study with the research made in previous studies. There will also be discussion on possible routes to experimental error as well as phenomena discovered.

The silver distribution ratio is a good indicator of the entire experimental procedure in this work, as the distribution ratio has been investigated by many previous researches, which can be compared to the distribution ratio of this study.

The $L_{Ag}^{Cu/wm}$ in this study are found to be affected by both temperature and $P(SO_2)$. Due to the high volatility of Ag in this system, the concentration in both phases dropped significantly from 0.3 wt. % to 0.02 wt. %. The $L_{Ag}^{Cu/Wm}$ is reported in this study to range from 3.3 at 1 atm $P(SO_2)$ and 1250 °C to 0.57 at 0.05 atm $P(SO_2)$ and 1350 °C. In their papers Taylor (1983), Schlitt and Richards (1957) and Asano (1971, 1965) report a low change if at all in the value of $L_{Ag}^{Cu/wm}$ as a result in temperature. The reported $L_{Ag}^{Cu/wm}$ values in the previous research papers are in the range of 2.93 to 2.17. However, what can be understood from all the literature data is that Ag is more concentrated to the metal phase. It is only Sinha et al. (1985) who report a change in the $L_{Ag}^{Cu/wm}$ as a function of temperature, changing from 2.13 to 2.21 when temperature changes from 1126 °C to 1226 °C. Kashima et al. (1978) show that the $L_{Ag}^{Cu/wm}$ increased with increasing $P(SO_2)$, increasing from 2.8 at 0.7 kPa to 3.6 at 20 kPa.

While some of the data points collected in this study are in agreement with the literature results it has been found that the $L_{Ag}^{Cu/wm}$ from the main series of experiments varies with both temperature and $P(SO_2)$. Concentrating more highly to the metal phase at high $P(SO_2)$ and low temperature with a $L_{Ag}^{Cu/wm}$ of 3.3, the second series is also in disagreement with the first series as it only shows the $L_{Ag}^{Cu/wm}$ to have a dependence on temperature. What is certainly different between this study and those made previously is that in certain conditions the $L_{Ag}^{Cu/wm}$ lowers past unity making Ag is more concentrated to the white metal phase.

The $L_{Co}^{Cu/Wm}$ appears to be only affected by the $P(SO_2)$, decreasing as $P(SO_2)$ is increased to 1 atm. The $L_{Co}^{Cu/wm}$ ranges from 0.85 at 0.01 atm $P(SO_2)$ to 0.15 at 1 atm $P(SO_2)$. In the previous works by Yazawa (1980) and Kashima (1978) the current study appears to be in

agreement with the trend of increased $P(SO_2)$ decreasing the $L_{Co}^{Cu/wm}$. Where there is difference between this work and the previous studies is that in the previous studies by Kashima et al (1978) and Yazawa (1980) state that the $L_{Co}^{Cu/wm}$ the trend is steeper, suggesting a greater effect of the $P(SO_2)$ on the $L_{Co}^{Cu/wm}$.

The results for $L_{Ni}^{Cu/wm}$ suggest that it is affected by both temperature and $P(SO_2)$. It is reported in this study that Ni was concentrated to the metal phase across all equilibrations. The highest $L_{Ni}^{Cu/wm}$ was found to exist at 1350 °C and 1 atm $P(SO_2)$ with a value of 5. The $L_{Ni}^{Cu/wm}$ was found to decrease from this point with both decreasing $P(SO_2)$ and temperature, decreasing to the minimum point at 1250 °C and 0.01 atm $P(SO_2)$ with a value of 2.

When comparing these results to those in the reviewed literature, the current study firstly agrees as to which phase the Ni is concentrated. Nagamori and Mackey (1978) report that the $L_{Ni}^{Cu/wm}$ decreases as the temperature increases, 3.07 at 1200 °C and 2.9 at 1250 °C. Asano and Ichio (1962) also found this same effect with temperature, and both sets of experiments were carried out under vacuum conditions, i.e. with very low $P(SO_2)$. When comparing the results from literature with the findings of the present study, it can be seen that the effect of temperature is in disagreement. In the study performed by Kashima (1978) the effect of $P(SO_2)$ is in agreement, as they state that the increased $P(SO_2)$ resulted in an increase for the value of $L_{Ni}^{Cu/wm}$. The study by Yazawa (1980) found no dependency on $P(SO_2)$. A number of different factors could cause the disagreement between this study and the previous literature, for example the fact that this current study reviews the compounding effects of both temperature and $P(SO_2)$ and the literature studies reviewed here focus on one variable each. Experimental error will also play a large role in the misrepresentation of trends. The present study agrees with some literature studies and not others, the fact that some data agrees with the data lends validity of the rest of the data gathered.

The $L_{Pd}^{Cu/wm}$ appears to have a functional dependence on the temperature and $P(SO_2)$, and the main series shows this. However, there are a number of peaks and troughs in the contour plot that confuse the trend of the plot. The second series does not show these peaks and troughs through the contour plot. Both plots suggest that the highest $L_{Pd}^{Cu/wm}$ is at 1 atm $P(SO_2)$ and at 1250 °C. The analogous values at certain points in the main series may be in part due to the fact that the second series was carried out second (as the name may suggest), and because of this the procedure was better known. In the later experiments, there were less procedural errors, but this could also be down to regular experimental error.

The $L_{Pd}^{Cu/wm}$ was found to decrease from 1 atm $P(SO_2)$ and at 1250 °C with a value of 54.5 to the minimum at 0.01 atm $P(SO_2)$ and at 1350 °C to a value 33.6. The concentration of Pd in the white metal phase was very low, very often below the detection limit. The concentrations found in the metal phase are highly ordered and the trends easy to observe. In the white metal phase though the actual weight percentage drop is comparatively much smaller to the drop in the metal phase, which would be useful information for a smelting operation aiming to recover this precious metal. However, across all experiments the concentration of Pd in the white metal phase above and including 0.5 atm $P(SO_2)$ are below the EPMA detection limit, and only the point at 1250 °C and 1300 °C and 0.1 atm $P(SO_2)$ is below the EPMA detection limit. Pd is highly concentrated to the metal phase, which is in agreement with what has been previously discovered by Schlitt and Richards (1975) and Burylev et al. (1974). However, there was a disagreement with Burylev et al. (1974) findings stating that the $L_{Pd}^{Cu/wm}$ is dependent on temperature, decreasing from 94 at 1150 °C to 62 at 1300 °C.

When it comes to $L_{Au}^{Cu/wm}$, in this study only the concentration of Au in the metal phase has been reliably measured, as all concentrations measurements in the white metal phase fell below the EPMA detection limit and the data presented in this paper are shown as the EPMA detection limit. So the presented dependencies on both temperature and $P(SO_2)$ are only due to the changing concentrations in the metal phase. The contour plots of the main series and the repetition series show that the lowest distribution coefficient is at 1350 °C and 1 atm $P(SO_2)$, the $L_{Au}^{Cu/wm}$ increases with decreasing temperature and decreasing $P(SO_2)$. The $L_{Au}^{Cu/wm}$ results presented here are not reliable and further experimentation is required to understand the true functional dependencies.

Comparing the experimental results of this study to those of the literature, gold is highly concentrated to the metal phase. Schlitt and Richards (1975) report the $L_{Au}^{Cu/wm}$ as 125 for 1200 °C, Asano (1971, 1965) found it to be 171–173 at 1200 °C also under vacuum conditions. These values are considerably higher than what has been found in this study. However, this is due to the detection limitation of the EPMA. The $L_{Au}^{Cu/wm}$ calculated from the data as presented by the EPMA is considerably higher. The work by Sinha et al. (1985) shows that the $L_{Au}^{Cu/wm}$ is a function of temperature, and this is in general agreement with the present study. However, Sinha et al. (1985) reported an increase in the $L_{Au}^{Cu/wm}$ with

increased temperature, and this aspect disagrees with the present study, but this is probably due to again to a detection limit issue.

The concentration of O_2 increases as $P(SO_2)$ increases in both phases, but the $L_{O_2}^{Cu/wm}$ decreases with increasing $P(SO_2)$. The temperature appears to have no effect on the $L_{O_2}^{Cu/wm}$.

Sulphur concentration decreases in the white metal phase (19.9 wt. % to 17.7 wt. %), while increasing in the metal phase as a function of $P(SO_2)$. It is hard to determine any kind of trend from the first series of experiments, but from the second series it can be seen that $L_S^{Cu/wm}$ is the highest at low temperature and $P(SO_2)$. However, because S is in high concentration, the other solute elements will have an impact on the concentrations in the white metal phase.

It was observed that both temperature and $P(SO_2)$ have an effect on the $L_{Cu}^{Cu/wm}$. Part of this effect could be because the solute elements are dependent on temperature and $P(SO_2)$. As the solute elements in the system find their respective equilibria, which accounts for 2.5 % of the total mass of each sample, the concentration of Cu in each phase will change. The concentration changed only from 1.199 to 1.219 wt. %, a change of only 0.02, but the effect can be clearly seen. Cu is more concentrated to the metal phase at high temperature and low $P(SO_2)$.

To begin with, the Fe concentration was very low before each equilibration, to simulate the second stage of the converter where most of the Fe had already been oxidized to the slag phase and been removed from the system. Despite this, the distributions were calculated, but as can be seen from Figure 71, the concentration of Fe in the metal phase falls below the EPMA detection limit. Comparing the distribution ratio with the literature, the overall coefficient is in agreement. The $L_{Fe}^{Cu/wm}$ reported in this study ranges from 0.04 to 0.2. Looking at the literature, Asano (1965) reports as 0.2 at 1200 °C, Coursol (2012) reports at a range of 0.1 to 0.14, and Krivsky and Schuhmann (1957) report the $L_{Fe}^{Cu/wm}$ increasing with temperatures 1150 °C to 1250 °C, increasing from 0.221 to 0.302. This means that there is good agreement with the literature as to the $L_{Fe}^{Cu/wm}$. The Fe contour plot for the first series of experiments shows the highest concentration is at low temperature and low $P(SO_2)$, but the temperature trend is then disagreement with the research by Krivsky and Schuhmann (1957).

Here are some generalizations as to what could possibly attribute to some poor results. As is the nature of any experimental work, there will be error in the procedural workings, as well as a certain amount of unpredictable variation. This also being my first study of this nature, this may also account for a larger amount of the error.

The comparatively long equilibration time will certainly affect the volatile components, particularly the Ag, as what was left in solution after quenching was significantly lower with wt. % combination in both phases than what was dissolved prior to the equilibration. This lowered concentration also makes the detection of these elements more difficult, especially the elements with very large or very small $L_X^{Cu/wm}$ values.

A phenomenon that occurred across all experiments is that inclusions of various sizes appeared in both the metal and white metal phases. In each case, the inclusions were comprised of one of the phases trapped in the other phase. The larger inclusions could be attributed to the mechanics of the drop and quench or some other unknown phenomena. The data collected with the EPMA avoided these larger inclusions. However, throughout both of the phases there were very small inclusions that the beam of the EPMA was unable to avoid, and these are included in the calculation of the results for concentrations and therefore could change the reported values for the distribution coefficients for each element. One possible explanation for these small inclusions is that they are an artefact of the quenching. Even though the quench must occur very rapidly, the saturation limit must rapidly change during the quenching, so there could be enough time for the inclusions to form but not enough time for them to separate from the respective phases.

High concentration areas of PGMs were found in many of the experiments. These areas were found at the boundary between the metal and white metal phase, and it is hard to determine which phase this high concentration is adsorbed into, or if it is at all. These high concentration areas of PGMs can also attribute to the low concentration of Pd, Ag and Au found at certain experimental points. An example of this can be seen in Figure 74, in which the concentration areas are highlighted. This can especially be seen at the lower portion of the micrograph, between the metal and white metal phases, at the point where the crack begins to form, separating the two phases continuing further up the boundary layer. On the white metal side a lighter area can be seen, which is lighter in colour than the metal phase. This was tested with the SEM-EDS and was found to have a higher concentration of PGMs and in shown in appendix 2.

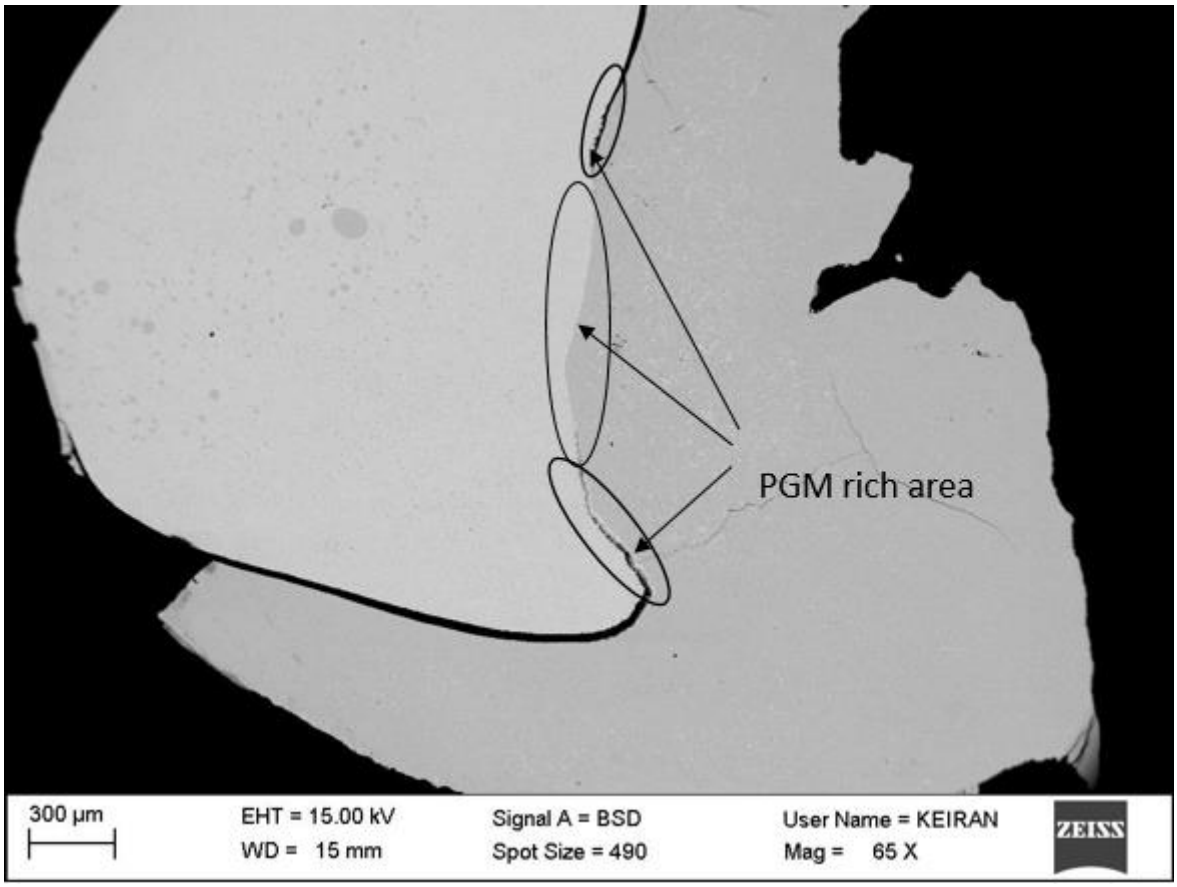

Figure 74 Micrograph of experiment 1 % 1300 °C showing an example of the PGM rich area

7 Summary

This work investigates the distribution coefficients of solute elements Au, Ag, Pd, Ni and Co between molten Cu and the white metal phase under varied temperature and partial pressure of sulphur dioxide. Each sample was equilibrated and rapidly quenched into an ice water bath. Cross sections were made by grinding and polishing, and they were analysed using SEM-EDS and EPMA. A total of 15 experiments were made in the first series at each point, 1250 °C, 1300 °C and 1350 °C by 0.01, 0.05, 0.1, 0.5 and 1 atm $P(SO_2)$. A second series of experiments was made from the extrema points from the first series plus two mid points. The solute atoms were added into the metal phase in their metallic forms prior to the equilibration. The partial pressures were achieved by diluting and mixing SO_2 with Ar prior to the work tube. Stabilized zirconia crucibles were used in all experiments.

The distribution coefficients for each solute element were calculated from the weight concentrations as found by the EPMA analysis. These distribution coefficients were plotted on scatter graphs against temperature and $P(SO_2)$ and plotted in contour plots with both temperature and $P(SO_2)$. All the solute elements showed functional dependency on temperature or $P(SO_2)$ or both. The results gathered in this study were compared with those found in literature reviewed in this study. The concentrations for certain elements were found to be extremely low in certain conditions, these results are not considered reliable and any trends cannot be determined.

The value of this work is that the effects of temperature and $P(SO_2)$ on the distribution coefficient are examined together. This is something has not been done for many of the elements in this study. The results in this work are often compared to previous research that only deals with one variable at a time. In some cases, the distribution coefficient dependency of a certain variable on an element has not been investigated previously or a relevant research paper was not found.

What is concluded is that temperature or sulphur dioxide partial pressure or both affect the distribution coefficients for each elements. The dependencies are presented in Table 121312. The conditions for the maximum distribution coefficient are presented when there is dependency on the variable as either the low or the high point of that variable. No or None is used if there appears to be no dependency found.

Table 12 The highest distribution coefficient conditions for each element.

Element	Temperature	$P(SO_2)$	Notes	Distribution
Ni	High	High	Decent concentration in both phases and agreement across both sets of data	1.58 to 5.17
Co	None	Low	Decent concentration in both phases and agreement across both sets of data	0.15 to 0.85
Ag	low	High/No	The first and second series of experiments are in disagreement about the effect of $P(SO_2)$	0.56 to 3.3*
Pd	None	High	Low concentrations in white metal phase led to some uncertain results.	33.6 to 54.5*
Au	Low	High	Low concentrations in white metal phase led to some uncertain results.	10.29 to 15.60*

Looking at the literature, $L_{Ag}^{Cu/wm}$ was found to increase as a function of temperature and with increasing $P(SO_2)$. In this study, the dependency on $P(SO_2)$ is in agreement with what was found, but as to the dependency of temperature this study found some disagreement. Co was found to only be affected by $P(SO_2)$, the distribution coefficient decreasing as $P(SO_2)$ increased, this agreed with what was found in the previous studies. Nickel distribution ratio trend as a function of temperature was found to be in disagreement with what was found in the literature. In this study, the $L_{Ni}^{Cu/wm}$ was found to increase with increasing temperature. However, the effects of $P(SO_2)$ are in agreement with what was found in the literature, the distribution ratio increasing with increasing $P(SO_2)$. The distribution of palladium between metal and white metal phases is found in this study to be mainly dependent on $P(SO_2)$. The distribution increases with increasing temperature, as is the case in the previous studies. However, Burylev et al. (1974) states that temperature affects the distribution of Pd, but this study showed no such relationship. The first experimental series showed no tendency either

way for temperature or $P(SO_2)$ because of low concentrations in the white metal phase. This seems to have skewed the results to the point where no conclusions could be reached. The second series of results shows better the functional dependency of temperature. The literature was found to agree with the temperature effects of the present study.

Due to the long equilibration time as there was some challenges in this study; Ag especially is volatile at these temperatures, which significantly reduced the concentration of it in both phases.

7.1 Plans for Further Research

Some opportunities were found to further investigate the functional dependency of temperature and $P(SO_2)$ on the distribution coefficients of Ni, Co, Ag, Au and Pd between copper and copper sulphide immiscible liquids in converting operations. This work was conducted between 1250 °C to 1350 °C, but the temperature range could be extended to typical matte converting temperature of 1200 °C (Schlesinger, 2011). The temperature could also be extended lower to 1130 °C, which is just above the point that Cu_2S becomes molten. The temperature range could also be extended beyond 1350 °C. Both temperature extensions would increase the size of the contour plots and give better validation to the current contour plots. Additional repetitions would also help to give validity to results found in this study.

The results gained by the EPMA in this study seem to offer reliable Ni and Co distributions, but concentrations gathered in the white metal phases for Au and Pd and in some cases the Ag concentrations in either phase are exceptionally below the detection limit for the EPMA, which affects the reliability of the distribution coefficients. To get reliable results for the distribution coefficients of Au, Ag and Pd, laser ablation inductively coupled mass spectrometry (LA-ICP-MS) could be employed to detect the lower concentration of these elements in the white metal phase, or some other method that could reliably detect those elements in low concentration.

8 References

AGA (2017) Product data Sheet. Liquid Argon, High Tech Quality [online] available at http://www.aga.fi/ [Accessed 8 Sept 2017]

Naraichiro Asano, Tadasu Ichio (1962) Distribution of Nickel and Lead between Copper and Cuprous Sulphide. Trans Min. Metall. Kyoto (Suiyokaishi (Japan)), Vol 14, P. 467 – 470.

Naraichiro Asano, Kuniomi Wase, Michiya Kobayashi (1971-4) Distribution of Gold and Selenium between liquid and Cuprous Sulfide. Japan Mining Journal. Vol 87. P. 347 – 352.

Asano N. (1965) Melting Smelting, Smelting by Gas Solid Reaction made in wet condition Showa 40 Mining Relations Association Joint Autumn Meeting (Kyoto). Subcommittee materials document. Melting Smelting, Smelting by Gas Solid Reaction made in wet condition. Japanese Mining Association / national coal mine Engineering Association. 40.10.23 – 24

Avarmaa K, Johto H. Taskinen P. (2015) Distribution of Precious Metals (Ag, Au, Pd, Pt and Rh) Between Copper Matte and Iron Silicate Slag. Metallurgical and Materials Transactions B.

Burylev, Mechev, Tsemekhan, Romonov, Vaisburd (1974) Distribution of Pd and Pt between metal and sulphide melt (Cu - S and Cu – Ni – S). Metals. Vol 2. P. 82 – 86.

D.J. Chakrabarti, D. E. Laughlin (1983) The Cu – S (Copper – Sulfur) System. Bulletin of Alloy Phase Diagrams. Vol. 4. No. 3. P. 254 – 271.

N. Choi, W.D. Cho (1997) Distribution Behaviour of Cobalt, Selenium and Tellurium between Nickel – Copper – Iron Matte and Silica – Saturated Iron Silicate Slag. Metallurgical and Materials Transactions B. Vol 28 B. P. 429 – 438

Pascal Coursol, Nubia Cardona Valencia, Phillip Mackey, Stacy Bell, Boyd Davis (2012) Minimization of Copper Losses in Copper Smelting Slag During Electric Furnace Treatment, Vol 64, Issue 11, P. 1305 – 1313.

Motonori Eguchi, Akira Yazawa (1977) Equilibrium Relations between Copper, White Metal and Silica – saturated Slag under Controlled SO_2 Pressure. Journal of the Mining and Metallurgical Institute of Japan, 99, 33, 191, (trans JIM, Vol 18).

D. R. Gaskell (2008) Introduction to the Thermodynamics of Materials. Fifth Edition, New York, USA, Taylor and Francis Group. P. 399 – 401. ISBN 9781498778589

Bob Hafner. Characterization Facility, University of Minnesota Energy Dispersive Spectroscopy on the SEM [online] available at http://www.charfac.umn.edu/instruments/eds_on_sem_primer.pdf [Accessed 10th Oct 2017].

Howard S. (2006) Ellingham Diagrams. [pdf], South Dakota School of Mines and Technology, Available at http://showard.sdsmt.edu/ [Accessed 15th May 2018].

Elizabeth A. Johnson, L. L. Oden, P. E. Sanker, and R. L. Fulton, 1984 Minor-Element Interactions in Copper Matte Smelting, Bureau of Mines Report of Investigations, united states department of the interior, Report of Investigations 8874.

Masaru Kashima, Motonori Eguchi, Akira Yazawa (1978) Distribution of Impurities between Crude Copper, White Metal and Silica saturated Slag, Trans JIM, Vol 19.

Masaru Kashima, Yuji Nishikawa, Motonori Eguchi, Akira Asano (1980). Distribution of Minor Elements among Liquid Copper, White Metal and Silica – Saturated Slag, Japanese Mining Association Journal. 96, 1114. P. 906 – 911.

Tak Seng Kho (2006) Microelement Distribution during Matte Smelting, Dissertation submitted in fulfilment of the requirements for the degree of Doctor of Philosophy in Engineering, RMIT University, School of Civil and Chemical Engineering. 206 p.

T.S. Kho, D.R. Swinbourne, T. Lehner (2006) Cobalt Distribution during Copper Matte Smelting. Metallurgical and Materials Transactions B. Vol 37 B, P. 209-211.

W. A. Krivsky and R. Schuhmann, Jr (1957) Thermodynamics of the Cu – Fe – S system at Matte Smelting Temperatures , The Journal of Metals, Transactions AIME, Vol 209, P. 981 – 988.

LentonFurnaces (2017) PTF – Three Zone Tube Furnaces: 1200, 1500 & 1600 °C. [Online] Available http://www.lentonfurnaces.com/content47/ptf-three-zone-tube-furnaces-1200C-and-1700C.aspx [Accessed 8 Sept 2017]

Myscope (2014). Accuracy, Precision and detection limits [online] available at http://www.ammrf.org.au/myscope/analysis/eds/accuracy/ [Accessed 10th Oct 2017].

M. Nagamori, P. J. Mackey (1978) Thermodynamics of Copper Matte Converting: Part II. Distribution of Au, Ag, Pb, Zn, Ni, Se, Te, Bi, Sb and As between Copper, Matte and Slag in the Noranda Process. Metallurgical Transactions B. Vol 9 B. P. 567 – 579.

Y. K. Rao (1984) Stoichiometry and Thermodynamics of Metallurgical Processes, Cambridge England, Cambridge University Press P. 516 – 519. ISBN 0 521 25856 1

M. Schlesinger, M. King, K Sole, W Davenport (2011) Extractive Metallurgy of Copper. 5th Edition, Oxford England, Elsevier, P. 441. ISBN: 978-0-08-096789-9

W. J. Schlitt, R. H. Craig, K. J. Richards (1973) The Miscibility Gap and Distribution of Nickel in the Molten System Cu – Ni – S, Metallurgical Transactions, Vol 4, P. 1994 – 1996.

W.J. Schlitt, K. J. Richards (1975) The Distribution of Silver, Gold, Platinum and Palladium in Metal – Matte Systems, Metallurgical Transactions B, Vol 6 B, P. 237 – 243.

Schmiedl J, Repcak V, Havlik M. (1977) Distribution of Ni and Sb among the Products of Copper Matte Converting (on a Laboratory Scale), Proc. Symp. on Advances in Extractive Metallurgy, P. 201 – 205.

R. Schuhmann, Jr (1950) A Survey of the Thermodynamics Copper Smelting, The Journal of Metals Transactions, Vol 188, p. 873 – 884.

S.N. Sinha, H.Y. Sohn, M. Nagamori (1985) Distribution of Gold and Silver between Copper and Matte, Metallurgical Transactions B, Vol 16 B, P. 53 – 59.

J. R. Taylor (1983) A Thermodynamic Study of the Distribution of Metals between Copper Matte and Bullion. In: H. Y. Sohn, D.B. George A. D. Zunkel. Proceedings of the 1983 International Sulfide Smelting Symposium on Advances in Sulfide Smelting, San Francisco, California, USA. November 6-9, 1983. Warrendale, Pennsylvania, USA. The Metallurgical Society of AIME. P 217 – 229. ISBN: 0-89520-463-0.

Akira Yazawa (1980) Distribution of Various Elements between Copper, Matte and Slag, Erzmetall Nr. 7 / 8, P. 377 – 382.

Yazawa, A (1974) Thermodynamic considerations of copper smelting. Can Metall Quart. Vol 13, (13). P. 443 – 455.

Alireza Zakeri, Mitsuhisa Hino, Kimio Itagaki (1998) Activity of Silver in Molten Copper Sulphide Saturated with Copper. Materials Transactions, JIM. Vol 39 No 11, p 1101 - 1107.

9 Appendix 1 Micrographs of samples

Main series of experiments; **0.01 atm P(SO_2) 1250 °C**

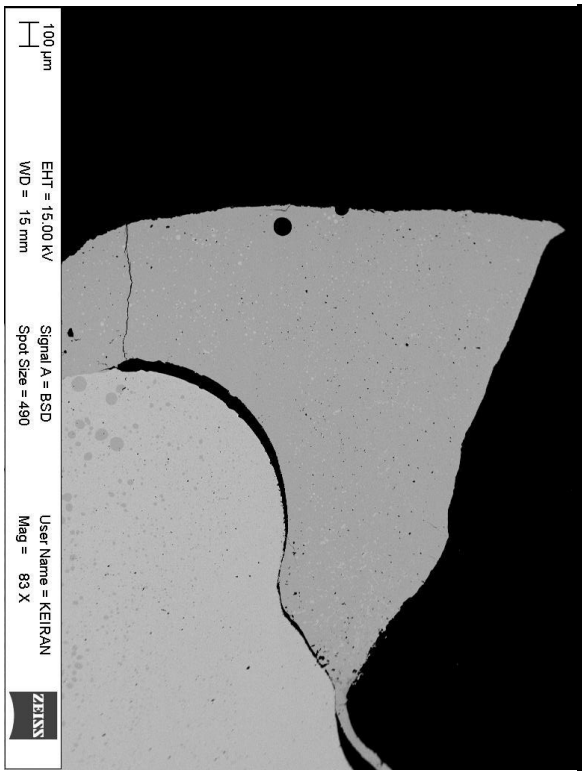

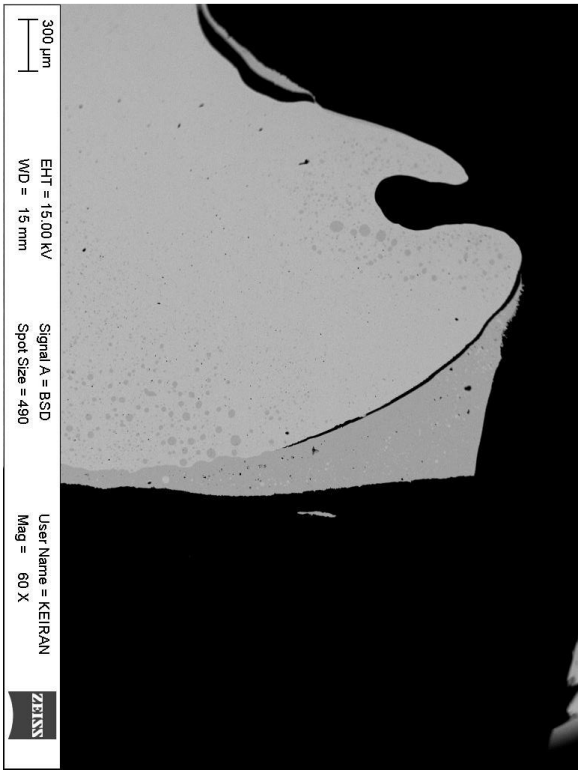

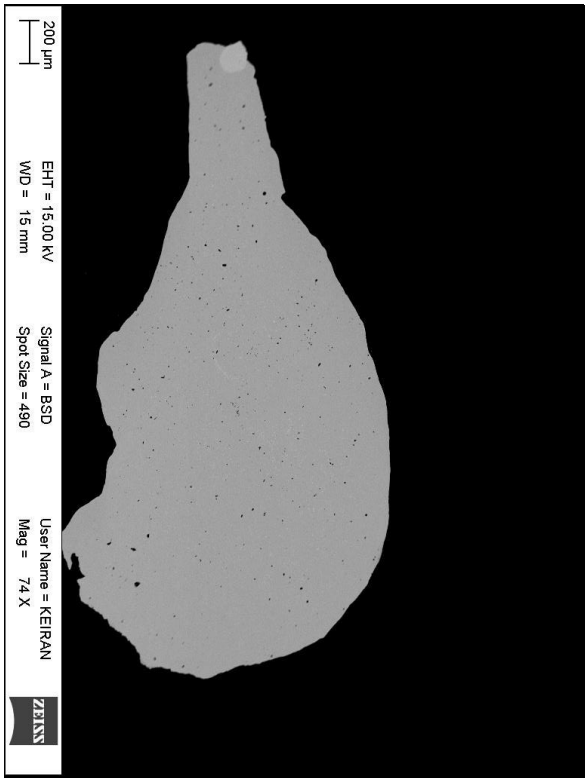

0.01 atm P(SO_2) 1300 °C

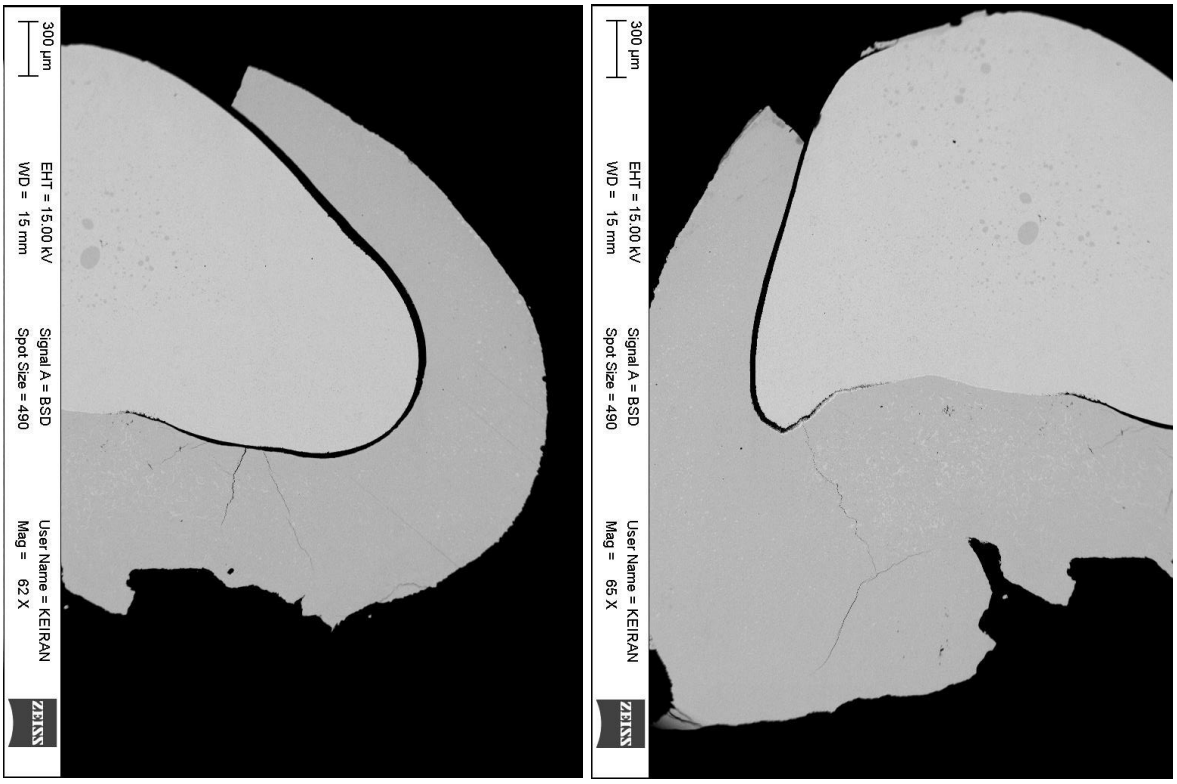

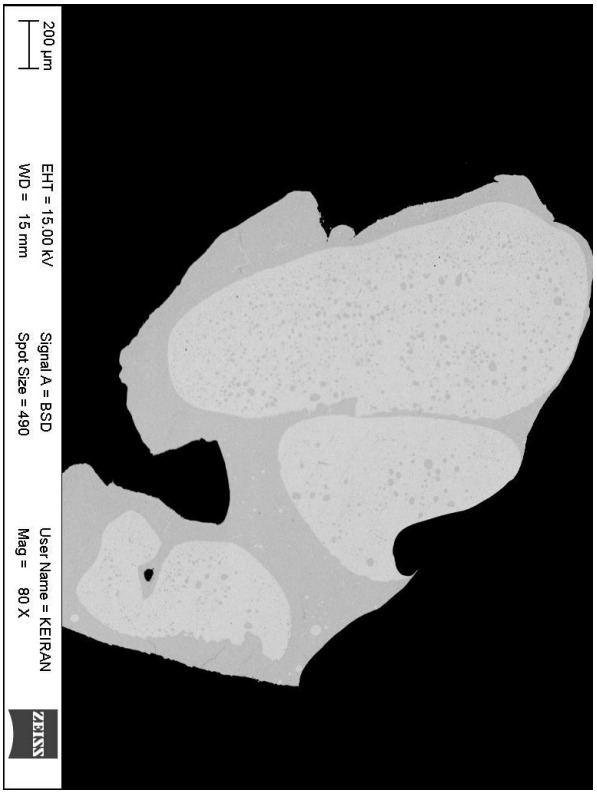

0.01 atm P(SO_2) 1350 °C

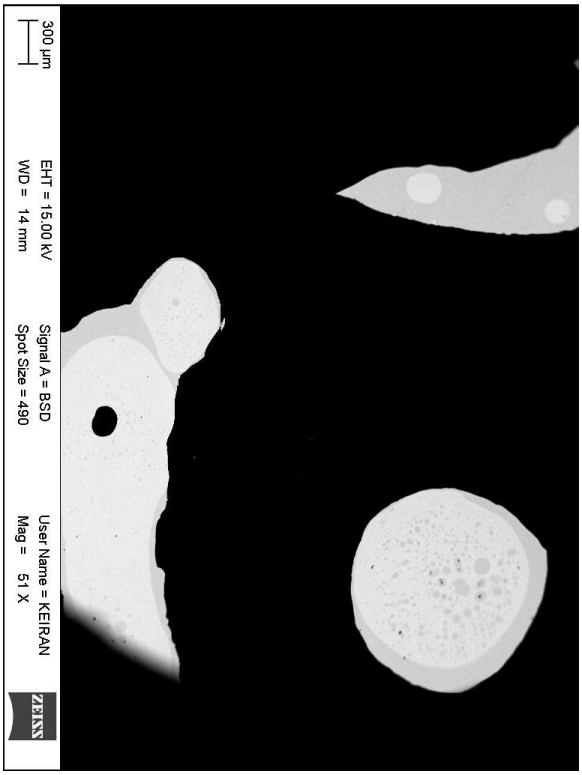

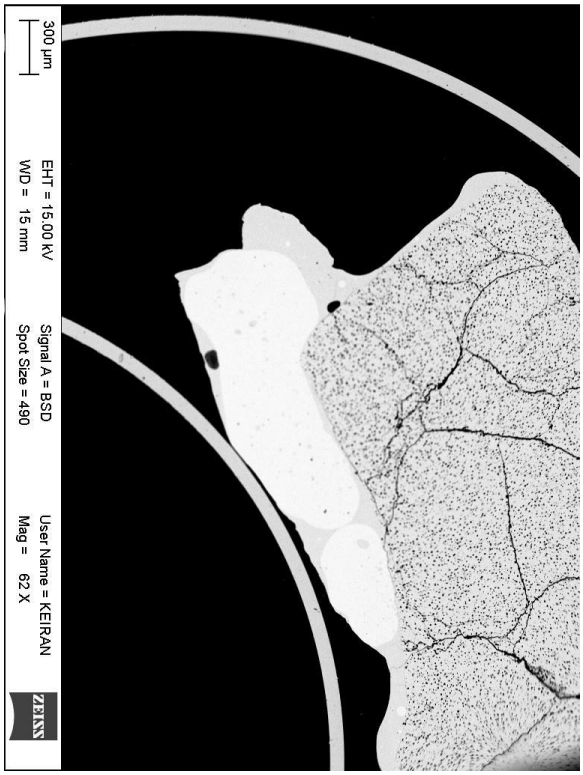

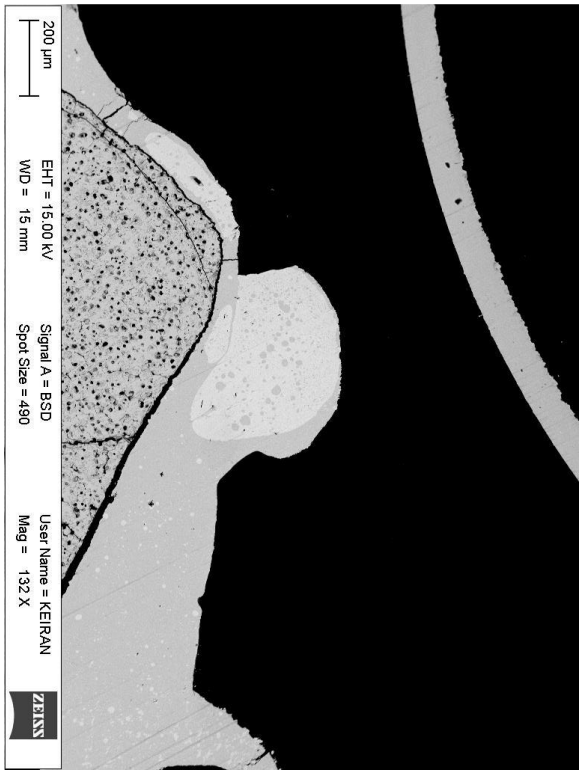

0.05 atm P(SO_2) 1250 °C

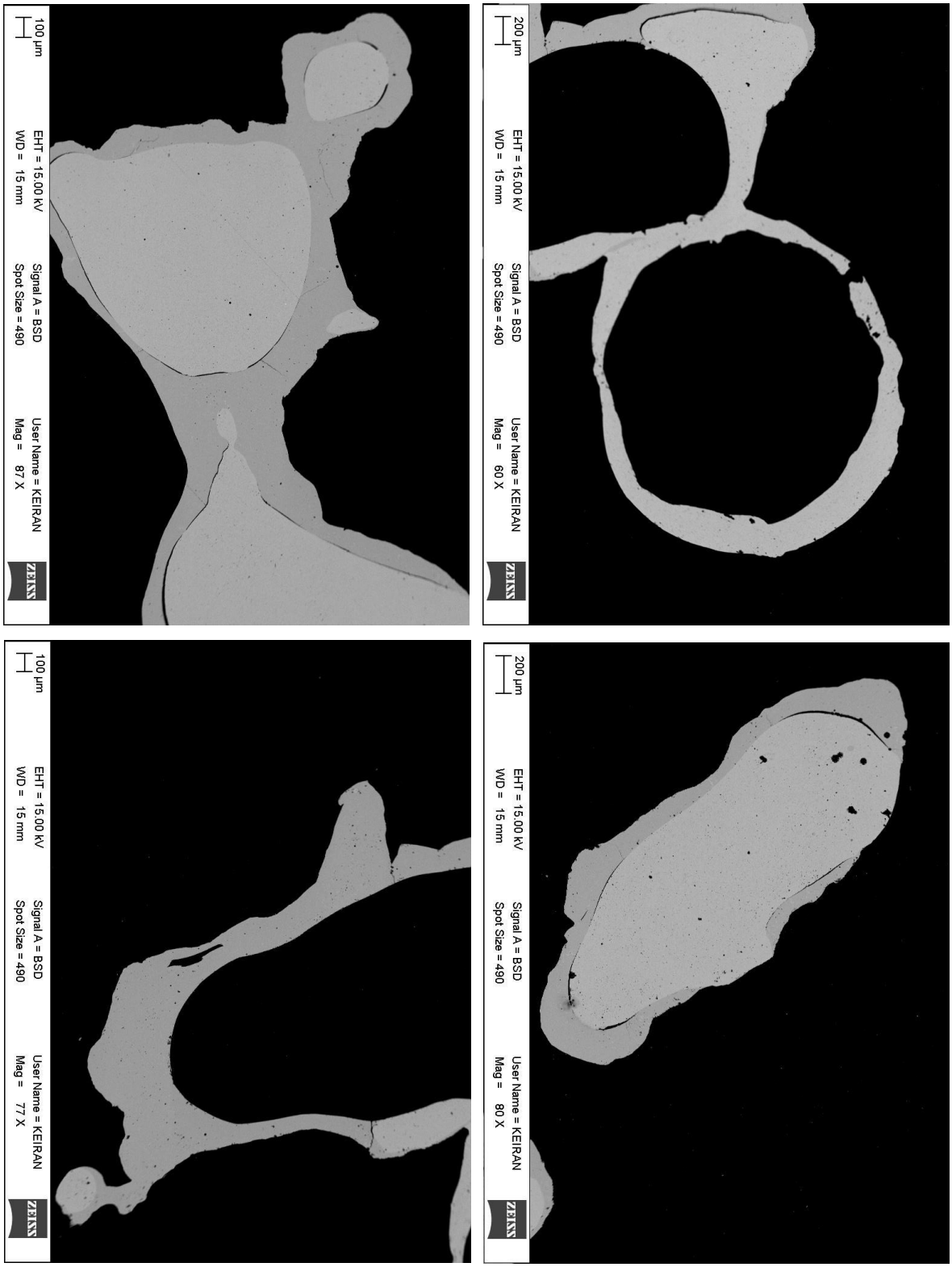

0.05 atm P(SO_2) 1300 °C

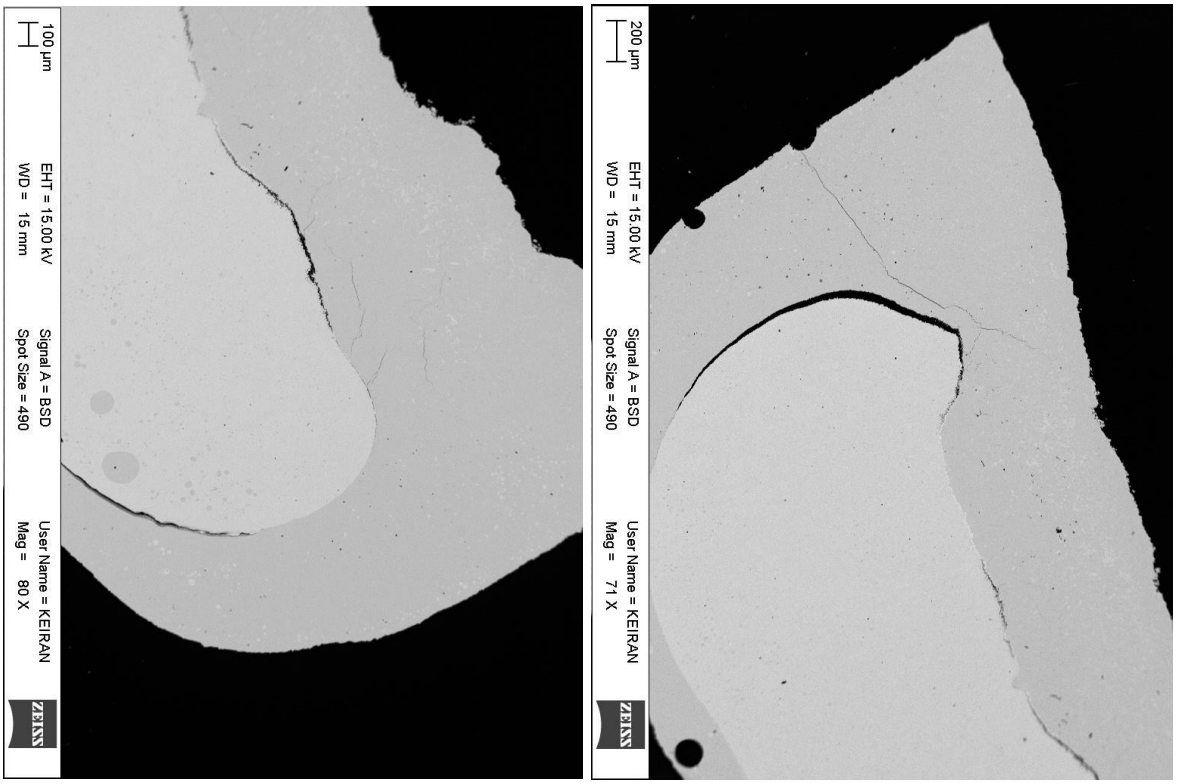

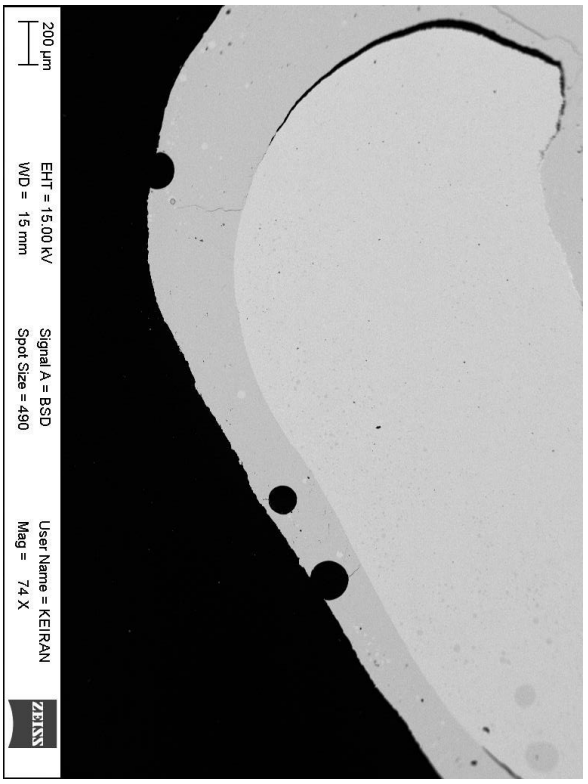

0.05 atm P(SO_2) 1350 °C

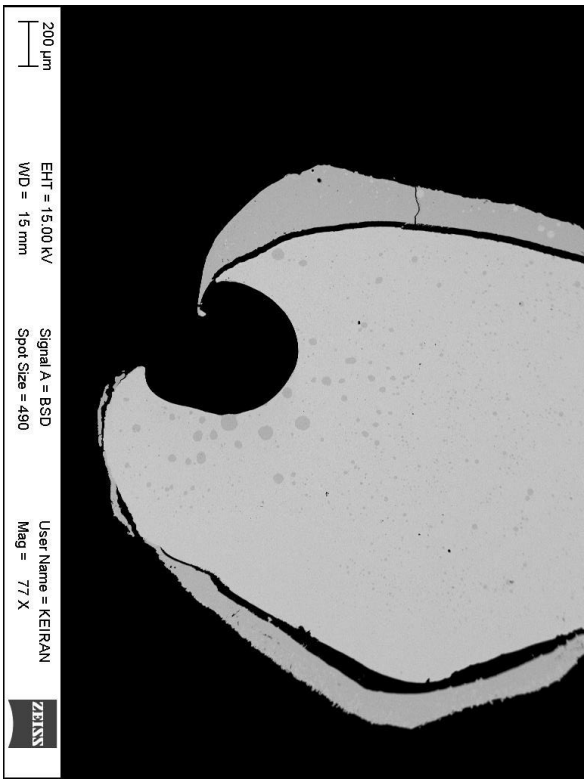

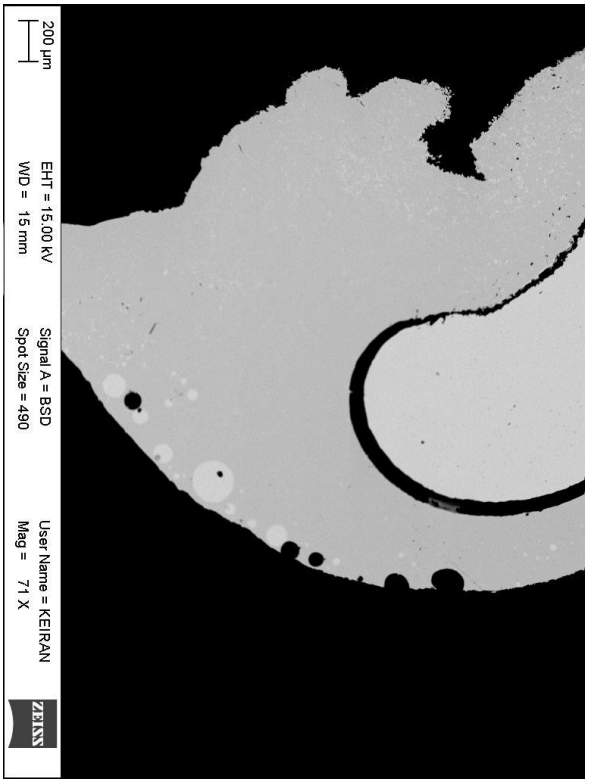

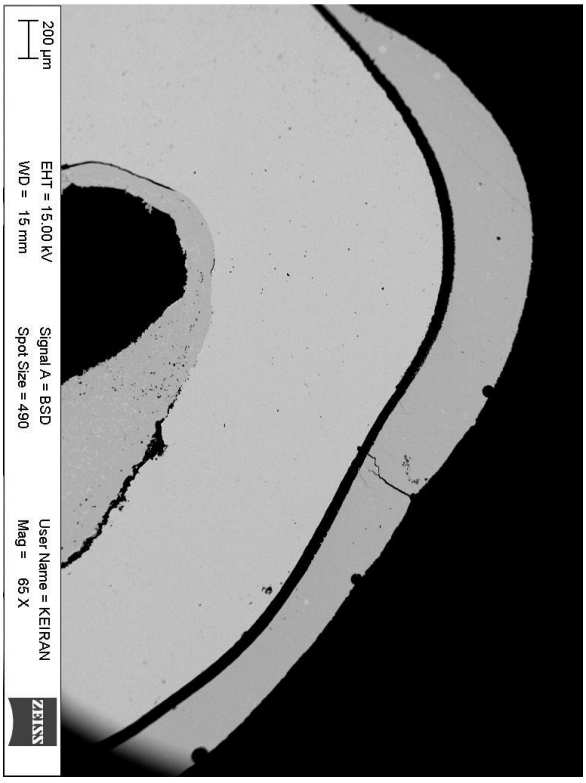

0.1 atm P(SO_2) 1250 °C

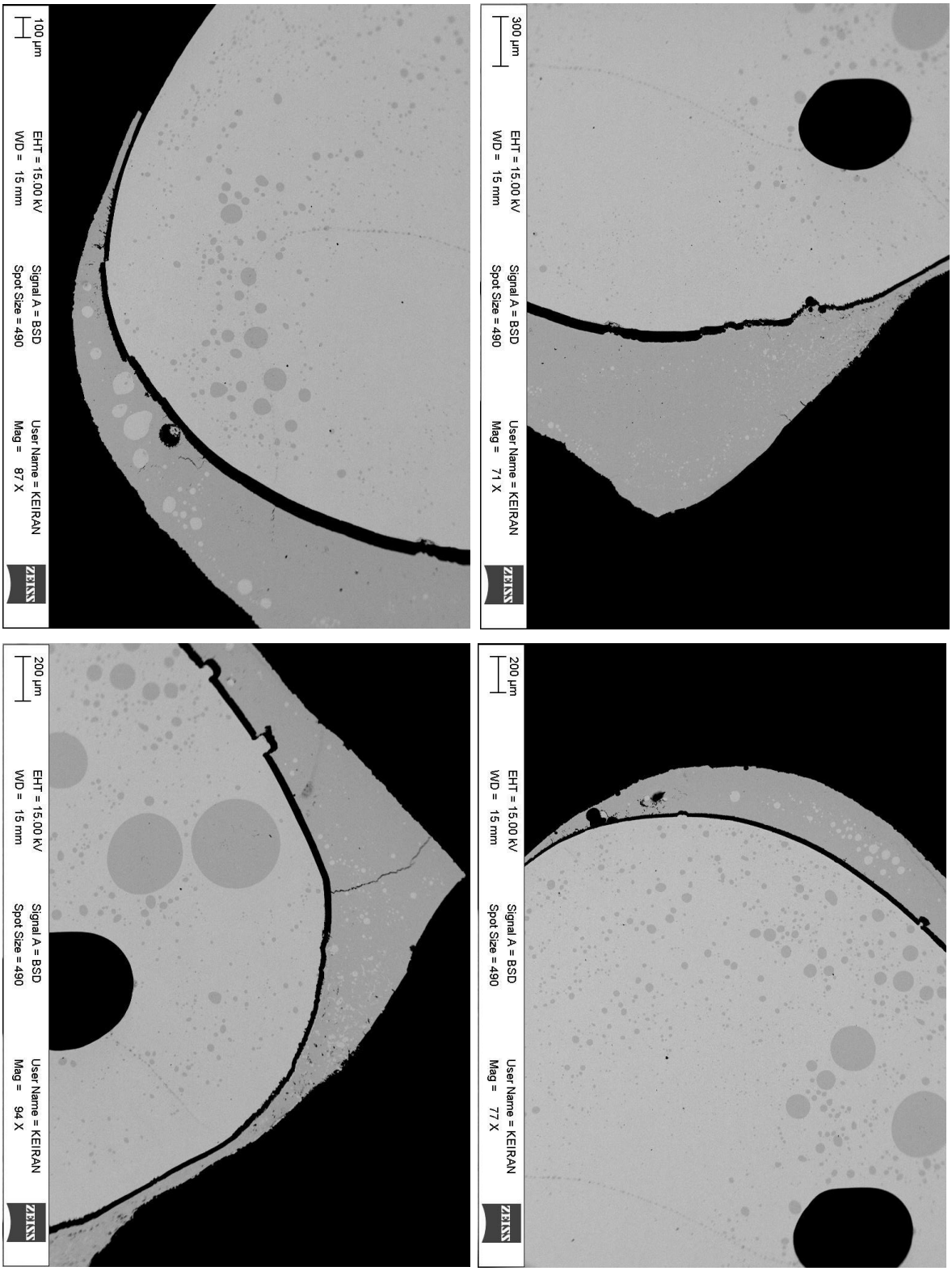

0.1 atm P(SO_2) 1300 °C

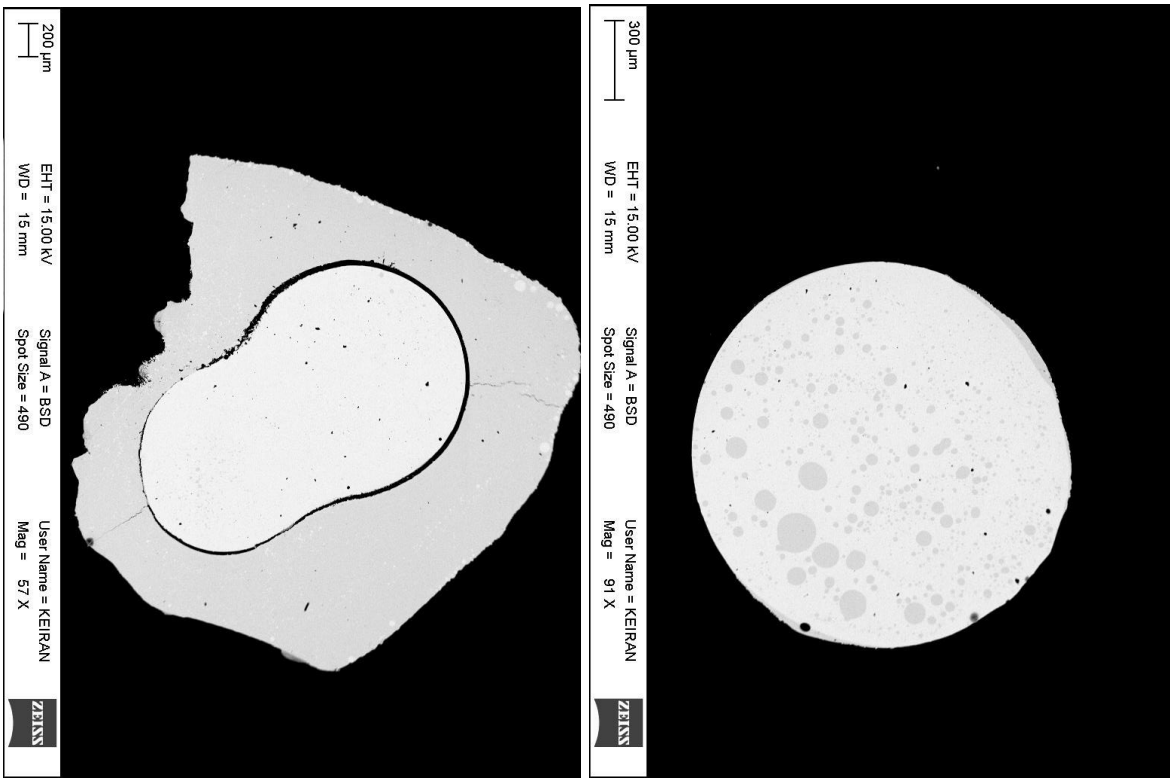

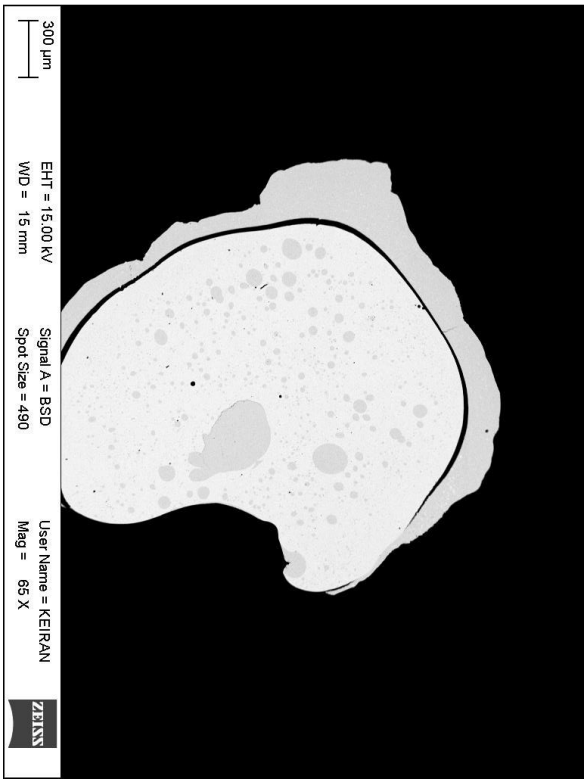

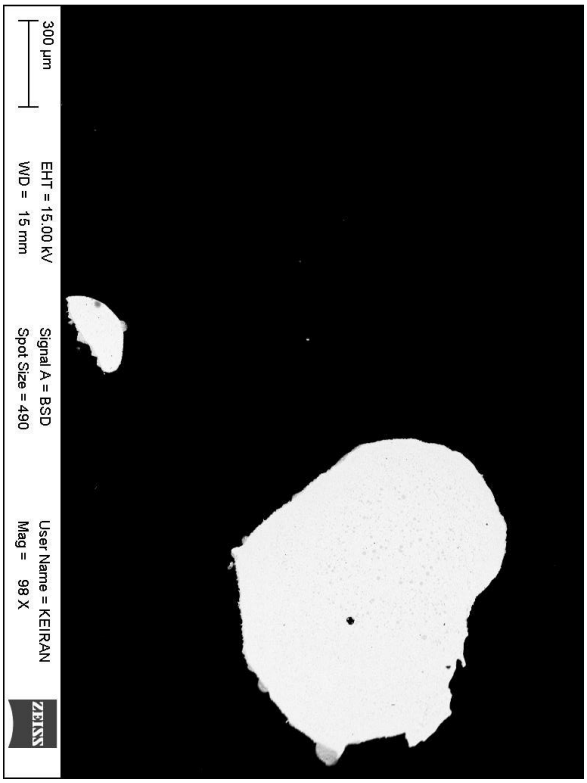

0.1 atm P(SO_2) 1350 °C

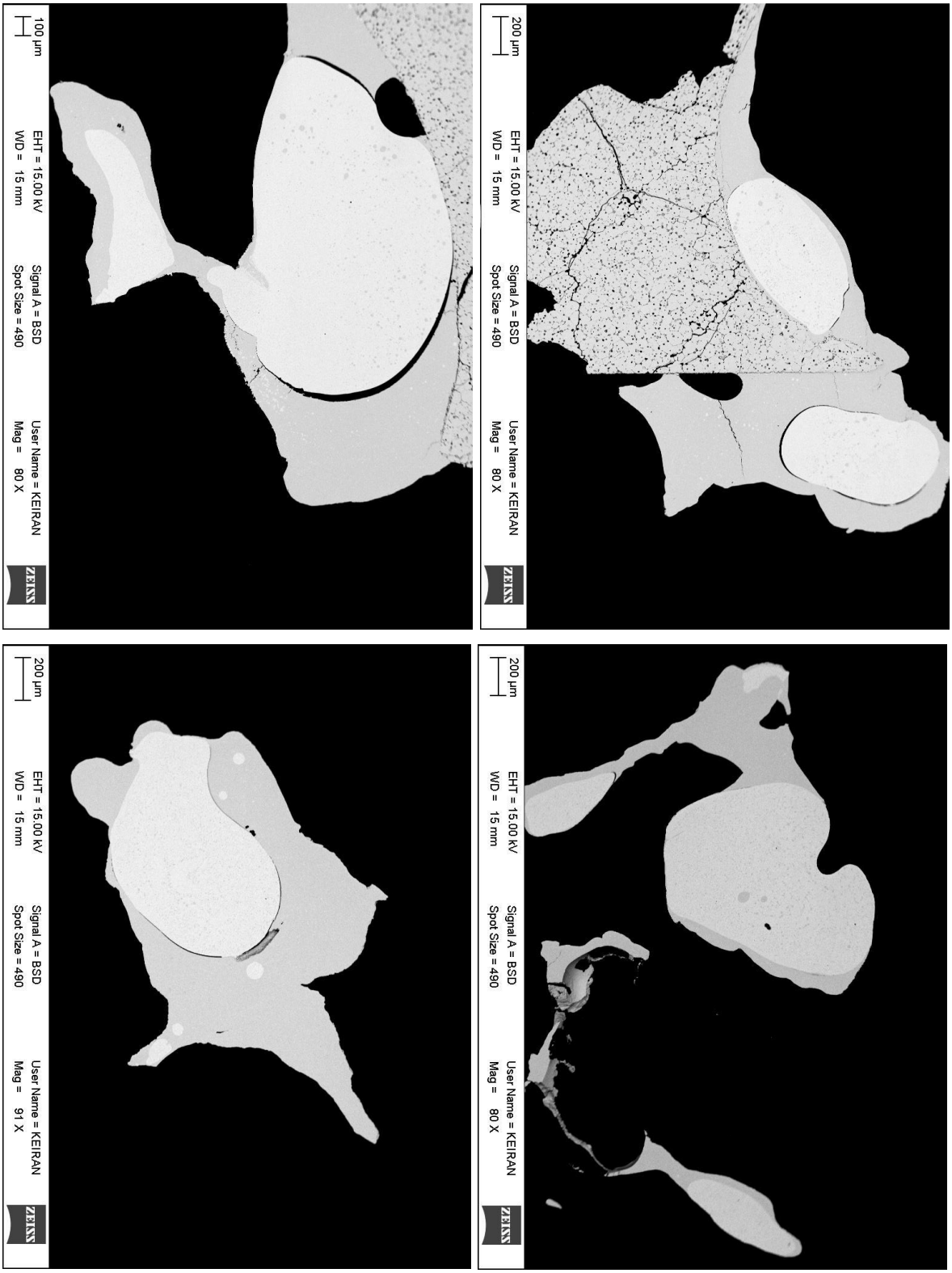

0.5 atm P(SO_2) 1250 °C

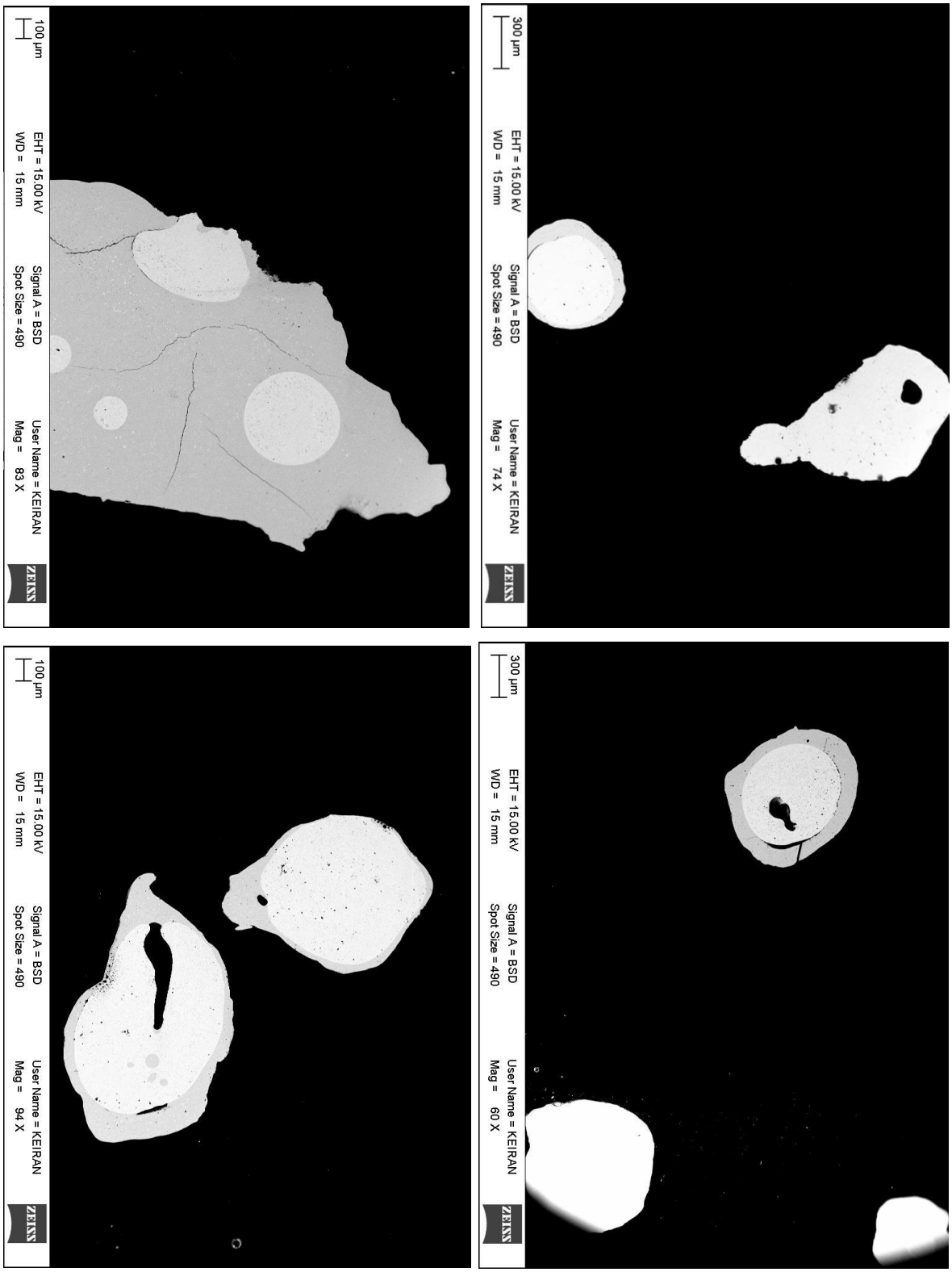

0.5 atm P(SO_2) 1300 °C

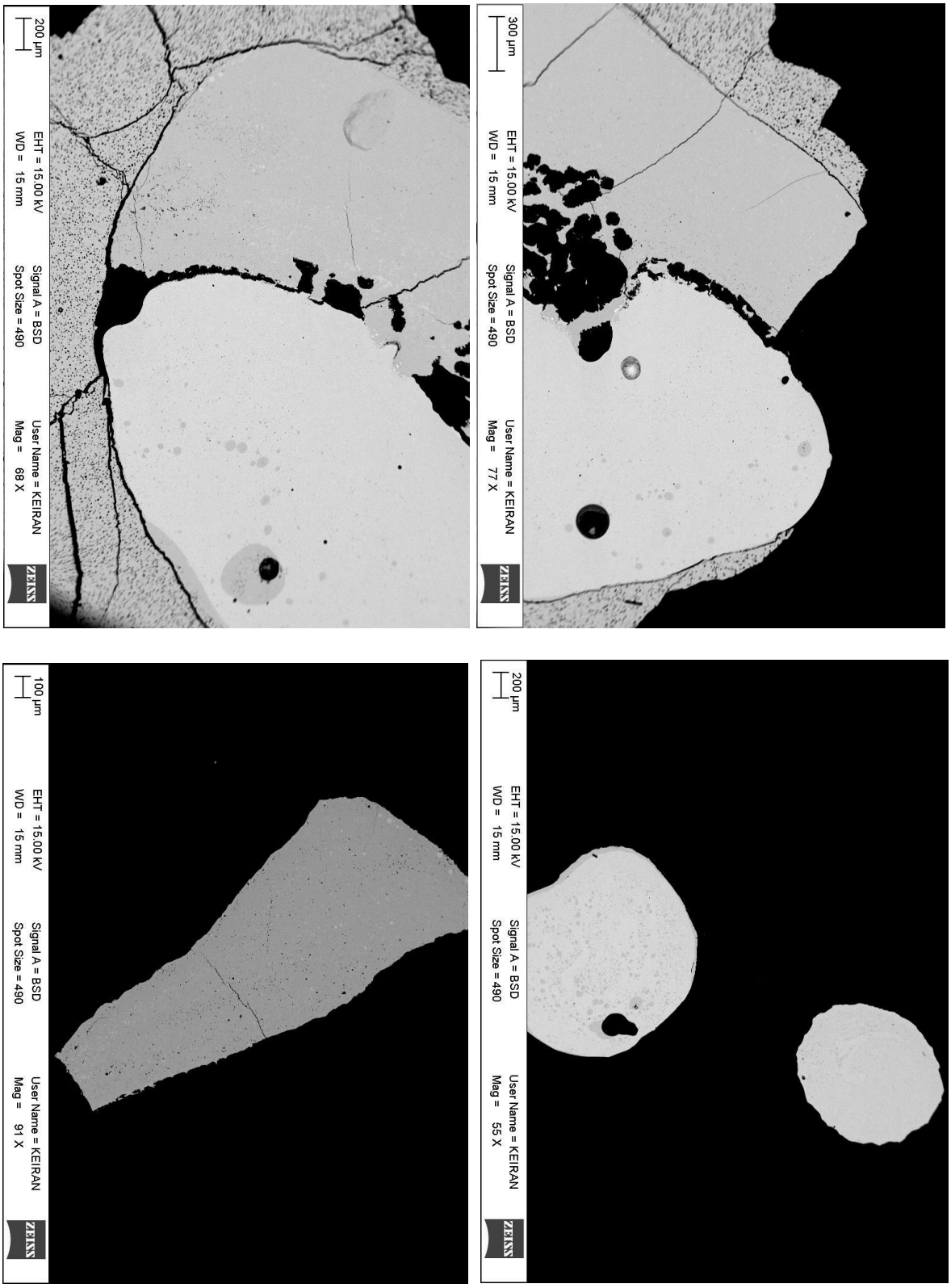

0.5 atm P(SO_2) 1350 °C

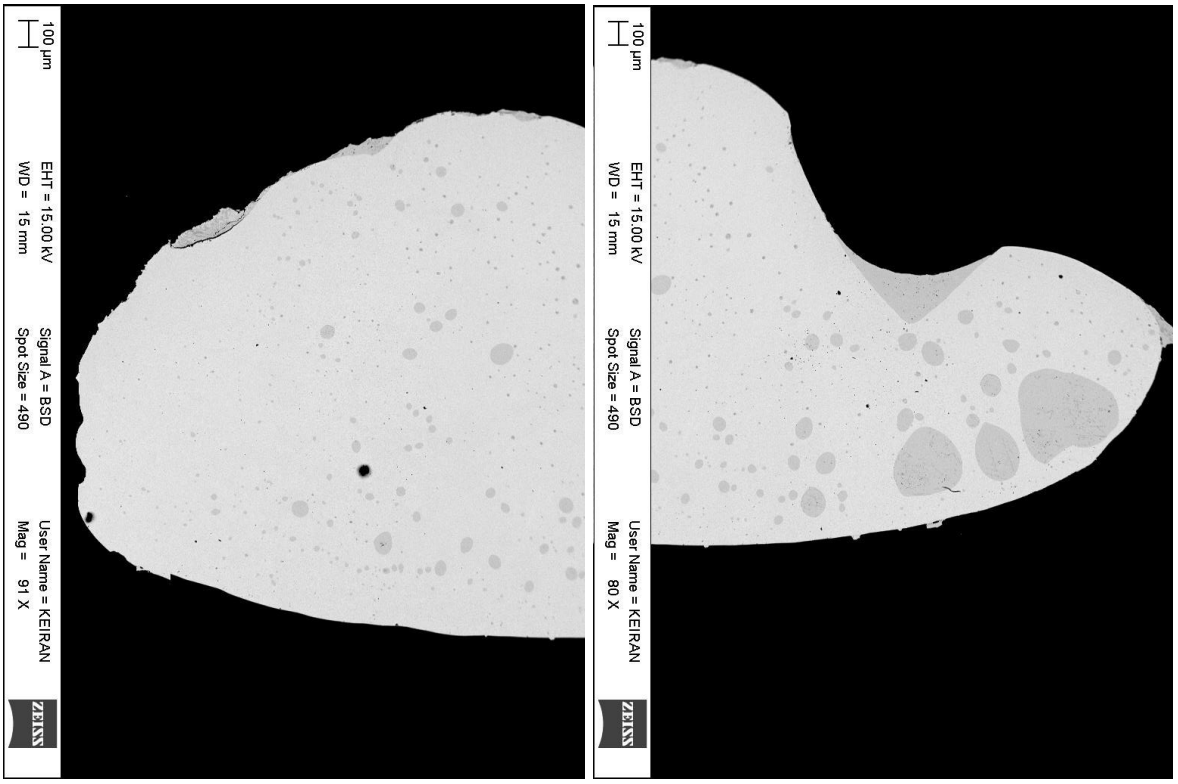

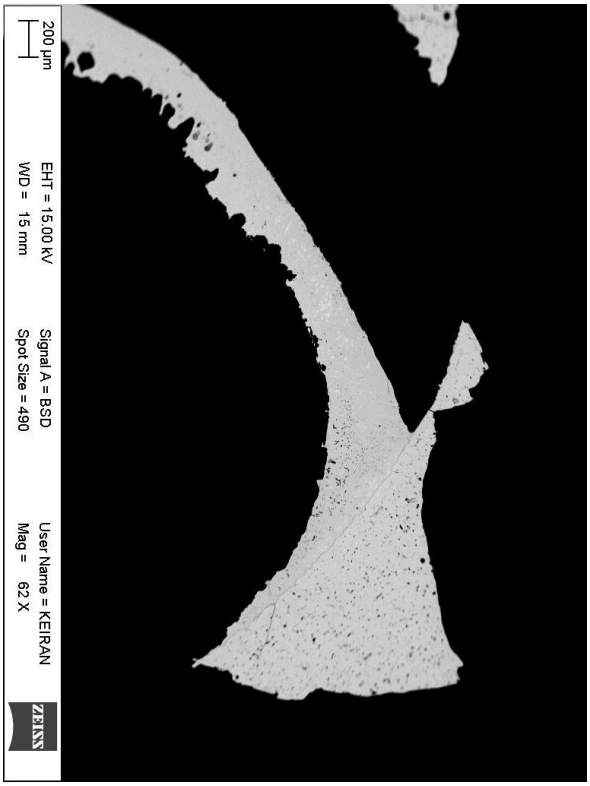

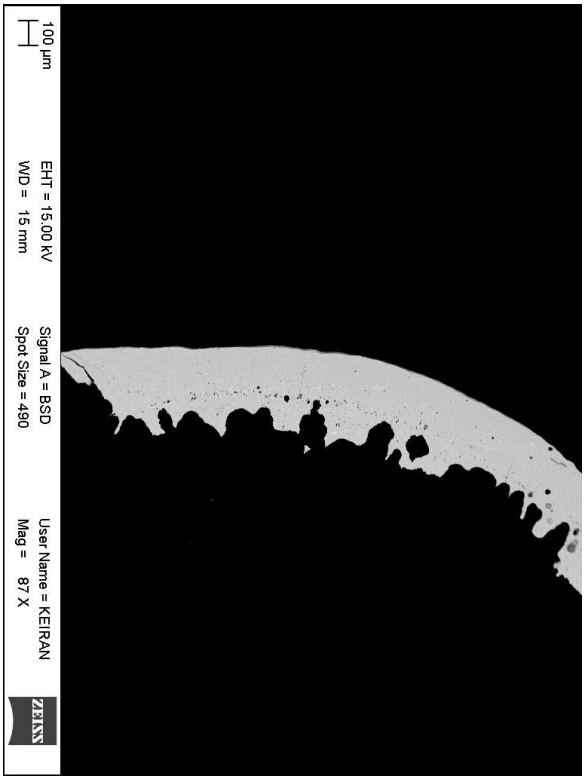

1 atm P(SO_2) 1250 °C

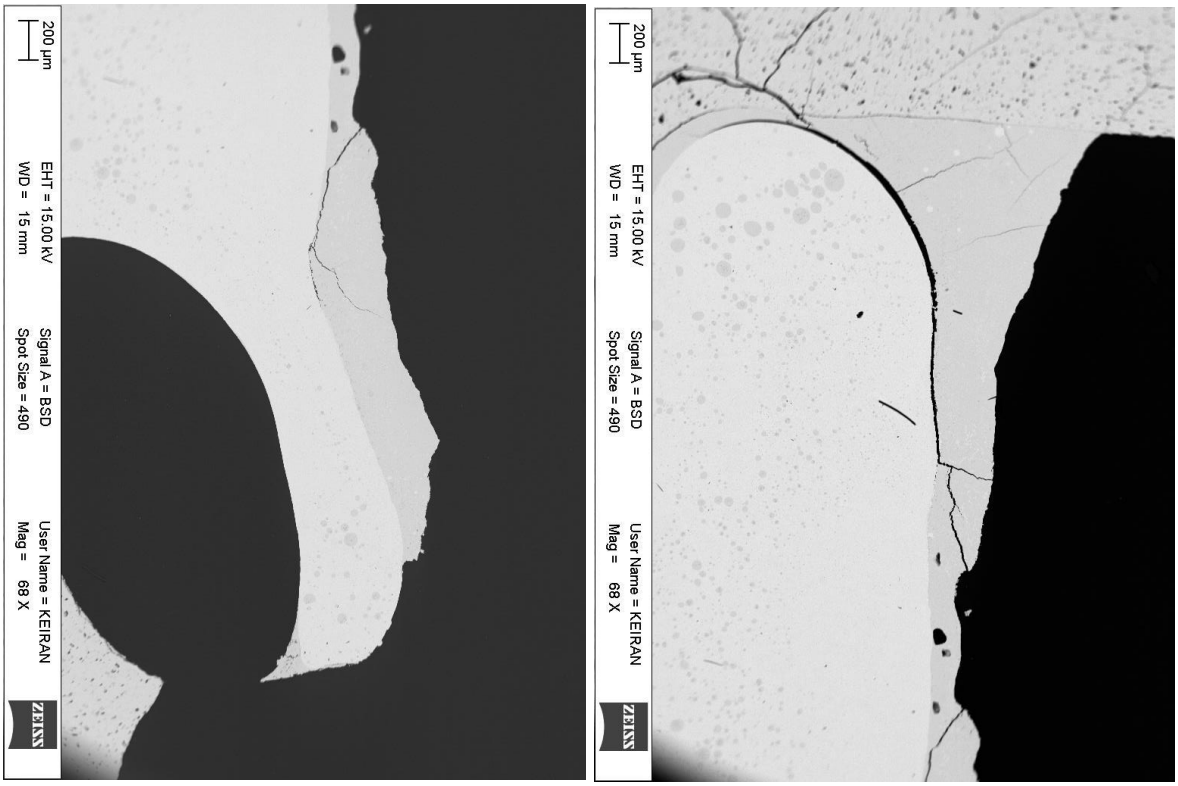

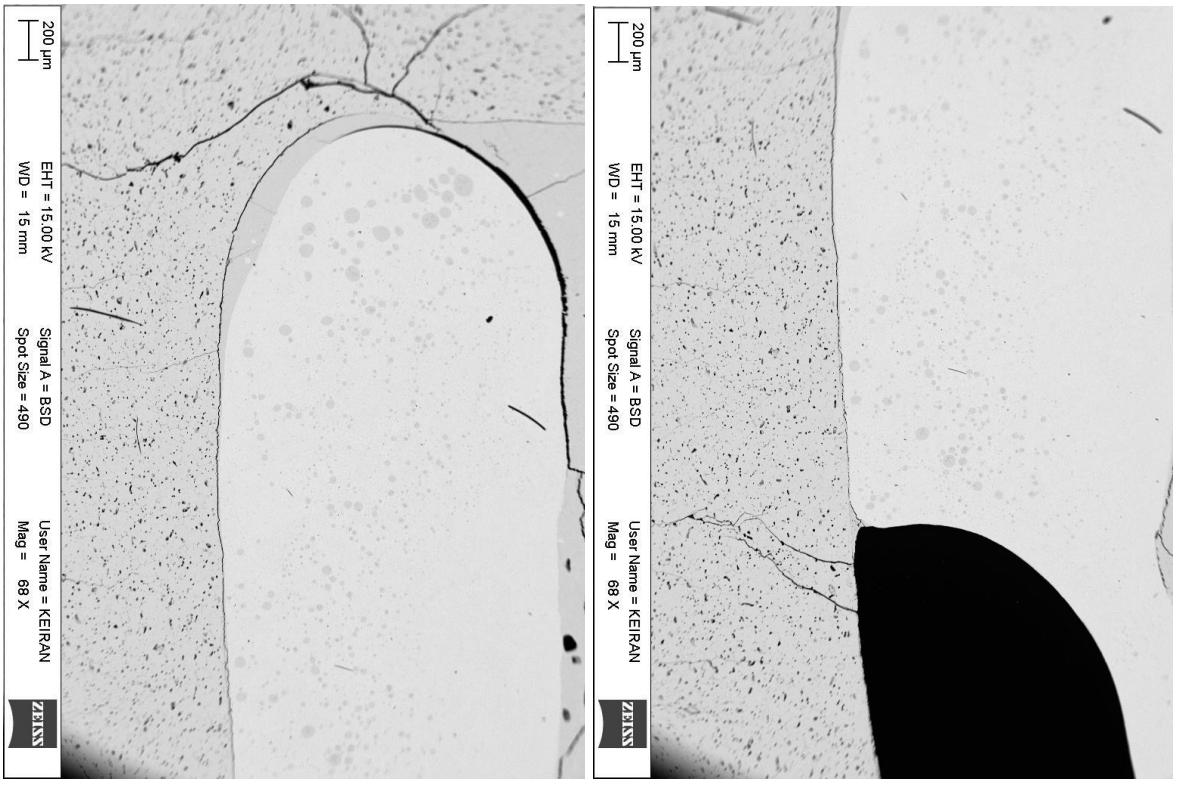

1 atm P(SO_2) 1300 °C

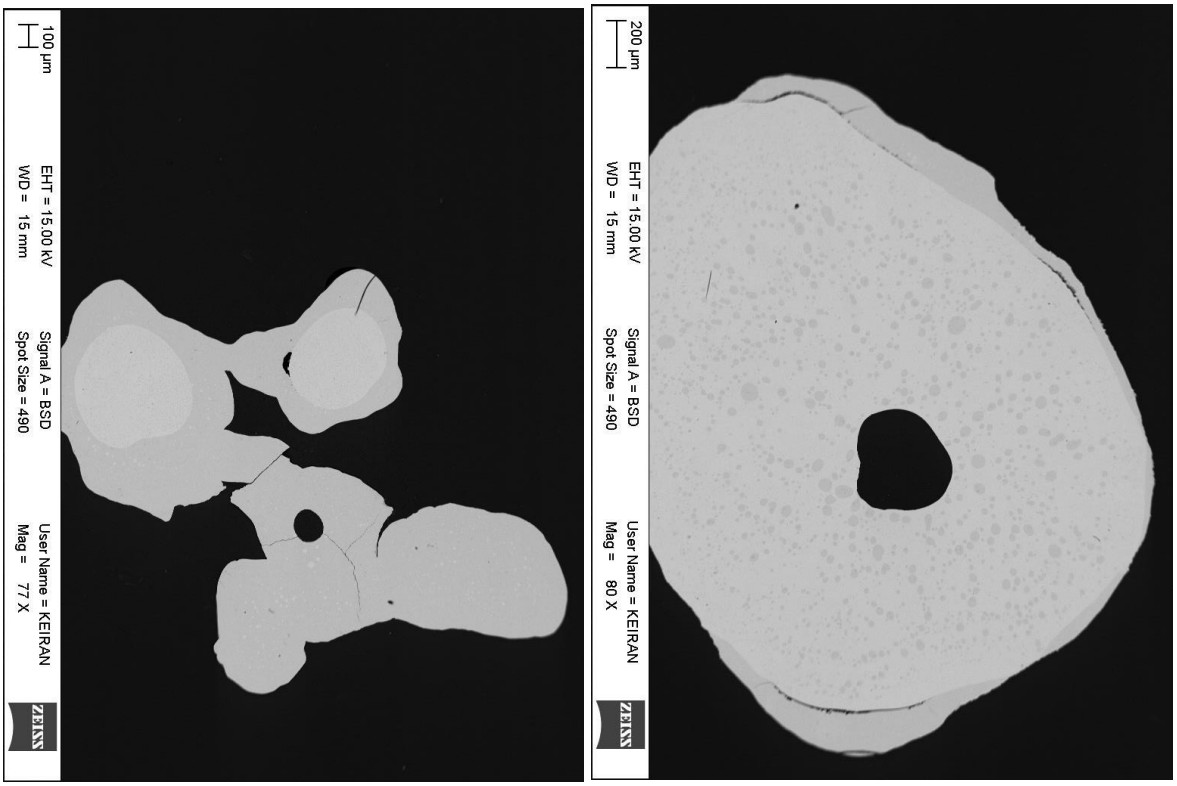

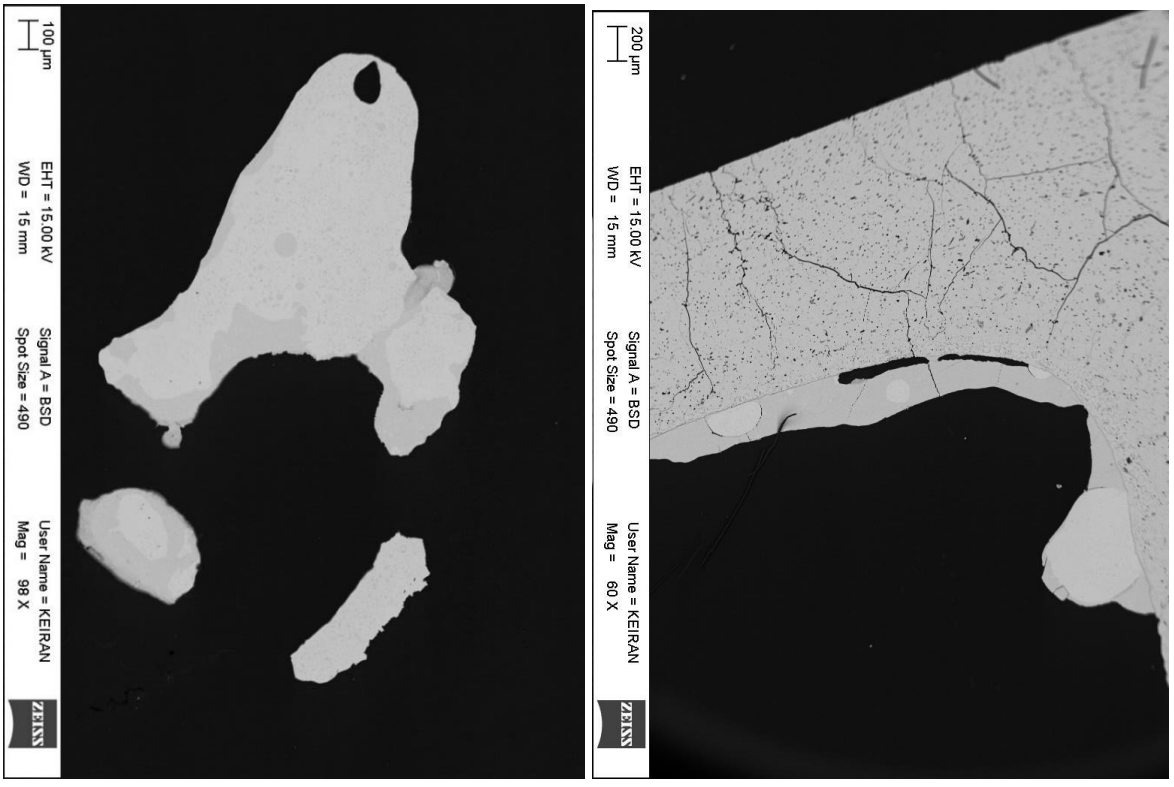

1 atm $P(SO_2)$ 1350 °C

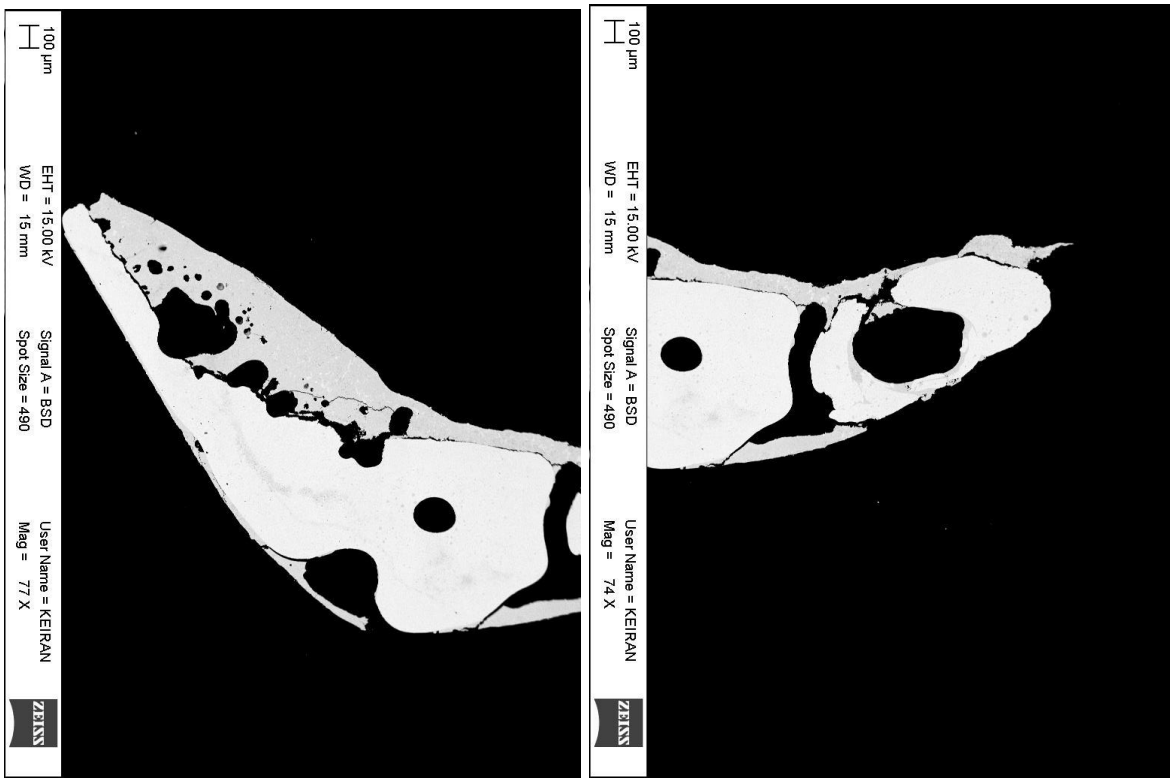

Second series **0.01 atm P(SO_2) 1250 °C**

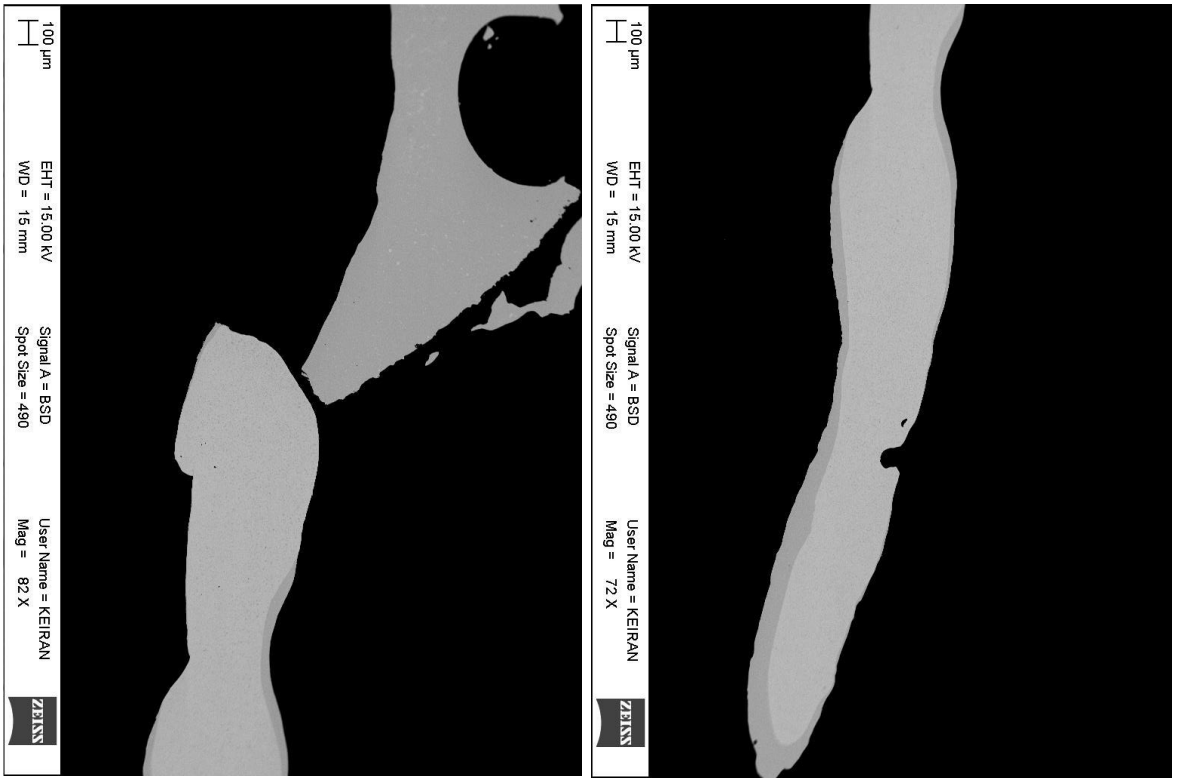

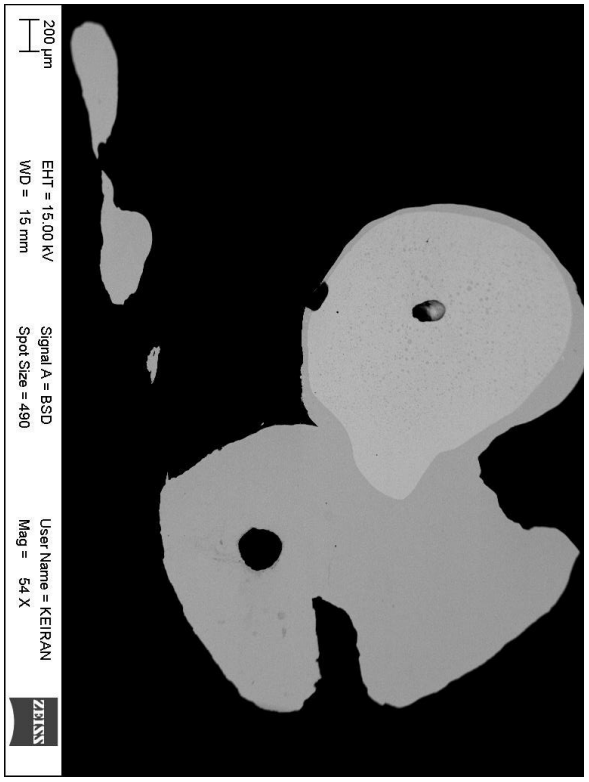

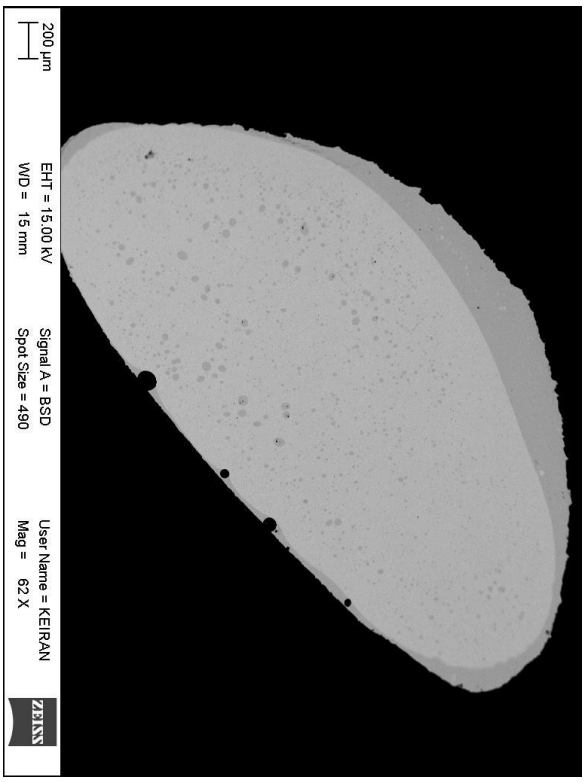

0.01 atm P(SO_2) 1350 °C

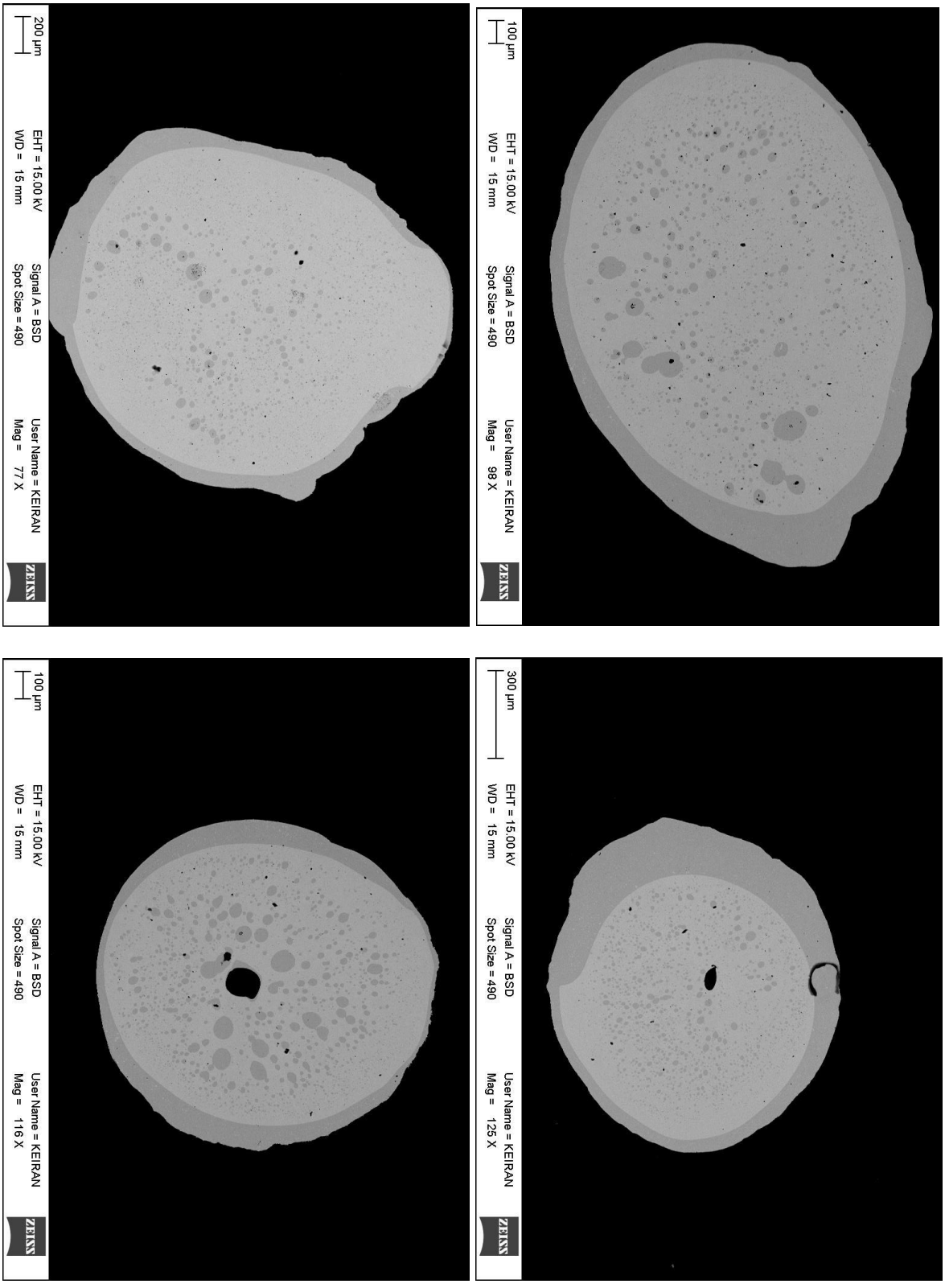

0.05 atm P(SO_2) 1300 °C

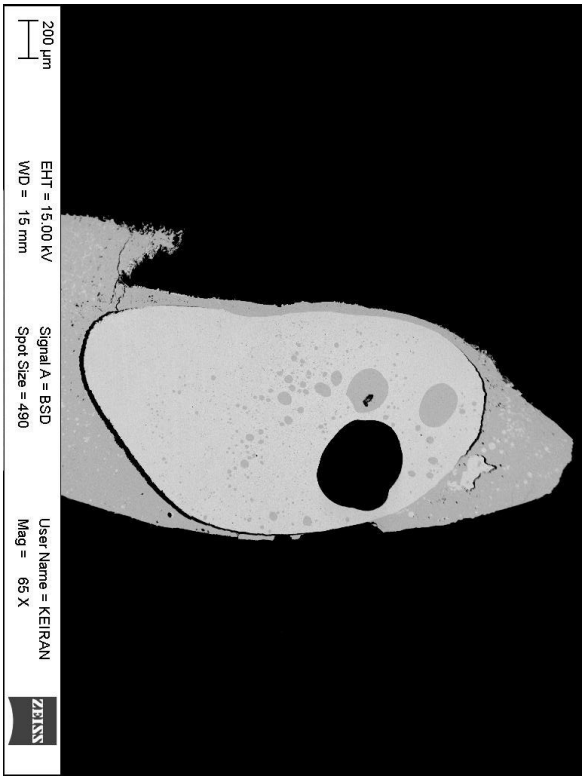

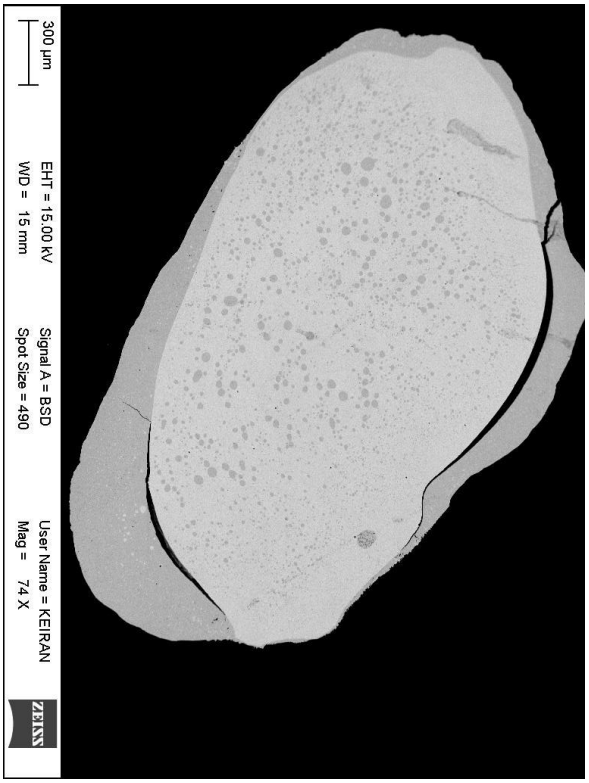

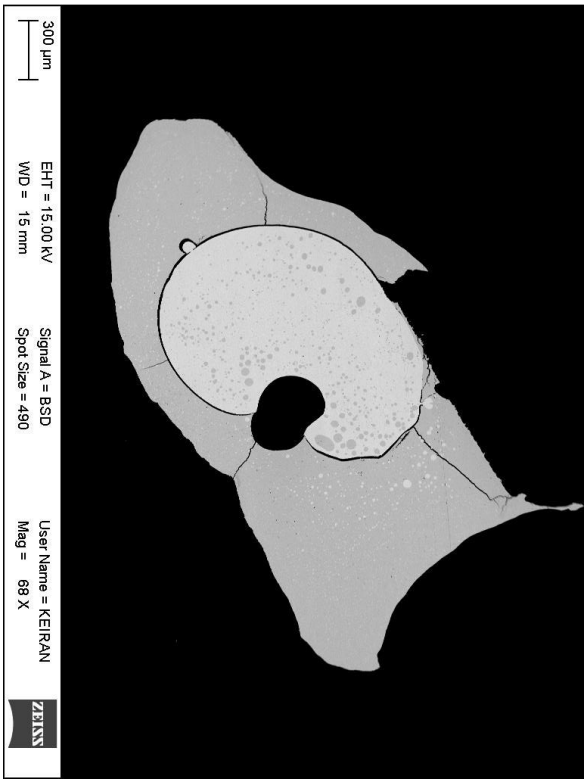

0.5 atm $P(SO_2)$ 1300 °C

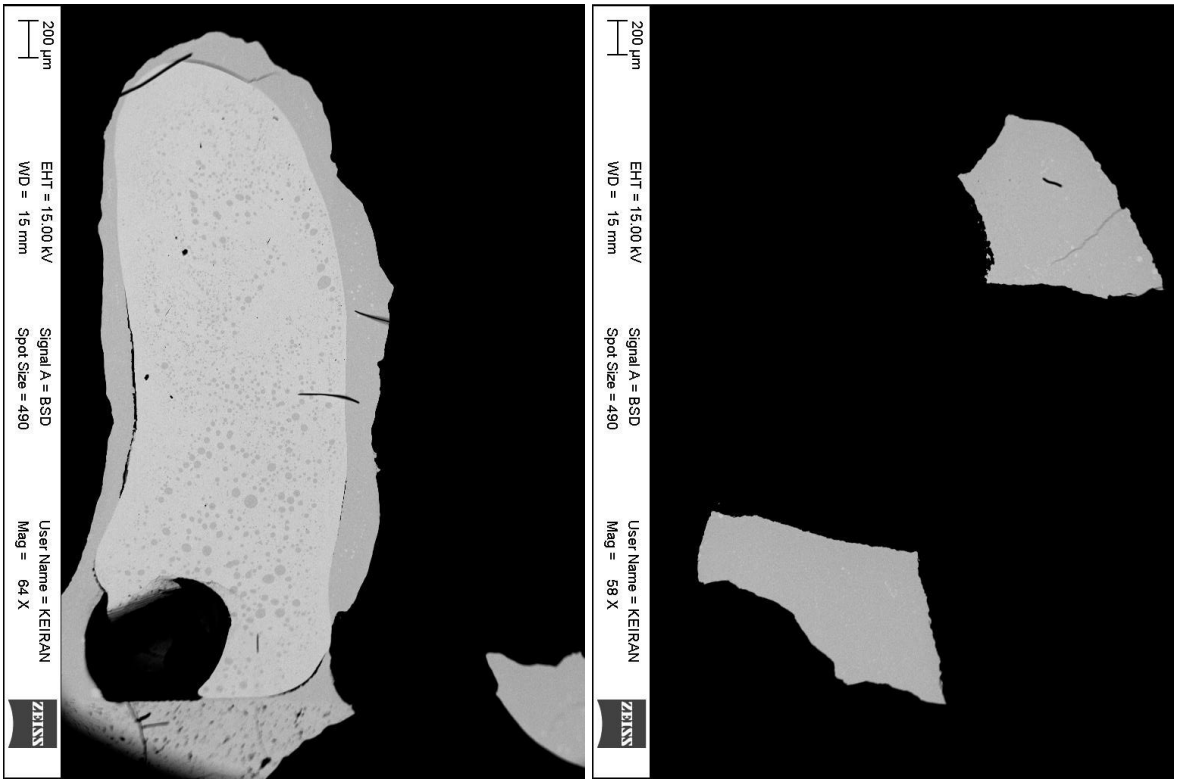

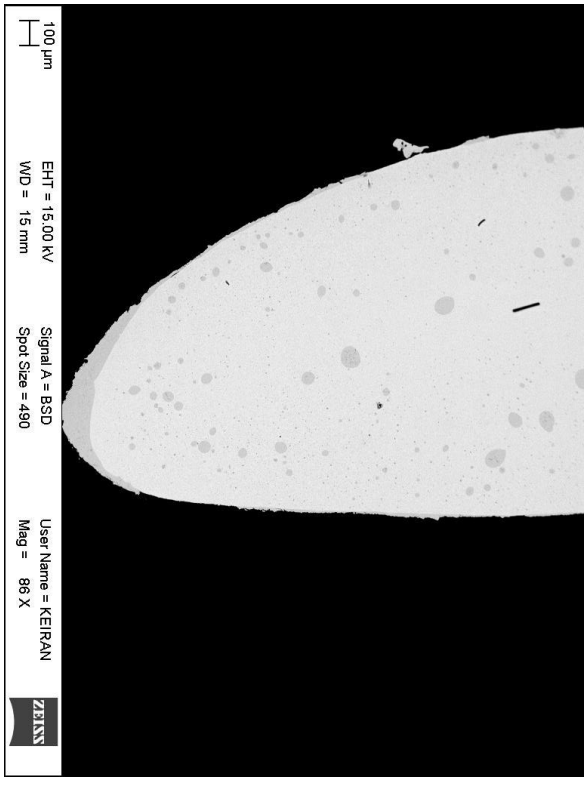

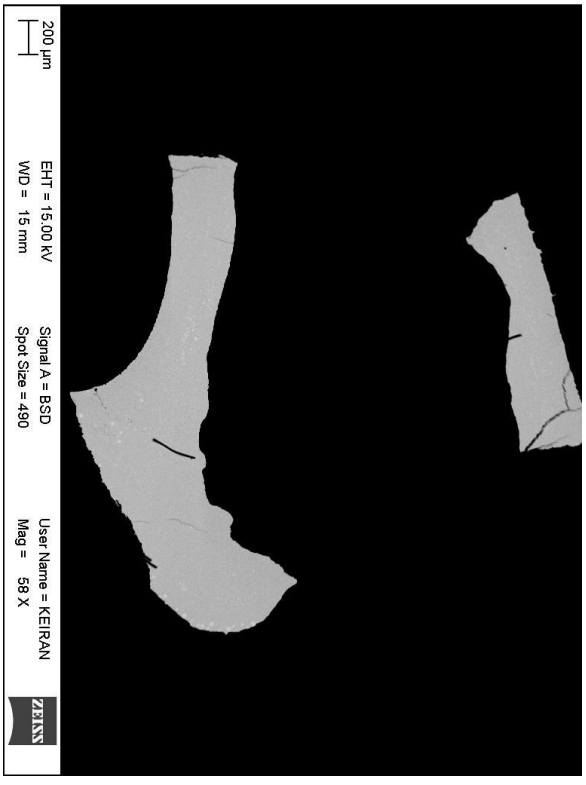

1 atm $P(SO_2)$ 1250 °C

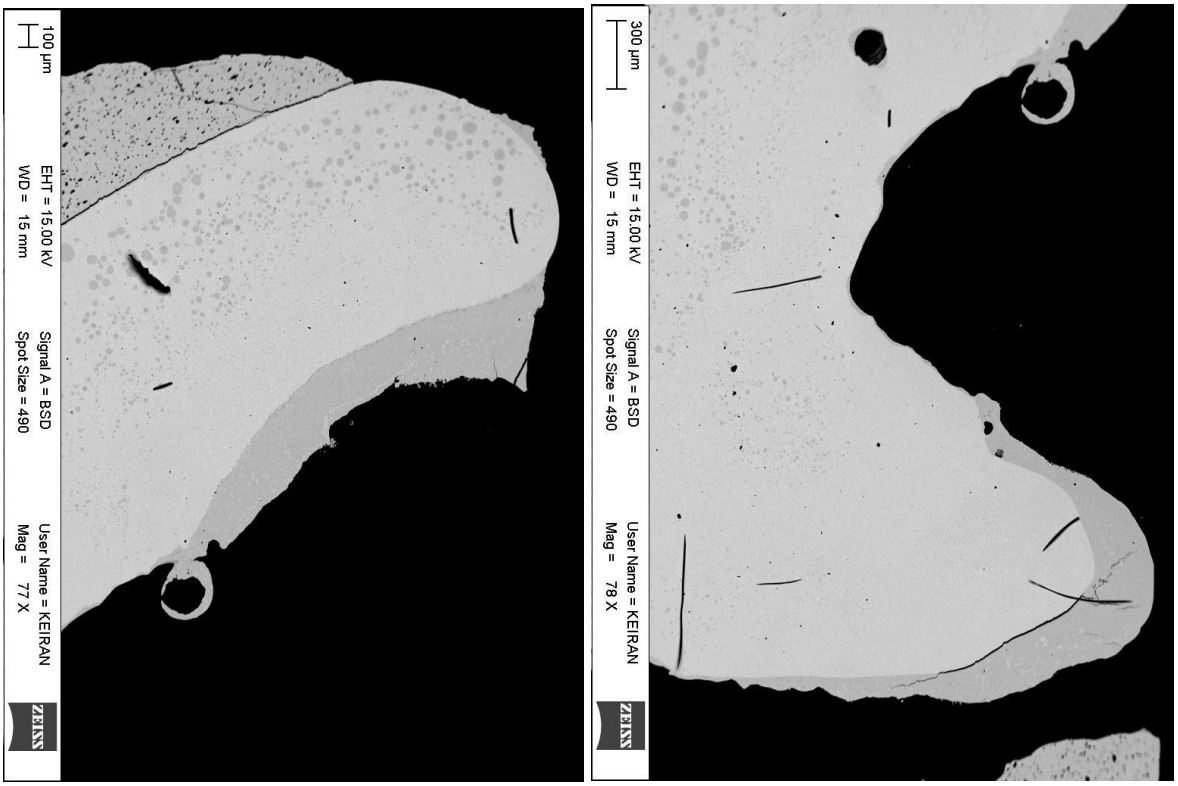

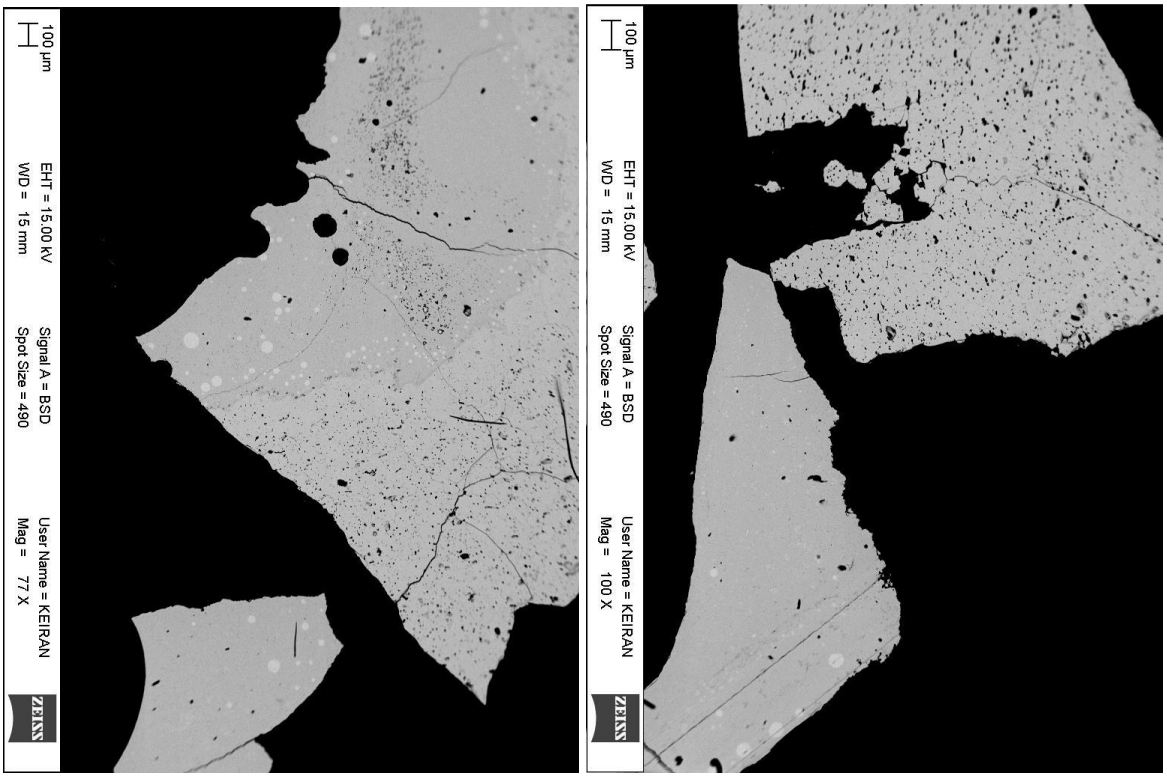

1 atm% P(SO_2) 1350 °C

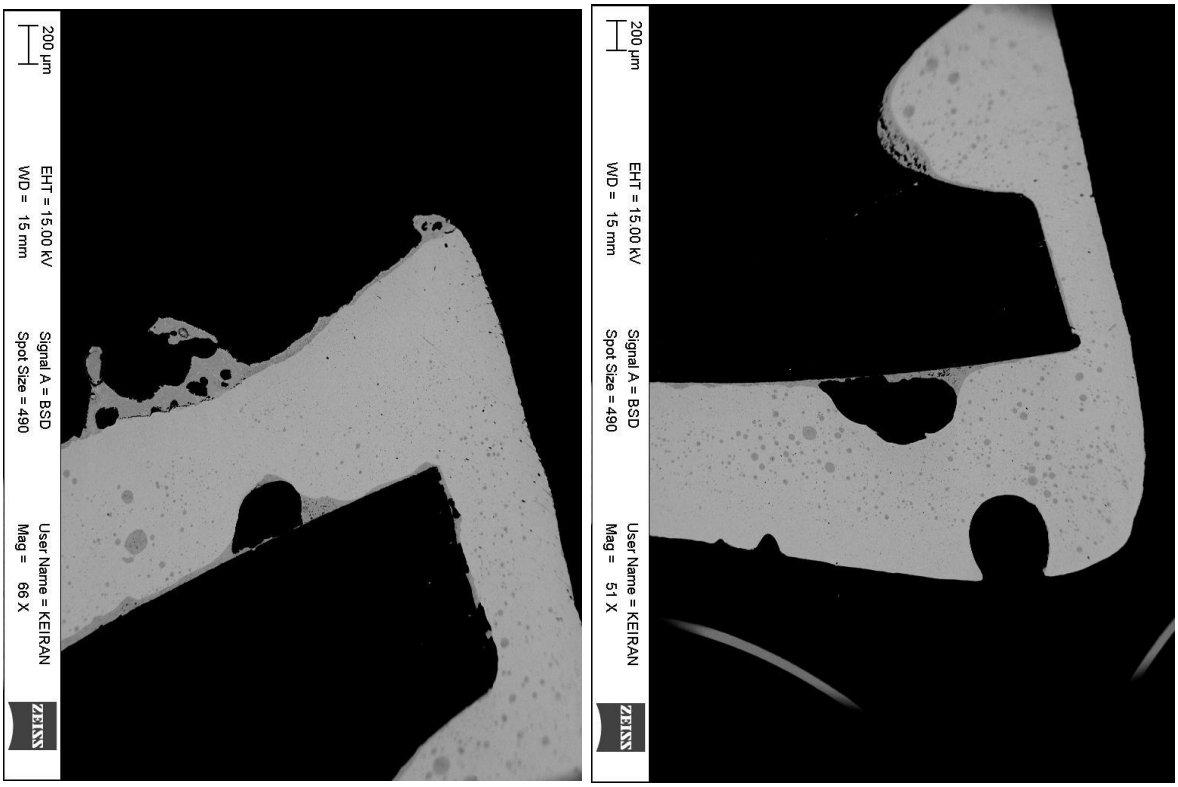

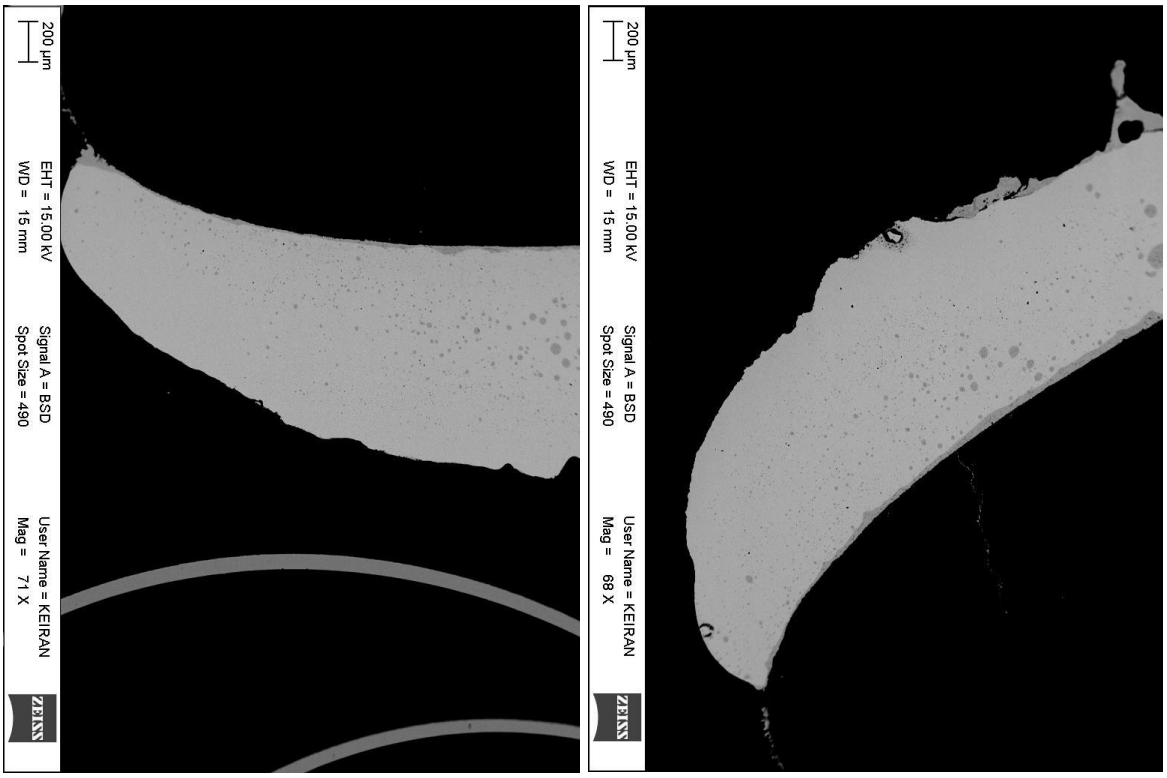

9.1 Appendix 2

Table 1 EPMA Analysis of main series, with values below detection limit presented as the detection limit.

	Wt % of each element in the Metal Phase								
0.01 atm P(SO_2) 1250 °C									
Site	**O**	**S**	**Fe**	**Co**	**Ni**	**Cu**	**Pd**	**Ag**	**Au**
S1	0.3127	2.2782	0.1061	0.4196	0.6679	94.493	0.8666	0.2235	0.7301
S2	0.4191	1.5834	0.1061	0.3815	0.7079	95.0089	0.8761	0.2383	0.7848
S3	0.4463	1.4542	0.1061	0.3913	0.6786	95.0788	0.9013	0.2265	0.808
S4	0.4408	1.5355	0.1061	0.3914	0.6782	95.0416	0.8745	0.2306	0.8046
S5	0.3477	1.1414	0.1061	0.3892	0.6928	95.4779	0.9102	0.2436	0.7876
S6	0.3898	1.2216	0.1061	0.3909	0.6875	95.3221	0.8964	0.2391	0.8475
S7	0.4246	1.0813	0.1061	0.4128	0.6743	95.4086	0.9216	0.2548	0.8114
S8	0.4416	1.1261	0.1061	0.4042	0.691	95.3513	0.8967	0.2565	0.8207
0.01 atm P(SO_2) 1300 °C									
S1	0.3144	1.2318	0.0176	0.4123	0.6875	95.6464	0.8805	0.0635	0.7605
S2	0.4413	1.0764	0.0176	0.3842	0.6687	95.7045	0.8672	0.0641	0.7876
S3	0.302	1.0999	0.0176	0.3916	0.7292	95.7935	0.8635	0.0356	0.7836
S4	0.2611	0.9304	0.0176	0.4059	0.6827	95.9434	0.8959	0.0824	0.795
S5	0.5319	1.2018	0.0176	0.4076	0.7084	95.4058	0.8617	0.0769	0.8023
S6	0.4456	1.2314	0.0176	0.4105	0.6917	95.446	0.8903	0.0626	0.8218
S7	0.6231	1.1907	0.0176	0.4008	0.6839	95.3814	0.8758	0.0648	0.7756
S8	0.5207	1.1263	0.0176	0.3998	0.6871	95.5135	0.8913	0.0627	0.7985
0.01 atm P(SO_2) 1350 °C									
S1	0.3771	0.9505	0.0176	0.4041	0.6964	95.8688	0.8846	0.0355	0.804
S2	0.3645	0.993	0.0176	0.3727	0.6735	95.8255	0.8873	0.0355	0.8702
S3	0.3518	0.5845	0.0176	0.4048	0.7473	96.1519	0.9054	0.0355	0.8118
S4	0.2254	0.9026	0.0176	0.4115	0.7539	95.9878	0.8972	0.0355	0.7924
S5	0.1715	1.0987	0.0176	0.3919	0.727	95.8955	0.8935	0.0355	0.8109
S6	0.2759	0.882	0.0176	0.3912	0.7198	95.9316	0.8935	0.0355	0.8783
S7	0.212	0.9892	0.0176	0.4156	0.7238	95.9339	0.8934	0.0355	0.814

S8	0.3163	0.8989	0.0176	0.4044	0.7273	95.9353	0.8833	0.0355	0.7951
0.05 atm P(SO_2) 1250 °C									
S1	0.3697	1.1735	0.0176	0.3021	0.6599	95.533	0.9011	0.2205	0.8402
S2	0.3924	2.5495	0.0176	0.3127	0.6522	94.3168	0.8291	0.1915	0.7445
S3	0.4159	2.3053	0.0176	0.2952	0.638	94.547	0.828	0.2105	0.7594
S4	0.3686	2.4863	0.0176	0.3032	0.6517	94.3993	0.8239	0.2132	0.7514
S5	0.4507	1.0708	0.0176	0.3313	0.7058	95.4946	0.9101	0.2215	0.8151
S6	0.3003	0.9432	0.0176	0.2736	0.6939	95.8123	0.9	0.2346	0.8406
S7	0.3929	1.54	0.0176	0.293	0.6821	95.1685	0.8973	0.2113	0.8062
S8	0.2773	1.0229	0.0176	0.2899	0.7018	95.7795	0.9086	0.1942	0.8258
0.05 atm P(SO_2) 1300 °C									
S1	0.3555	1.1425	0.0176	0.3046	0.743	95.686	0.8796	0.0957	0.7931
S2	0.374	1.1271	0.0176	0.3246	0.7118	95.7575	0.8363	0.081	0.7826
S3	0.377	1.0501	0.0176	0.3192	0.6994	95.8063	0.8538	0.1026	0.7852
S4	0.3973	1.0868	0.0176	0.3257	0.6944	95.788	0.859	0.1056	0.7411
S5	0.4029	1.2003	0.0176	0.3206	0.6994	95.6558	0.8438	0.0973	0.7754
S6	0.3546	1.1767	0.0176	0.3191	0.7081	95.7433	0.8676	0.096	0.7333
S7	0.3821	1.104	0.0176	0.3137	0.6909	95.7631	0.8622	0.0968	0.7813
S8	0.2747	1.2403	0.0176	0.3308	0.686	95.727	0.8491	0.111	0.781
0.05 atm P(SO_2) 1350 °C									
S1	0.3923	1.2122	0.0176	0.3401	0.6612	95.8202	0.8127	0.0355	0.74
S2	0.3612	1.0332	0.0176	0.3153	0.6736	96.0038	0.8285	0.0355	0.7539
S3	0.3993	1.15	0.0176	0.3342	0.6829	95.9342	0.7987	0.0355	0.6945
S4	0.4196	1.1556	0.0176	0.3405	0.6957	95.8729	0.7978	0.0355	0.7179
S5	0.4535	1.1289	0.0176	0.3396	0.6815	95.8473	0.8187	0.0355	0.7226
S6	0.4564	1.0783	0.0176	0.3347	0.6563	95.905	0.8167	0.0355	0.7511
S7	0.3951	0.9894	0.0176	0.3065	0.6578	96.0779	0.8105	0.0355	0.7371
S8	0.4286	1.0447	0.0176	0.3322	0.705	95.9325	0.8232	0.0355	0.7338
0.1 atm P(SO_2) 1250 °C									
S1	0.4783	1.104	0.0176	0.212	0.6493	95.6621	0.8823	0.2239	0.7846
S2	0.5249	1.0032	0.0176	0.2147	0.6694	95.6937	0.8945	0.2315	0.7681
S3	0.5689	0.9928	0.0176	0.2526	0.6593	95.585	0.8922	0.2428	0.8037

S4	0.4451	1.1352	0.0176	0.2187	0.6499	95.6428	0.8896	0.2393	0.7656
S5	0.5743	2.2436	0.0176	0.2461	0.6296	94.4606	0.8514	0.2292	0.7652
S6	0.6272	2.237	0.0176	0.2359	0.615	94.519	0.8174	0.2206	0.7262
S7	0.5367	2.1377	0.0176	0.2511	0.6543	94.6095	0.8424	0.2301	0.7351
S8	0.5495	1.9288	0.0176	0.2469	0.6263	94.8346	0.8435	0.2079	0.7626
0.1 atm P(SO_2) 1300 °C									
S1	0.471	1.069	0.0176	0.2288	0.6607	95.876	0.8587	0.095	0.7364
S2	0.4958	1.1037	0.0176	0.2357	0.6544	95.8435	0.85	0.0944	0.7191
S3	0.4693	1.2107	0.0176	0.2394	0.6459	95.737	0.8352	0.1095	0.7484
S4	0.4622	1.1142	0.0176	0.2432	0.6804	95.8036	0.8475	0.0847	0.7639
S5	0.4357	1.0373	0.0176	0.2303	0.644	95.968	0.8549	0.099	0.7308
S6	0.4547	0.991	0.0176	0.2161	0.6549	95.981	0.8551	0.0852	0.76
S7	0.4838	1.3141	0.0176	0.2447	0.6291	95.6408	0.8424	0.1045	0.7406
S8	0.4569	1.1264	0.0176	0.2386	0.6287	95.8583	0.8432	0.1117	0.7347
0.1 atm P(SO_2) 1350 °C									
S1	0.5506	1.588	0.0178	0.2624	0.6211	95.5146	0.768	0.0355	0.657
S2	0.5828	1.5854	0.0178	0.2578	0.6288	95.5414	0.7346	0.0355	0.6527
S3	0.5564	1.1056	0.0178	0.2539	0.6607	95.9684	0.7648	0.0355	0.6823
S4	0.4271	1.191	0.0178	0.2573	0.6701	95.9917	0.7579	0.0355	0.6692
S5	0.4468	1.5214	0.0178	0.263	0.6197	95.6906	0.7462	0.0355	0.6895
S6	0.3706	1.7013	0.0178	0.2674	0.617	95.6805	0.7415	0.0355	0.6114
S7	0.4029	1.1933	0.0178	0.2433	0.6722	96.0227	0.7843	0.0355	0.6664
S8	0.5185	1.3861	0.0178	0.2468	0.6484	95.7606	0.7607	0.0355	0.6745
0.5 atm P(SO_2) 1250 °C									
S1	0.8401	0.9957	0.0176	0.1045	0.6324	95.5868	0.8646	0.2327	0.7411
S2	0.6592	1.1931	0.0176	0.1278	0.6098	95.5599	0.8581	0.2495	0.7425
S3	0.7012	0.9319	0.0176	0.2069	0.6481	95.634	0.8881	0.2143	0.7651
S4	0.7631	2.4025	0.0176	0.1954	0.5993	94.3267	0.8021	0.2042	0.6973
S5	0.7371	2.7645	0.0176	0.2036	0.5987	93.998	0.7835	0.2393	0.6681
S6	0.6236	2.4546	0.0176	0.1863	0.6113	94.4134	0.8071	0.2049	0.6881
S7	0.5627	1.8404	0.0176	0.1691	0.6388	95.0202	0.8386	0.2108	0.7154
S8	0.7193	2.2659	0.0176	0.1775	0.6061	94.5304	0.7962	0.2265	0.6781

0.5 atm P(SO_2) 1300 °C									
S1	0.7755	1.1956	0.0176	0.1312	0.6061	95.7552	0.7707	0.1149	0.6508
S2	0.6606	1.1556	0.0176	0.113	0.5982	95.8979	0.759	0.1316	0.6842
S3	0.7144	1.0036	0.0176	0.1114	0.6166	96.0058	0.763	0.1206	0.6596
S4	0.7366	0.9169	0.0176	0.0895	0.6181	96.0633	0.763	0.1253	0.6821
S5	0.6116	1.0309	0.0176	0.1175	0.6266	96.0975	0.7699	0.1152	0.6309
S6	0.687	1.0299	0.0176	0.1095	0.6008	96.0666	0.7651	0.1069	0.6308
S7	0.8385	3.194	0.0176	0.1689	0.5789	93.8696	0.6758	0.119	0.5534
S8	0.7634	0.9607	0.0176	0.1081	0.6201	95.9865	0.7613	0.1259	0.6711
0.5 atm P(SO_2) 1350 °C									
S1	0.675	1.0393	0.0176	0.2055	0.6093	96.1664	0.6972	0.0355	0.5897
S2	0.726	1.1486	0.0176	0.2022	0.6068	96.017	0.6789	0.0355	0.5882
S3	0.6542	1.045	0.0176	0.128	0.5665	96.2801	0.6956	0.064	0.557
S4	0.6124	0.9698	0.0176	0.1791	0.6059	96.3592	0.6803	0.0355	0.5613
S5	0.7352	1.0102	0.0176	0.2028	0.6079	96.1322	0.6855	0.0355	0.5988
S6	0.7071	1.0475	0.0176	0.1591	0.5921	96.2213	0.6765	0.0355	0.5773
S7	0.5869	0.9832	0.0176	0.1874	0.597	96.3042	0.6885	0.0355	0.6211
S8	0.6901	1.0146	0.0176	0.1034	0.5754	96.2819	0.6845	0.0355	0.6139
1 atm P(SO_2) 1250 °C									
S1	0.8073	1.0212	0.0176	0.1217	0.6211	95.376	0.9192	0.2898	0.8437
S2	0.78	0.9913	0.0176	0.0762	0.6422	95.438	0.9483	0.2924	0.8297
S3	0.8238	0.9981	0.0176	0.0967	0.6258	95.3831	0.9179	0.3117	0.843
S4	0.883	1.053	0.0176	0.0988	0.6147	95.261	0.9457	0.3227	0.8144
S5	0.7487	0.978	0.0176	0.0747	0.6084	95.5206	0.921	0.3047	0.839
S6	0.7049	0.8407	0.0176	0.0431	0.6067	95.6871	0.9522	0.3246	0.8348
S7	0.7143	1.188	0.0176	0.1008	0.6544	95.2817	0.9253	0.3298	0.8057
S8	0.8153	0.9187	0.0176	0.0851	0.6325	95.4079	0.9555	0.329	0.856
1 atm P(SO_2) 1300 °C									
S1	0.7479	1.8168	0.0176	0.1356	0.5871	95.2065	0.7684	0.1234	0.6143
S2	0.7637	0.9941	0.0176	0.1134	0.5961	95.9146	0.8006	0.1441	0.6733
S3	0.9344	2.8175	0.0176	0.1591	0.5752	94.0489	0.717	0.141	0.6034
S4	0.7845	2.6059	0.0176	0.1495	0.5906	94.3431	0.7326	0.1537	0.6401

S5	0.687	1.5089	0.0176	0.114	0.5821	95.5102	0.7712	0.1496	0.6702
S6	0.7327	0.8546	0.0176	0.0704	0.6121	95.9914	0.8247	0.1549	0.7592
S7	0.7774	1.0622	0.0176	0.0917	0.6171	95.8069	0.7839	0.1398	0.7138
S8	1.0988	1.647	0.0176	0.1193	0.6075	94.9969	0.7817	0.1205	0.6255
1 atm $P(SO_2)$ 1350 °C									
S1	0.5478	0.963	0.0176	0.1109	0.5639	96.5847	0.6599	0.047	0.5184
S2	0.5429	0.9526	0.0176	0.0709	0.5392	96.6352	0.6492	0.0462	0.5636
S3	0.6187	1.2905	0.0176	0.1847	0.5722	96.1498	0.6298	0.0355	0.5338
S4	0.6133	0.9941	0.0176	0.1174	0.5883	96.4668	0.6364	0.0359	0.5479
S5	0.4918	0.8223	0.0176	0.0373	0.5444	96.901	0.6495	0.0355	0.5263
S6	0.5726	0.8389	0.0176	0.0644	0.532	96.7315	0.641	0.0489	0.5706
S7	0.5436	0.9405	0.0176	0.0397	0.5356	96.6578	0.6401	0.0423	0.5949
S8	0.5528	0.8382	0.0176	0.0337	0.5454	96.8065	0.6587	0.0355	0.5417
	Wt % of each element in the white metal phase								
0.01 atm $P(SO_2)$ 1250 °C									
Site	**O**	**S**	**Fe**	**Co**	**Ni**	**Cu**	**Pd**	**Ag**	**Au**
S1	0.5506	19.8898	0.0335	0.4500	0.2665	78.6130	0.0218	0.1633	0.0534
S2	0.6097	20.0447	0.0439	0.4600	0.2708	78.3884	0.0375	0.1276	0.0534
S3	0.6861	19.8277	0.0489	0.4711	0.2579	78.5121	0.0384	0.1579	0.0534
S4	0.5739	19.8835	0.0475	0.4804	0.2743	78.5113	0.0368	0.1716	0.0534
S5	0.6145	20.0754	0.0379	0.4815	0.2252	78.4350	0.0171	0.1263	0.0534
S6	0.5646	19.9677	0.0371	0.4794	0.2254	78.5525	0.0171	0.1553	0.0534
S7	0.6578	20.0833	0.0340	0.4644	0.2290	78.3939	0.0171	0.1335	0.0534
S8	0.5824	20.1108	0.0364	0.4692	0.2666	78.3881	0.0171	0.1302	0.0534
0.01 atm $P(SO_2)$ 1300 °C									
S1	0.5495	19.9896	0.0459	0.4524	0.2044	78.7259	0.0171	0.0347	0.0534
S2	0.553	19.9474	0.042	0.466	0.2263	78.7116	0.0171	0.0425	0.0534
S3	0.5206	19.976	0.0472	0.467	0.2413	78.6892	0.0171	0.0479	0.0534
S4	0.4335	20.025	0.0495	0.4846	0.2553	78.6935	0.0196	0.0391	0.0534
S5	0.4712	19.4012	0.0381	0.4484	0.2576	79.2946	0.0362	0.0347	0.0534
S6	0.6843	19.8537	0.0464	0.4643	0.2987	78.5654	0.0228	0.0644	0.0534
S7	0.6401	19.1082	0.0477	0.4644	0.3077	79.3234	0.045	0.0598	0.0534

S8	0.7478	19.5373	0.0401	0.4542	0.3072	78.7873	0.0366	0.0751	0.0534
0.01 atm P(SO_2) 1350 °C									
S1	0.5162	19.9596	0.0844	0.5052	0.1082	78.7927	0.0171	0.0347	0.0534
S2	0.5664	20.0505	0.0643	0.4805	0.161	78.6415	0.0171	0.0347	0.0534
S3	0.5623	19.6201	0.0826	0.5226	0.2451	78.8971	0.0414	0.0347	0.0534
S4	0.5769	19.8511	0.0725	0.4912	0.242	78.7114	0.0176	0.0374	0.0534
S5	0.4838	19.9976	0.079	0.5251	0.2641	78.5951	0.0171	0.0502	0.0534
S6	0.5365	19.8774	0.0797	0.5306	0.1894	78.7227	0.0171	0.0576	0.0534
S7	0.402	20.0253	0.0776	0.5465	0.1342	78.7543	0.0171	0.0474	0.0534
S8	0.5596	20.0562	0.0635	0.5046	0.2202	78.5644	0.0171	0.0347	0.0534
0.05 atm P(SO_2) 1250 °C									
S1	0.7943	19.6306	0.0378	0.4505	0.2707	78.6425	0.0171	0.1653	0.0534
S2	0.7691	19.5039	0.0254	0.4301	0.3046	78.8185	0.0171	0.1484	0.0534
S3	0.7421	19.4744	0.0328	0.4379	0.2981	78.7978	0.0171	0.2023	0.0534
S4	0.8208	19.6371	0.0484	0.5241	0.2723	78.5345	0.0171	0.1567	0.0534
S5	0.7975	19.5569	0.0419	0.5405	0.363	78.4937	0.0171	0.2065	0.0534
S6	0.7549	19.506	0.0322	0.4341	0.3022	78.759	0.0171	0.2009	0.0534
S7	0.8154	19.5818	0.0448	0.4694	0.3069	78.5662	0.0171	0.209	0.0534
S8	0.6934	19.5773	0.0378	0.4979	0.248	78.762	0.0171	0.1836	0.0534
0.05 atm P(SO_2) 1300 °C									
S1	0.8062	19.9237	0.032	0.423	0.2766	78.4329	0.0171	0.0951	0.0534
S2	0.7548	19.4971	0.0297	0.4261	0.3307	78.8652	0.0364	0.0531	0.0534
S3	0.644	19.5237	0.0299	0.3824	0.2902	79.0371	0.0224	0.0704	0.0534
S4	0.5688	19.9397	0.0374	0.4199	0.247	78.6745	0.0171	0.0972	0.0534
S5	0.519	19.9671	0.0322	0.4858	0.2203	78.7105	0.0171	0.0652	0.0534
S6	0.6952	20.0584	0.0272	0.439	0.2837	78.4494	0.0171	0.0463	0.0534
S7	0.678	20.0352	0.0384	0.4346	0.2731	78.4607	0.0171	0.0521	0.0534
S8	0.6641	20.1368	0.0281	0.4402	0.2824	78.3588	0.0171	0.0794	0.0534
0.05 atm P(SO_2) 1350 °C									
S1	0.8108	19.6756	0.0629	0.611	0.2677	78.5234	0.0171	0.0485	0.0534
S2	0.7228	19.6743	0.0642	0.6411	0.2447	78.5673	0.0171	0.081	0.0534
S3	0.7437	19.6706	0.052	0.5048	0.2831	78.695	0.0171	0.0505	0.0534

S4	0.6969	19.6804	0.0613	0.4804	0.2766	78.7332	0.0171	0.0712	0.0534
S5	0.7539	19.713	0.0609	0.5421	0.2243	78.662	0.0171	0.0374	0.0534
S6	0.6689	19.7975	0.0381	0.3944	0.3194	78.6738	0.0171	0.1078	0.0534
S7	0.4842	19.8084	0.0304	0.2956	0.1917	79.1269	0.0171	0.0628	0.0534
S8	0.7151	19.7212	0.0628	0.4839	0.3149	78.6394	0.0171	0.0398	0.0534
0.1 atm P(SO_2) 1250 °C									
S1	0.8808	19.2487	0.041	0.4243	0.2738	78.9895	0.0171	0.139	0.0534
S2	1.0894	19.1573	0.0335	0.3726	0.3191	78.8948	0.0171	0.1166	0.0534
S3	1.0141	19.2385	0.0535	0.6457	0.4179	78.466	0.0171	0.1642	0.0534
S4	1.0387	19.1123	0.0364	0.4003	0.3033	78.9195	0.0171	0.1743	0.0534
S5	0.8451	19.1852	0.0359	0.3793	0.2479	79.0717	0.0171	0.2268	0.0534
S6	0.9295	19.1386	0.0412	0.5686	0.384	78.7559	0.0171	0.1823	0.0534
S7	0.9064	19.194	0.0345	0.4122	0.2951	78.9557	0.0171	0.2016	0.0534
S8	0.9542	19.0268	0.0349	0.3507	0.2323	79.1961	0.0171	0.1998	0.0534
0.1 atm P(SO_2) 1300 °C									
S1	1.1304	19.2008	0.0342	0.4183	0.317	78.8269	0.0171	0.0724	0.0534
S2	0.9984	19.2752	0.0331	0.4336	0.3181	78.8584	0.0171	0.0781	0.0534
S3	0.9999	19.3197	0.0259	0.4072	0.2826	78.8695	0.0171	0.0905	0.0534
S4	1.0299	19.324	0.0217	0.4248	0.2261	78.9179	0.0171	0.0493	0.0534
S5	1.0554	19.3739	0.019	0.4902	0.2333	78.7591	0.0171	0.0687	0.0534
S6	1.0594	19.2102	0.0237	0.5149	0.2643	78.8599	0.0171	0.0674	0.0534
S7	1.0569	19.3379	0.0275	0.3192	0.3035	78.8566	0.0171	0.0946	0.0534
S8	1.0059	19.3603	0.0314	0.4354	0.286	78.7914	0.0171	0.0719	0.0534
0.1 atm P(SO_2) 1350 °C									
S1	1.0362	19.1076	0.0275	0.4166	0.3341	78.9957	0.0215	0.0458	0.0534
S2	1.1188	19.1176	0.0428	0.413	0.3293	78.923	0.0171	0.0471	0.0534
S3	1.0861	19.0242	0.0463	0.4372	0.2945	79.0785	0.0171	0.0347	0.0534
S4	0.846	19.3793	0.0267	0.4129	0.3253	78.9883	0.0171	0.0347	0.0534
S5	0.9489	18.8193	0.0333	0.4007	0.3096	79.4612	0.0171	0.0347	0.0534
S6	0.9739	18.5443	0.0277	0.4054	0.3217	79.6428	0.0425	0.0347	0.0534
S7	1.0389	18.9043	0.0368	0.4031	0.3341	79.2469	0.0218	0.0347	0.0534
S8	1.0949	18.2405	0.0239	0.4013	0.3027	79.8999	0.0241	0.0347	0.0534

0.5 atm P(SO_2) 1250 °C									
S1	1.9826	18.1376	0.0469	0.4498	0.3	78.9485	0.0171	0.128	0.0534
S2	1.7794	18.3044	0.0592	0.4792	0.2863	78.915	0.0171	0.1764	0.0534
S3	1.383	18.4848	0.058	0.511	0.3028	79.0718	0.0171	0.1671	0.0534
S4	1.6516	18.1162	0.0648	0.6686	0.3787	78.9408	0.0171	0.161	0.0534
S5	1.5535	18.4826	0.0625	0.4158	0.2494	79.0273	0.0171	0.2089	0.0534
S6	1.5595	18.102	0.0438	0.4046	0.2608	79.4314	0.0171	0.1901	0.0534
S7	1.5727	18.1852	0.0602	0.4406	0.2826	79.2434	0.0171	0.2048	0.0534
S8	1.7622	18.3199	0.0666	0.5323	0.3804	78.7305	0.0171	0.189	0.0534
0.5 atm P(SO_2) 1300 °C									
S1	1.97	18.2064	0.064	0.4144	0.3603	78.8837	0.0171	0.0942	0.0534
S2	1.9562	18.1743	0.0537	0.3813	0.3035	79.0614	0.0171	0.0616	0.0534
S3	1.5223	18.4138	0.052	0.3997	0.3112	79.1854	0.0171	0.103	0.0534
S4	1.8138	18.2814	0.0662	0.4398	0.3459	78.9679	0.0171	0.0828	0.0534
S5	1.9108	18.2179	0.0555	0.3815	0.33	79.0418	0.0171	0.0624	0.0534
S6	1.8451	18.3038	0.0673	0.4031	0.3528	78.9486	0.0171	0.0793	0.0534
S7	1.9392	18.1411	0.077	0.5753	0.3983	78.7771	0.0171	0.092	0.0534
S8	1.9606	18.0807	0.0717	0.4914	0.35	78.9799	0.0171	0.0572	0.0534
0.5 atm P(SO_2) 1350 °C									
S1	1.6678	18.4601	0.0318	0.2644	0.1176	79.3666	0.0171	0.0713	0.0534
S2	1.5123	18.3823	0.0182	0.1736	0.0449	79.8294	0.0171	0.0433	0.0534
S3	1.478	18.5273	0.0182	0.1478	0.0272	79.7654	0.0171	0.0368	0.0534
S4	1.7266	18.1683	0.0656	0.9112	0.2839	78.7799	0.0171	0.061	0.0534
S5	1.5545	18.2448	0.0368	0.6235	0.2417	79.1981	0.0171	0.0775	0.0534
S6	1.2453	18.6626	0.0268	0.1454	0.0453	79.7709	0.0171	0.0791	0.0534
S7	1.8171	17.7754	0.0552	0.6197	0.19	79.4408	0.0171	0.1018	0.0534
S8	1.7123	18.2905	0.08	0.9018	0.3152	78.6465	0.0171	0.0516	0.0534
1 atm P(SO_2) 1250 °C									
S1	2.0079	17.6067	0.0687	0.6147	0.333	79.3293	0.0171	0.0383	0.0534
S2	1.772	16.9568	0.0461	0.4338	0.2456	80.3852	0.0177	0.14	0.0534
S3	2.024	16.4569	0.0706	0.6461	0.3338	80.3453	0.0171	0.1097	0.0534
S4	1.7698	17.7499	0.057	0.3604	0.1529	79.7805	0.0171	0.1256	0.0534

S5	2.0564	17.6471	0.0826	0.8889	0.4235	78.7389	0.0171	0.1559	0.0534
S6	2.3662	17.6005	0.0573	0.4376	0.224	79.2542	0.0171	0.0602	0.0534
S7	2.3013	17.3398	0.0454	0.4546	0.2614	79.5257	0.0171	0.057	0.0534
S8	2.0216	17.6069	0.073	0.7277	0.4021	79.0971	0.0171	0.0716	0.0534
1 atm P(SO_2) 1300 °C									
S1	1.9379	17.9427	0.0521	0.5123	0.3571	79.0241	0.0171	0.1727	0.0534
S2	1.7998	18.0602	0.0639	0.57	0.4012	78.9436	0.0171	0.1282	0.0534
S3	2.2179	17.6883	0.071	0.4186	0.2903	79.1268	0.0171	0.1871	0.0534
S4	2.2947	17.541	0.0851	0.7808	0.5185	78.6468	0.0171	0.1302	0.0534
S5	1.8657	17.7795	0.0611	0.5746	0.3701	79.2158	0.0171	0.1204	0.0534
S6	2.633	17.6724	0.0524	0.5008	0.3397	78.7195	0.0171	0.0822	0.0534
S7	2.3458	18.1031	0.0649	0.535	0.3752	78.4966	0.0171	0.078	0.0534
S8	1.7364	18.2815	0.0637	0.5341	0.3845	78.9597	0.0171	0.0401	0.0534
1 atm P(SO_2) 1350 °C									
S1	1.2667	18.4357	0.0219	0.4446	0.0507	79.7431	0.0171	0.0372	0.0534
S2	1.8646	17.5067	0.0394	0.3055	0.1357	80.122	0.0171	0.0347	0.0534
S3	1.3573	18.128	0.0182	0.0617	0.0257	80.4019	0.0171	0.0347	0.0534
S4	2.0801	17.3866	0.0274	0.3597	0.2332	79.8764	0.0171	0.0347	0.0534
S5	1.6476	17.9699	0.0294	0.154	0.1083	79.9798	0.0171	0.1034	0.0534
S6	2.0331	17.5737	0.0714	0.6785	0.2643	79.2743	0.0171	0.0996	0.0534
S7	1.7791	17.9282	0.0193	0.1794	0.0257	80.0064	0.0171	0.0729	0.0534
S8	1.2958	18.8273	0.0244	0.1735	0.0398	79.5889	0.0171	0.0436	0.0534

Table 2 EPMA Analysis of repetition series, with values below detection limit presented as the detection limit.

Wt. % of elements in metal phase of the repetitious series									
0.01 atm P(SO_2) 1250 °C									
Site	**O**	**S**	**Fe**	**Co**	**Ni**	**Cu**	**Pd**	**Ag**	**Au**
S1	0.2877	1.1714	0.0176	0.4282	0.6992	95.4134	0.9092	0.2717	0.812
S2	0.323	1.2637	0.0176	0.4494	0.69	95.3028	0.8932	0.2845	0.7902

S3	0.3597	1.7037	0.0176	0.4642	0.7138	94.7626	0.8987	0.2871	0.8053
S4	0.3458	0.9624	0.0176	0.421	0.7195	95.5475	0.9196	0.2452	0.8333
S5	0.3832	1.1718	0.0176	0.4404	0.6966	95.3327	0.891	0.2601	0.8164
S6	0.3143	1.0629	0.0176	0.4354	0.7026	95.5117	0.9216	0.2647	0.7867
S7	0.398	2.2413	0.0176	0.4507	0.6718	94.3436	0.8699	0.2686	0.7528
S8	0.3653	2.1205	0.0176	0.4393	0.6911	94.4922	0.8557	0.2516	0.7705
0.01 atm P(SO_2) 1350 °C									
S1	0.2771	1.0918	0.0176	0.4579	0.7032	95.8012	0.8975	0.0355	0.7623
S2	0.2949	1.1793	0.0176	0.4454	0.6776	95.7916	0.8563	0.0355	0.7488
S3	0.4412	1.1668	0.0176	0.4587	0.6983	95.5975	0.8779	0.0355	0.7447
S4	0.3439	1.3656	0.0176	0.4783	0.6872	95.4879	0.8429	0.0355	0.7763
S5	0.3423	1.7536	0.0176	0.461	0.6841	95.1598	0.8425	0.0355	0.7418
S6	0.4334	1.4267	0.0176	0.4535	0.6974	95.414	0.8351	0.0355	0.7176
S7	0.3848	1.3276	0.0176	0.4492	0.6973	95.5117	0.8675	0.0355	0.7443
S8	0.2723	1.0208	0.0176	0.4595	0.7008	95.8784	0.874	0.0355	0.7739
0.05 atm P(SO_2) 1300 °C									
S1	0.5908	1.3493	0.0176	0.3562	0.6691	95.3422	0.8401	0.1029	0.7493
S2	0.5451	1.2117	0.0176	0.3612	0.6657	95.4913	0.8631	0.1276	0.7308
S3	0.516	1.156	0.0176	0.3596	0.6681	95.5922	0.8632	0.0998	0.7334
S4	0.4492	1.2108	0.0176	0.3351	0.6677	95.6149	0.8619	0.1258	0.7346
S5	0.465	1.0228	0.0176	0.3523	0.6664	95.8026	0.8558	0.0892	0.7458
S6	0.5593	1.1793	0.0176	0.3432	0.6788	95.4798	0.8729	0.1155	0.7674
S7	0.547	1.1002	0.0176	0.3595	0.668	95.6333	0.8706	0.099	0.7224
S8	0.5798	1.3085	0.0176	0.3657	0.6704	95.3598	0.8697	0.1158	0.7274
0.5 atm P(SO_2) 1300 °C									
S1	0.5689	0.9659	0.0176	0.2012	0.6333	95.9999	0.8092	0.125	0.6913
S2	0.4749	0.8911	0.0176	0.0591	0.6058	96.3145	0.7906	0.1594	0.7047
S3	0.6727	0.9644	0.0176	0.2246	0.646	95.8657	0.7927	0.1515	0.6824
S4	0.4951	0.9339	0.0176	0.1559	0.648	96.1418	0.7874	0.1298	0.708

S5	0.6012	0.8909	0.0176	0.1522	0.6278	96.0717	0.8269	0.1211	0.7082
S6	0.5142	0.8539	0.0176	0.1407	0.6263	96.2513	0.7833	0.1431	0.6864
S7	0.5255	0.8864	0.0176	0.1807	0.6329	96.0951	0.8095	0.135	0.7337
S8	0.5537	0.9499	0.0176	0.1534	0.623	96.0635	0.7921	0.1484	0.7159
1 atm P(SO_2) 1250 °C									
S1	0.7993	1.0875	0.0176	0.0857	0.6207	95.4035	0.9219	0.2886	0.7893
S2	0.8449	1.3707	0.0176	0.1074	0.6301	95.0397	0.9168	0.2804	0.8091
S3	0.8314	1.3624	0.0176	0.1022	0.6411	94.96	0.9714	0.2893	0.8373
S4	0.8594	1.0836	0.0176	0.0672	0.6352	95.1492	0.995	0.326	0.8795
S5	1.0146	1.0473	0.0176	0.0983	0.6284	95.1495	0.93	0.2986	0.8263
S6	0.7248	1.0058	0.0176	0.1024	0.6306	95.469	0.9524	0.2865	0.8202
S7	0.6741	1.028	0.0176	0.0896	0.6106	95.591	0.9083	0.2936	0.7944
S8	0.7663	1.1542	0.0176	0.1059	0.6407	95.2998	0.9139	0.277	0.8319
1 atm P(SO_2) 1350 °C									
S1	0.7374	0.9708	0.0176	0.096	0.558	96.4146	0.6396	0.0355	0.5493
S2	0.6578	0.9406	0.0176	0.1642	0.5854	96.4127	0.6554	0.0428	0.5411
S3	0.6186	1.1014	0.0176	0.1128	0.5376	96.5502	0.5789	0.0355	0.4909
S4	0.6497	0.9103	0.0176	0.09	0.5641	96.6484	0.6082	0.0355	0.5035
S5	0.799	1.0145	0.0176	0.1031	0.5303	96.3803	0.5975	0.0409	0.5342
S6	0.6843	1.0256	0.0176	0.1444	0.5829	96.3879	0.6125	0.0355	0.527
S7	0.5993	0.9914	0.0176	0.0968	0.5304	96.6333	0.6034	0.0355	0.5117
S8	0.6576	1.1021	0.0176	0.1837	0.5709	96.2346	0.645	0.0388	0.5598
Wt. % of elements in white metal phase in the repetitious series									
0.01 atm P(SO_2) 1250 °C									
S1	0.6329	19.3179	0.0737	0.5173	0.2777	79.034	0.0285	0.118	0.0534
S2	0.6989	19.106	0.0763	0.506	0.3054	79.1422	0.0303	0.131	0.0534
S3	0.7092	19.249	0.0699	0.5124	0.2734	79.0441	0.0391	0.1028	0.0534
S4	0.6171	19.6826	0.078	0.5462	0.2686	78.6564	0.0228	0.1283	0.0534
S5	0.6179	19.6583	0.079	0.525	0.2184	78.7651	0.0171	0.1286	0.0534
S6	0.7393	19.5831	0.0818	0.5338	0.266	78.6375	0.0189	0.1395	0.0534
S7	0.6171	19.7851	0.0773	0.5281	0.239	78.6188	0.0171	0.1218	0.0534

S8	0.6049	19.6951	0.077	0.5589	0.229	78.6492	0.0171	0.1457	0.0534
0.01 atm P(SO_2) 1350 °C									
S1	0.589	18.847	0.0709	0.5189	0.3021	79.6066	0.045	0.0347	0.0534
S2	0.6507	18.4988	0.0863	0.5285	0.3282	79.8665	0.0382	0.0347	0.0534
S3	0.613	19.7112	0.078	0.5269	0.2315	78.8282	0.0171	0.0347	0.0534
S4	0.7949	19.4943	0.0728	0.538	0.2781	78.7729	0.0171	0.0347	0.0534
S5	0.4785	19.62	0.0875	0.5169	0.1134	79.1758	0.0171	0.0347	0.0534
S6	0.4261	19.8835	0.078	0.4564	0.1672	78.9887	0.0171	0.0347	0.0534
S7	0.454	19.6582	0.0656	0.3922	0.2274	79.1015	0.0873	0.0347	0.0534
S8	0.4952	19.7658	0.0811	0.4914	0.2146	78.9455	0.0171	0.0347	0.0534
0.05 atm P(SO_2) 1300 °C									
S1	0.6338	19.7616	0.0499	0.4343	0.2772	78.7542	0.0171	0.089	0.0534
S2	0.8591	19.7787	0.0533	0.5381	0.3236	78.3539	0.0171	0.0868	0.0534
S3	0.8129	19.7597	0.0713	0.5476	0.2745	78.4591	0.0171	0.0738	0.0534
S4	0.8432	19.7519	0.0535	0.4731	0.3211	78.4373	0.0171	0.0974	0.0534
S5	0.8406	19.5779	0.0518	0.4782	0.2813	78.6345	0.02	0.1157	0.0534
S6	0.8627	19.7221	0.0494	0.4601	0.2815	78.5247	0.0171	0.08	0.0534
S7	0.7889	19.8715	0.0611	0.498	0.2649	78.4114	0.0171	0.1042	0.0534
S8	0.9018	19.6113	0.0714	0.5417	0.3435	78.4196	0.0171	0.0998	0.0534
0.5 atm P(SO_2) 1300 °C									
S1	1.7133	18.2116	0.0778	0.6308	0.3374	78.9362	0.0171	0.0867	0.0534
S2	1.8295	18.2146	0.0808	0.6733	0.3488	78.7435	0.0171	0.1066	0.0534
S3	1.7973	18.2857	0.0335	0.4942	0.2452	79.0207	0.0171	0.1121	0.0534
S4	1.7815	18.2285	0.064	0.5733	0.3075	78.9294	0.0171	0.0849	0.0534
S5	1.6891	18.2188	0.0607	0.5696	0.2727	79.0705	0.0171	0.1125	0.0534
S6	1.7052	18.2265	0.0721	0.6884	0.3098	78.8686	0.0171	0.1219	0.0534
S7	1.6816	18.2629	0.0567	0.596	0.283	79.0132	0.0171	0.1066	0.0534
S8	1.7587	18.2076	0.072	0.6141	0.3188	78.9121	0.0171	0.1144	0.0534
1 atm P(SO_2) 1250 °C									

S1	1.8901	18.0462	0.0791	0.7162	0.3905	78.7167	0.0171	0.1567	0.0534
S2	2.0802	17.6671	0.0619	0.6412	0.3353	79.0898	0.0171	0.1244	0.0534
S3	2.2711	17.4501	0.0839	0.8375	0.528	78.6622	0.0171	0.1583	0.0534
S4	2.1979	17.4281	0.0645	0.5905	0.3249	79.3123	0.0171	0.0818	0.0534
S5	2.4837	17.2507	0.0776	0.5105	0.2804	79.2758	0.0171	0.1213	0.0534
S6	1.8423	17.4789	0.0182	0.1963	0.0633	80.3199	0.0171	0.0835	0.0534
S7	2.2856	16.8755	0.0475	0.1597	0.0257	80.4281	0.0171	0.1733	0.0534
S8	1.7562	17.7559	0.0251	0.1625	0.0337	80.1802	0.0171	0.0808	0.0534
1 atm P(SO_2) 1350 °C									
S1	1.2667	18.4357	0.0219	0.4446	0.0507	79.7431	0.0171	0.0372	0.0534
S2	1.8646	17.5067	0.0394	0.3055	0.1357	80.122	0.0171	0.0347	0.0534
S3	1.3573	18.128	0.0182	0.0617	0.0257	80.4019	0.0171	0.0347	0.0534
S4	2.0801	17.3866	0.0274	0.3597	0.2332	79.8764	0.0171	0.0347	0.0534
S5	1.6476	17.9699	0.0294	0.154	0.1083	79.9798	0.0171	0.1034	0.0534
S6	2.0331	17.5737	0.0714	0.6785	0.2643	79.2743	0.0171	0.0996	0.0534
S7	1.7791	17.9282	0.0193	0.1794	0.0257	80.0064	0.0171	0.0729	0.0534
S8	1.2958	18.8273	0.0244	0.1735	0.0398	79.5889	0.0171	0.0436	0.0534